

*Tumor-targeted immunotherapy using an
engineered adenoviral vector platform*

Inauguraldissertation

zur

Erlangung der Würde eines Doktors der Philosophie

vorgelegt der Philosophisch-Naturwissenschaftlichen Fakultät der
Universität Basel

von

Nicole Kirchhammer

Basel, 2021

Genehmigt von der Philosophisch-Naturwissenschaftlichen Fakultät auf Antrag von

Prof. Dr. Alfred Zippelius, Prof. Dr. Christoph Hess und Prof. Dr. Mikaël Pittet

Basel, den 25. Mai 2021

Prof. Dr. Marcel Mayor

“The important thing is not to stop questioning. Curiosity has its own reason for existence. One cannot help but be in awe when he contemplates the mysteries of eternity, of life, of the marvelous structure of reality. It is enough if one tries merely to comprehend a little of this mystery each day.”

Albert Einstein

Table of Contents

1	INTRODUCTION.....	2
1.1	CANCER IMMUNOLOGY.....	2
1.1.1	NK cells in cancer.....	3
1.1.2	DCs in cancer.....	3
1.2	CANCER IMMUNOTHERAPY.....	4
1.2.1	Cytokines in cancer immunotherapy.....	6
1.2.2	Adenoviral vectors for cancer gene therapy.....	7
2	RESULTS AND DISCUSSION.....	9
2.1	IMATCH - AN INTEGRATED MODULAR ASSEMBLY-SYSTEM FOR THERAPEUTIC COMBINATION HIGH-CAPACITY ADENOVIRUS GENE THERAPY.....	9
2.1.1	Abstract.....	10
2.1.2	Introduction.....	10
2.1.3	Results.....	13
2.1.4	Discussion.....	26
2.1.5	Materials and methods.....	29
2.1.6	Acknowledgments.....	34
2.1.7	Authors contributions.....	34
2.1.8	Conflict of interest.....	34
2.1.9	Supplemental information.....	35
2.2	TARGETING INTRA-TUMORAL CROSSTALK BETWEEN ADAPTIVE AND INNATE IMMUNITY ENHANCES CANCER IMMUNE CONTROL.....	43
2.2.1	Abstract.....	44
2.2.2	Introduction.....	45
2.2.3	Results.....	46
2.2.4	Extended discussion.....	63
2.2.5	Methods.....	68
2.2.6	Acknowledgments.....	79
2.2.7	Authors contributions.....	79
2.2.8	Declaration of interests.....	79
2.2.9	Supplementary figures.....	80
3	SUMMARY.....	84
4	ACKNOWLEDGEMENTS.....	85
5	REFERENCES.....	86
6	CURRICULUM VITAE.....	97

1 Introduction

1.1 Cancer immunology

Cancer is a genetic disease that is characterized by the accumulation of mutations and epigenetic changes (Flavahan et al., 2017; Takeshima and Ushijima, 2019). These changes in gene regulation underlie the malignant transformation of cells and are necessary for the development of the hallmarks of cancer (Hanahan and Weinberg, 2011). However, an increased tumor mutational burden heightens the risk for detection by the immune system as non-self, which would elicit cellular immune responses and result in the elimination of the tumor (Samstein et al., 2019). The tumor-eliminating potential of the immune system can be seen as a process of selection of tumor variants with reduced immunogenicity, termed immunoediting, representing one common mechanism of cancer immune escape (Schreiber et al., 2011). Reduced immunogenicity is mainly the result of the downregulation of antigen-presentation, the upregulation of immunoregulatory pathways, including surface receptor-mediated interactions (e.g. the PD-1/PD-L1 axis) or the secretion of immunosuppressive cytokines (e.g. IL-10, TGF- β), as well as the accumulation of pro-tumorigenic cell types (e.g. regulatory T cells, tumor-associated macrophages and monocyte-derived suppressor cells; Garrido et al., 1997; Saleh and Elkord, 2020; Sharma et al., 2017; Yang et al., 2008). These stages of tumor “Elimination, Editing, and Escape” have been described in multiple models, as well as in patients. Strategies aiming to tip the balance towards tumor-elimination are still a current area of research and the goal of immunotherapeutic interventions (Dunn et al., 2004; O’Donnell et al., 2019).

The immunological steps involved in the successful generation of an anti-tumor immune response have been described in the “cancer-immunity cycle” by Chen and Mellman (2013). The cycle begins with the release of tumor antigens due to the death of cancer cells. These antigens can then be presented by antigen-presenting cells (APCs) to CD8 T cells preferentially in tumor-draining lymph nodes. Tumor-specific T cells then become activated and migrate into the tumor, where they are able to recognize tumor cells presenting their cognate peptides on major histocompatibility complex I (MHC I) molecules. This leads to the T cell-mediated killing of the cancer cells, setting the cycle in motion anew. Although cytotoxic T cells have been shown to be essential for successful cancer immunity, they still commonly fail to control tumors. CD8 T cell cytotoxicity can be limited through a state of exhaustion or dysfunction induced by chronic T cell receptor (TCR) stimulation which is accompanied by a reduced expression of effector cytokines and upregulation of inhibitory receptors such as T-cell immunoglobulin and mucin domain-3 (TIM-3), lymphocyte activation gene-3 (LAG-3), programmed cell death protein-1 (PD-1) and T-lymphocyte-associated protein-4 (CTLA-4; Baitsch et al., 2011; Blank et al., 2019; Zippelius et

al., 2004). However, there is increasing evidence that these intratumoral T cells are not fully “exhausted” but exhibit other functions in the tumor microenvironment including the secretion of C-X-C motif chemokine 13 (CXCL13), which mediates immune cell recruitment to tertiary lymphoid structures (Thommen et al., 2018).

1.1.1 NK cells in cancer

While the cancer-immunity cycle focuses predominantly on T cells, natural killer (NK) cells – a type of innate lymphoid cells – can similarly control cancers by the rapid killing of tumor cells (Herberman et al., 1975; Huntington et al., 2020). In contrast to T cells, NK cells do not require presentation of tumor antigen in order to elicit anti-tumor functions, and instead respond either to the expression of activating ligands or the specific lack of inhibitory ligands on tumor cells during transformation (Kärre, 2002). Thereby, NK cells are able to eliminate tumors with very low mutational burdens and those that lack neoantigen presentation, complementing the cytotoxic activity of CD8 T cells.

Upon activation, NK cells secrete a variety of cytokines, including interferon γ (IFN γ) and tumor necrosis factor (TNF). These pleiotropic proteins have potent anti-proliferative and pro-apoptotic effects on cancer cells, in addition to their ability to enhance cytotoxic CD8 T cell responses (Myers and Miller, 2021). Furthermore, NK cells improve CD8 T cell immunity by recruiting and fostering the survival and maturation of dendritic cells (DCs) through the production of C-C motif chemokine ligand 5 (CCL5) and XC-chemokine ligand 1 (XCL1), as well as FMS-related tyrosine kinase 3 ligand (FLT3L) and granulocyte-macrophage colony-stimulating factor, respectively (GM-CSF; Barry *et al.*, 2018; Böttcher *et al.*, 2018).

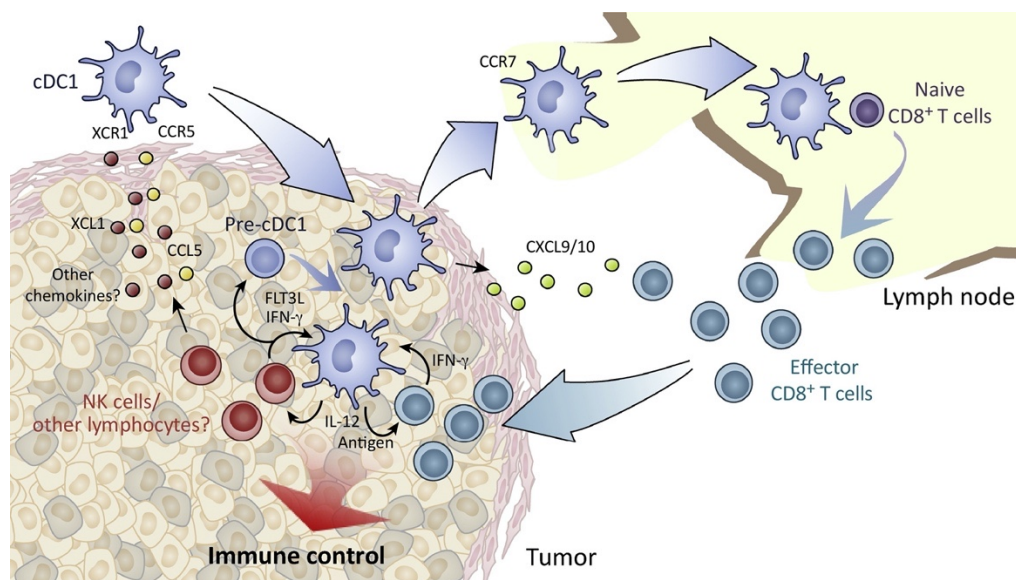
1.1.2 DCs in cancer

DCs are a diverse group of specialized antigen-presenting cells with key roles in the initiation and regulation of innate and adaptive immune responses, particularly in the priming and activation of T cells (Hildner et al., 2008; Roberts et al., 2016; Sánchez-Paulete et al., 2016). DCs can be resident within lymphoid organs, or they can surveil peripheral tissues and blood (Cabeza-Cabrerizo et al., 2019). Inflammatory conditions, including cancer, enhance DC accumulation within tissues, as well as their maturation and trafficking to draining lymph nodes, subsequently enhancing T cell immunity by presenting captured antigens (Roberts et al., 2016).

Multiple sub-classifications of DCs exist and are furtherer expanded with the advance of increasingly sophisticated profiling techniques (Gerhard et al., 2021). Broadly, DCs can be grouped into conventional type 1 DCs (cDC1), conventional type 2 DCs (cDC2) and plasmacytoid DCs (pDCs). An additional subset of DCs arises from blood monocytes which traffic to peripheral

tissues and differentiate into monocyte-derived DCs (moDCs). cDC1 are the DC subset best known for their ability to process and cross-present exogenous antigens on MHC1 molecules to activate CD8 T cells and for their ability to prime type 1 T helper cell (Th1) responses (Hildner et al., 2008). Furthermore, cDC1s have been described as the main producers of interleukin 12 (IL-12) which further potentiates the effector function of CD8 T cells and NK cells by inducing IFN γ (Garris et al., 2018; Tugues et al., 2015). In turn, IFN γ enhances cDC1's secretion of the chemokines CXCL9 and CXCL10, both of which further attract effector CD8 T cells (Figure 1; Böttcher and Reis e Sousa, 2018). The importance of this immune signaling cascade in cancer is emphasized by the fact that gene expression signatures characteristic for the cellular components of this axis, as well as a signature of IFN γ signaling and CXCL9 and CXCL10, are all prognostic for patient survival and predictive of improved response to immune checkpoint inhibition (Ayers et al., 2017; Böttcher et al., 2018; Bronger et al., 2016; Cursons et al., 2019; Lee, 2019; Zhao et al., 2019).

Recently, single-cell RNA sequencing revealed an additional subtype of DCs which is conserved in different cancers, called DC3. These DCs are only found in tissues and may arise from either cDC1s or cDC2s/moDCs and are defined by the expression of C-C chemokine receptor 7 (CCR7) and their high capability to produce IL-12 (Gerhard et al., 2021).



Trends in Cancer

Figure 1. Orchestration of cancer immune control by cDC1 (Böttcher and Reis e Sousa, 2018).

1.2 Cancer immunotherapy

Immunotherapy, aiming to boost host immune responses in order to eliminate malignant cells, is a monumental breakthrough for cancer treatment and has revolutionized the field of oncology

(Hegde and Chen, 2020; Ribas and Wolchok, 2018; Wolchok et al., 2017). Multiple cancer entities have shown sustained, durable clinical responses, albeit with limited response rates and ultimately unclear underlying mechanisms (Kalbasi and Ribas, 2020).

Initiated by a pioneering study demonstrating that blocking CTLA-4 induces effective immune responses and leads to tumor regression, utilizing antibodies to release the brakes on immune cells and reinforce anti-tumor immune responses opened the era of immune checkpoint inhibitors (ICIs) in clinical practice (Leach et al., 1996). CTLA-4 is upregulated and trafficked to the immune cell synapse following TCR engagement and can inhibit T cell priming by competing with the co-stimulatory molecule CD28 for binding to their shared ligands CD80 and CD86 (Egen and Allison, 2002; Masteller et al., 2000; Pentcheva-Hoang et al., 2004). Using CTLA-4-blocking antibodies allows unrestrained CD28 co-stimulation and reduces the immunosuppressive capacity of regulatory T cells (Tregs) resulting in improved anti-tumor immunity (Li et al., 2020). Besides CTLA-4-based ICI, the most widely and successfully used immunotherapies are based on the inhibition of the PD-1/PD-L1 axis. Binding of PD-1 to its ligand PD-L1 triggers recruitment of SHP2, a phosphatase that dephosphorylates TCR and CD28-co-stimulatory signaling components, therefore restricting T cell activity (Waldman et al., 2020). Investigations are ongoing to achieve a comprehensive, mechanistic understanding of the mentioned pathways. It is apparent, however, that CTLA-4 and PD-1/PD-L1 inhibition act in a non-redundant manner resulting in an improved treatment success when combined in patients (Wei et al., 2019).

The success of ICI demonstrates that harnessing the immune system, particularly T cells, can eliminate cancer cells. However, despite their clinical efficacy, only a fraction of patients show response. Following the successful example of utilizing non-redundant mechanisms to achieve synergistic therapeutic benefits, approved immunotherapies are often combined with conventional, targeted and/or other immunotherapeutic agents (Mokhtari et al., 2017; Seliger, 2019). Although a number of these combinations show increased efficacy, the systemic administration of many immunotherapeutic agents, including co-administration of anti-CTLA-4 and anti-PD-1 antibodies, can cause pronounced side effects (Algazi et al., 2020; Chan and Bass, 2020; Motzer et al., 2019). This toxicity is likely due to the action of these agents not being restricted to the tumor site. Therefore, recent research has aimed to improve the toxicity profiles and the clinical responses of ICIs through the modification of existing antibodies and the engineering of novel delivery methods (Riley et al., 2019). In addition, targeted delivery also allows the use of therapeutic agents with high therapeutic potential but limited tolerability or half-life such as immune-stimulating cytokines (Algazi et al., 2020; Diab et al., 2020).

1.2.1 Cytokines in cancer immunotherapy

Cytokines function as messengers of the immune system, orchestrating cellular interactions and communication. They play an indispensable role in immune regulation while being involved in cell proliferation, cell death, inflammation, tissue repair, and cellular homeostasis. Because of their pleiotropic effects on immune cells and their role in immune activation, cytokines have emerged as potential candidates for cancer immunotherapy (Sudan, 2020).

The history of cytokines as agents to treat cancer, began in the mid-1990s when the anti-cancer effect of high-dose interleukin 2 (IL-2) therapy was first demonstrated (West, 1989). IL-2 binding to its receptor leads to an increased activation and proliferation of T cells and NK cells (Cornish et al., 2006; Fehniger et al., 2003; Hinrichs et al., 2008). Furthermore, it has been shown to reduce the expression of PD-1 and to partly restore cytokine production in dysfunctional CD8 T cells (Thommen et al., 2018). A major drawback of IL-2-based therapies is the strong expression of the high affinity IL-2 receptor on Tregs which upon engagement results in their expansion and the suppression of the anti-tumor immune response (Ahmadzadeh and Rosenberg, 2006; Zorn et al., 2006).

In contrast, the cytokine IL-12, while equally potent at inducing CD8 T cell- and NK cell-mediated tumor killing, has been shown to reduce the number of Tregs in the tumor microenvironment (TME). This occurs by driving the differentiation of naïve CD4 T cells towards IFN γ and TNF secreting Th1 cells, as well as by inducing apoptosis in Tregs through Fas-mediated killing by CD8 T cells (Kennedy et al., 1994; Kilinc et al., 2009; Lasek et al., 2014). Beyond these functions, IL-12 has been shown to inhibit or reprogram immunosuppressive cells, such as tumor-associated macrophages (TAMs) and is the main driver of the cytostatic and anti-angiogenic IFN γ . Importantly, IFN γ is able to upregulate MHC I and II expression on tumor cells, resulting in their enhanced recognition and lysis (Tugues et al., 2015). Furthermore, IL-12 is required for effective anti-PD-1 immunotherapy, fully licensing T cell-mediated anti-tumor immunity (Garris et al., 2018). Consequently, IL-12 has been extensively investigated for its use in cancer immunotherapy. In clinical studies, however, IL-12 induced high toxicity when administered systemically, resulting in low efficacy at tolerated doses (Hurteau et al., 2001; Weiss et al., 2003). A possible explanation for its limited clinical efficacy is the lack of targeting IL-12 into the tumor microenvironment. Most cytokines, including IL-12, act locally in the tumor and nearby lymph nodes in paracrine or autocrine fashions, rather than systemically on lymphocytes in circulation (Nguyen et al., 2020). Therefore, maximizing the amount of IL-12 effectively reaching the tumor seems critical for a robust anti-tumor response.

1.2.2 Adenoviral vectors for cancer gene therapy

Local delivery strategies can be divided into three general approaches: (1) gene therapy approaches using viral or non-viral vectors, (2) fusion of the therapeutic payload to a targeting moiety such as antibodies, and (3) controlled release of the protein from a sustained delivery system (Neshat et al., 2020; Riley et al., 2019).

Virus-mediated gene delivery utilizes the natural ability of a virus to transfer genetic material (DNA or RNA) into host cells to produce the encoded proteins. Over the past decades, dozens of pathogens have been vectorized into viral gene vectors, out of which lentiviral (LV), adeno-associated (AAV) and human adenoviral vectors (AdV) are the most frequently used in gene therapy (Lundstrom, 2018). In contrast to LV, both AAV and AdV are non-integrative vectors, in that they do not stably integrate their viral genes into the host genome. This reduces the risk of integration-induced toxicity and malignancies, while leading to transient expression of payloads, overall increasing their safety profiles for clinical use (Cavazzana-Calvo et al., 2000; Gaspar et al., 2004). Of note, stable integration of LV-delivered DNA might be desired for some oncological applications such as gene corrections and CAR T cell therapies (Maude et al., 2014). Non-replicative AAV vectors are frequently used in preclinical and clinical applications, in particular in oncology, due to the low immunological responses against these vectors in humans and the efficient production of high yields (Chahal et al., 2014; Mingozzi and High, 2013). However, the use of AAV vectors for combination therapies is limited since AAVs have a packaging capacity of below 4.5 kb. In contrast, adenoviral vectors are well suited for combination therapy approaches due to their large packaging capacity of 2-36 kb, even though they appear to be more immunogenic in humans (Lee et al., 2017).

Until now, four types of adenoviral gene vectors can be distinguished: conditionally replicative, first-generation (FG), second-generation (SG) and high-capacity/gutless adenoviral (HCAAdV) vectors (Figure 2; Ricobaraza et al., 2020). The most prominent conditionally replicative vectors are oncolytic viruses (additional packaging capacity: 2 kb) which specifically replicate in cancer cells, inducing their lysis (Baker et al., 2018). FG, SG and high capacity adenoviral vectors are non-replicative vectors due to deletion of the early adenoviral gene 1 (E1), which instead is supplied in *trans* from the producer cell line during the production of the adenoviral vector. FG viral vectors have an additional deletion of the gene E3 resulting in a packaging capacity of 8-10 kb. FG vectors can be rapidly produced in high titers with producer cell lines supplementing E1 and E3 (Danthinne and Imperiale, 2000). For SG vector production, the producer cell line needs to provide the genes E1, E2, E3 and E4 which makes viral production less efficient while only moderately increasing packaging capacity (14 kb; Gorziglia et al., 1999). Therefore, SG vectors have not frequently been used as gene therapy vectors. HCAAdV lack all viral genes resulting in a

substantial increase of packaging capacity up to 36 kb and decreased immunogenicity of transduced cells due to the lack of residual viral protein expression (Rosewell et al., 2011). To produce gutless HCAAdV vectors, all viral genes need to be provided by the producer cell line and a helper virus, which can lead to helper virus contamination of the final product (Dormond and Kamen, 2011). Despite the elaborate production procedure, HCAAdV vectors offer unique advantages for combinatorial gene therapies, driving the development of scalable production and purification techniques (Ricobaraza et al., 2020).

In the following parts of this thesis, I will first introduce an efficient platform for the generation and production of HCAAdVs (Section 2.1) and second introduce a strategy how one can apply these vectors for improved cancer immunotherapy (Section 2.2). The second part was still performed using first generation adenoviral vectors, as both projects were initiated in parallel.

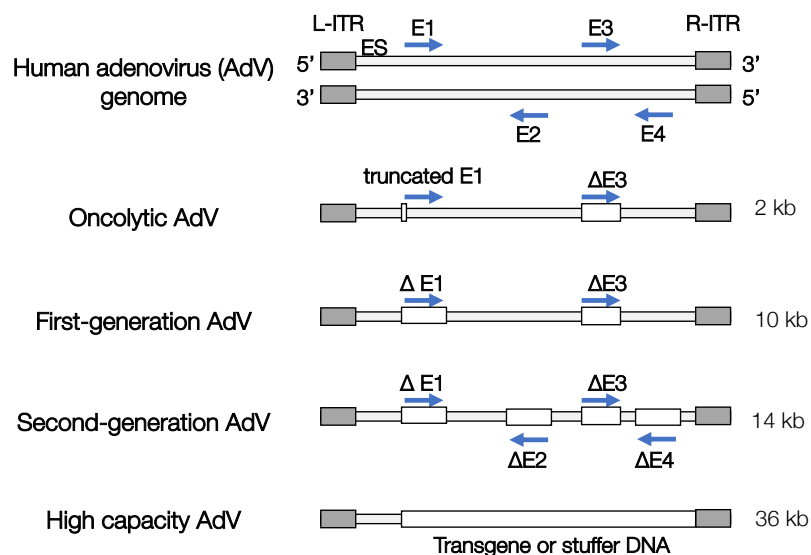


Figure 2: Schematic representation of adenoviral vector generations.

The position of the early genes (E), the encapsulation signal (ES), left (L-ITR) and right (R-ITR) inverted terminal repeats and the insertion position of the transgenes or stuffer DNA (white boxes) are listed. The orientation of the early genes is indicated by arrows. In addition to truncating the E1 gene oncolytic vectors can also be generated by encoding E1 under tumor-specific promoters (not depicted here).

2 Results and Discussion

2.1 iMATCH - an integrated modular assembly-system for therapeutic combination high-capacity adenovirus gene therapy

Short Title: Modular production system for combination vectors

Dominik Brücher^{1,*}, Nicole Kirchhammer^{2,*}, Sheena N. Smith¹, Jatina Schumacher¹, Nina Schumacher¹, Jonas Kolibius¹, Patrick C. Freitag¹, Markus Schmid^{1,3}, Fabian Weiss^{1,4}, Corina Keller^{1,5}, Melanie Grove⁶, Urs Greber⁶, Alfred Zippelius^{2,7} and Andreas Plückthun¹

1) Department of Biochemistry, University of Zurich, Winterthurerstrasse 190, 8057 Zurich, Switzerland.

2) Department of Biomedicine, University of Basel, Hebelstrasse 20, 4031 Basel, Switzerland.

3) Present address: Roche Diagnostics GmbH, Nonnenwald 2, 82377 Penzberg, Germany

4) Institute of Pharmacology, University of Bern, Inselspital, INO-F, 3010 Bern

5) Present address: MBV AG, Industriestrasse 9, 8712, Stäfa, Switzerland

6) Department of Molecular Life Sciences, University of Zurich, 8057 Zurich, Switzerland

7) Medical Oncology, University Hospital Basel, 4031 Basel, Switzerland

*: These authors contributed equally to this work

Correspondence should be addressed to Andreas Plückthun, Department of Biochemistry, University of Zurich, plueckthun@bioc.uzh.ch

Adapted from the publication: Brücher, D., Kirchhammer, N., Smith, S.N., Schumacher, J., Schumacher, N., Kolibius, J., Freitag, P.C., Schmid, M., Weiss, F., Keller, C., et al. (2021). iMATCH - an integrated modular assembly-system for therapeutic 2 combination high-capacity adenovirus gene therapy. *Mol. Ther. - Methods Clin. Dev.*

Published: 12th of March 2021

DOI: 10.1016/j.omtm.2021.01.002.

2.1.1 Abstract

Adenovirus-mediated combination gene therapies have shown promising results in vaccination or treating malignant and genetic diseases. Nevertheless, an efficient system for the rapid assembly and incorporation of therapeutic genes into high-capacity adenoviral vectors (HCAAdV) is still missing. Here, we developed the iMATCH platform which enables the generation and production of HCAAdVs encoding therapeutic combinations in high quantity and purity within three weeks. Our modular cloning system facilitates the efficient combination of up to four expression cassettes and the rapid integration into HCAAdV genomes with defined sizes. Helper viruses (HVs) and purification protocols were optimized to produce HCAAdVs with distinct capsid modifications and unprecedented purity (0.1 ppm HVs). The constitution of HCAAdVs, with adaptors for targeting and a shield of trimerized scFv for reduced liver clearance, mediated cell- and organ-specific targeting of HCAAdVs. As proof of concept, we showed that a single HCAAdV encoding an anti PD-1 antibody, IL-12 and IL-2 produced all proteins, and led to tumor regression and prolonged survival in tumor models, comparable to a mixture of single-payload HCAAdVs *in vitro* and *in vivo*. Therefore, the iMATCH system provides a versatile platform for the generation of high-capacity gene therapy vectors with a high potential for clinical development.

Keywords:

high-capacity vectors, helper-dependent adenovirus, gutless adenovirus, gene therapy, combination therapy, cancer therapy, immunotherapy, gene vectors, PD-1, IL-12, IL-2

2.1.2 Introduction

Gene therapy comprises viral, bacterial and cellular vectors with cellular therapies, also including stem cell therapies (De Luca et al., 2019; Sedighi et al., 2019). Viral gene therapy has come a long way since the early 1990s, when human adenoviruses (HAdV) were first vectorized and applied in attempts to treat monogenic cystic fibrosis lung disease (Baker et al., 2018; Gao et al., 2019; Greber, 2020; Greber and Flatt, 2019; Slade, 2001). Today, viral gene therapy with a variety of viruses is used in oncology, vaccination, and many other disciplines in clinical science (Bjorklund, 2018; Gordon et al., 2019; Ura et al., 2014; Wirth and Ylä-Herttuala, 2014). Gene therapy vectors have been used preclinically for host genome editing and clinically for the expression of intracellular proteins, surface receptor presentation and/or the secretion of therapeutics (Ehrke-Schulz et al., 2017; Hubberstey et al., 2002; Palmer et al., 2020; Ruan et al., 2016). Recently, multiple gene delivery vectors have been developed in the expanding field of cancer immunotherapy (Neshat et al., 2020). Cancer immunotherapy approaches modulate the

activity of immune cells against cancer cells in various ways, e.g., by rendering the immunosuppressive state of the tumor microenvironment (e.g., by blocking the PD-1/PD-L1 axis) or by stimulating immune cell activation (e.g., by cytokine IL-12 or IL-2 release) to eradicate cancer cells (Sharma and Allison, 2020).

Despite numerous successes in different types of cancer such as melanoma, non-small cell lung carcinoma (NSCLC), urothelial carcinoma, and Hodgkin's lymphoma (Ansell et al., 2015; Garon et al., 2015; Topalian et al., 2012), immunotherapies with checkpoint inhibitors have only been effective in a subset of patients (Haslam and Prasad, 2019), at least in part due to the complex immunosuppressive interactions of cancer cells within the tumor microenvironment (Galluzzi et al., 2018). Certain combinations of immunotherapeutics have shown synergistic effects e.g., anti-PD-1 with IL-12 or IFN- γ (Garris et al., 2018) but also severe side effects upon systemic application, e.g., anti-CTLA-4 with anti-PD-1 (Chan and Bass, 2020).

In contrast, immunotherapeutics delivered by viral or non-viral vectors to the tumor site have provided increased efficacy with less severe side effects due to the tumor-restricted expression of immunotherapeutic combinations (Huang et al., 2020; Nakao et al., 2020; Porter et al., 2020). Non-replicative high-capacity adenoviral vectors (HCAAdV), also called helper-dependent (HdV) or gutless adenoviral vectors, are especially well suited for the gene delivery of multiple transgenes due to their high packaging capacity up to 36 kb (Rosewell et al., 2011), the efficient and long-lasting transgene expression of up to 7 years (Brunetti-Pierri et al., 2013) and the attenuated immune clearance of transduced cells (Muruve et al., 2004). The latter is largely a result of the absence of viral genes and their products.

Despite these advantages, the broad use of HCAAdV vectors is currently hampered by the notoriously complex cloning and production schemes of HCAAdVs (Dormond and Kamen, 2011; Jager et al., 2009; Lee et al., 2019). During HCAAdV production, helper viruses (HVs) provide sufficient viral proteins in *trans* to achieve high HCAAdV yields. HV particles are typically first-generation adenoviral vectors derived from HAdV-C5 lacking the E1 and E3 gene clusters (Zhou et al., 2002). Due to the high immunogenicity of HVs and the potential interference of HV-expressed viral proteins with the target cells, HV must be removed from any HCAAdV formulation. To suppress HV particle formation, the packaging signal of the HV DNA is typically flanked by loxP sites, which permits a Cre recombinase-mediated excision of the HV packaging signal in HCAAdV producer cells, e.g., in the cell line 116 (Sandig et al., 2000). This strategy reduces HV contamination to 0.01-0.2 % of the HCAAdV, that is 100-2000 HV particles per million HCAAdV particles (ppm; Jager et al., 2009; Palmer and Ng, 2003).

For gene therapy applications, the natural tropism of HAdV-C5 vectors for coxsackievirus and adenovirus receptor (CAR) has been ablated by genomic modifications to the adenovirus fiber

knob (Barry et al., 2020). The tropism of adenoviral vectors has been redirected to defined biomarkers using genetically-encoded tags, or exogenously added adaptor proteins (Barry et al., 2020; Dreier et al., 2013). While genetic modifications can lead to virion instability and low vector yields (Poulin et al., 2020), exogenously-added adaptors do not affect vector production and thus allow for versatile use of the vector in different cell types (Poulin et al., 2020). Previously, our group has developed a trimerized adaptor that binds in a quasi-covalent manner to the HAdV-C5 knob by coupling the trimerizing SHP domain of the lambdaoid phage 21 linked to a knob-binding designed ankyrin repeat protein (DARPin; Dreier et al., 2013). Cell specificity is then mediated by a second retargeting DARPin coupled to the SHP domain. Retargeting DARPins against new proteins can be selected rapidly via ribosomal display (Dreier and Plückthun, 2012), produced efficiently in *E. coli* in large scale, and the adaptors constructed from simply added to the virus (Dreier et al., 2013). The receptor specificity of a given virus can thus be changed rapidly. Off-target infection of HAdV-C5 vectors, especially liver infection, can further be reduced by genetic ablation of the hypervariable region 7 (HVR7) of the hexon, which facilitates blood factor X binding; however, HVR7 deletion also results in increased adenoviral depletion by neutralizing antibodies (Allen and Byrnes, 2019; Xu et al., 2013). To decrease the rapid clearance of modified or unmodified HAdV-C5 by neutralizing antibodies following systemic injection, our group has developed a trimerized scFv-based shield that covers the adenoviral surface (Schmid et al., 2018). The combined implantation of capsid mutation (Δ HVR7) and exogenously-added shield and adaptor proteins increases tumor specificity and transgene expression of non-replicative first generation (E1 and E3 deleted) adenoviral vectors upon intravenous and intratumoral injection in murine models (Schmid et al., 2018).

To enhance the versatility of HAdV vectors, we designed a system that facilitates the rapid and efficient assembly of multiple transgenes into high-capacity adenoviral vectors with very low HV contamination for gene therapy approaches. Our platform iMATCH (integrated Modular Assembly for Therapeutic Combination High-capacity adenoviral vectors) combines a highly efficient assembly system with a novel purification strategy for generating combinations of HCAV vectors, compatible with adenoviral retargeting and shielding strategies that can be used for the specific delivery of complex combinations of genes to target cells in a broad range of diseases. We validated the efficacy of the iMATCH system using reporter vectors as well as vectors harboring multiple immunotherapeutic genes for expression in cell culture and immune-competent murine tumor models.

2.1.3 Results

2.1.3.1 A modular assembly system for combing therapeutic genes

The generation and production of high-capacity adenoviral vectors (HCA_{AdV}) has so far been cumbersome, inefficient and time-consuming (Lee et al., 2019). Overall, this is due to technical challenges in cloning of large (>28 kb) plasmids which is required in standard HCA_{AdV} preparations. To enhance the cloning efficiency, we designed four size-optimized plasmids of 3-5 kb (pUniversal plasmids), each with an orthogonal expression cassette containing one of the following constitutive promoters: CMV, EF1 α , SV40 or PGK (Fig. 1a). The four promoters vary in the efficiency of transgene expression relative to each other, depending on the targeted cell (Qin et al., 2010). Expression levels of transgenes can thus be tuned relative to each other and relative to the chosen producer cell line. The expression cassettes were designed with minimal sequence similarity to each other, to the HCA_{AdV} backbone and to the HV genome in order to reduce inter- and intra-vector homologous recombination events. Notably, the number of payloads encoded on the pUniversal plasmid is not limited by the number of promoters, as polycistronic gene expression elements (e.g., 2A peptides (Chng et al., 2015) or internal ribosomal entry sites (IRES; Renaud-Gabardos et al., 2015) can be utilized within each open reading frame (ORF). Payloads encoding expression cassettes were flanked in each pUniversal plasmid by a unique pair of restriction sites and payload assembly overlaps (Fig 1a).

Upon restriction enzyme digestion, payloads encoded under the CMV, EF1- α or PGK promoter are released and can be integrated into a linearized pUniversal plasmid of choice, which was beforehand linearized with the same restriction enzyme pair. Payload integration thus can be achieved either by cost-effective ligation or, alternatively, by Gibson Assembly (Gibson et al., 2009). The assembly of multiple expression cassettes was done sequentially or simultaneously, allowing for the assembly of up to four expression cassettes on a single pUniversal plasmid within one day. Plasmid encoded correctly assembled payloads were selected by antibiotic resistance and validated by sequencing confirming a cloning efficacy of above 80 %. To verify this approach, reporter proteins were encoded within each expression cassette and combined on a single plasmid. Cells transfected with a combination of pUniversal plasmids containing all reporter expression cassettes showed similar or greater protein expression compared to a mixture of single reporter encoding plasmid transfection (Sup. Fig. 1).

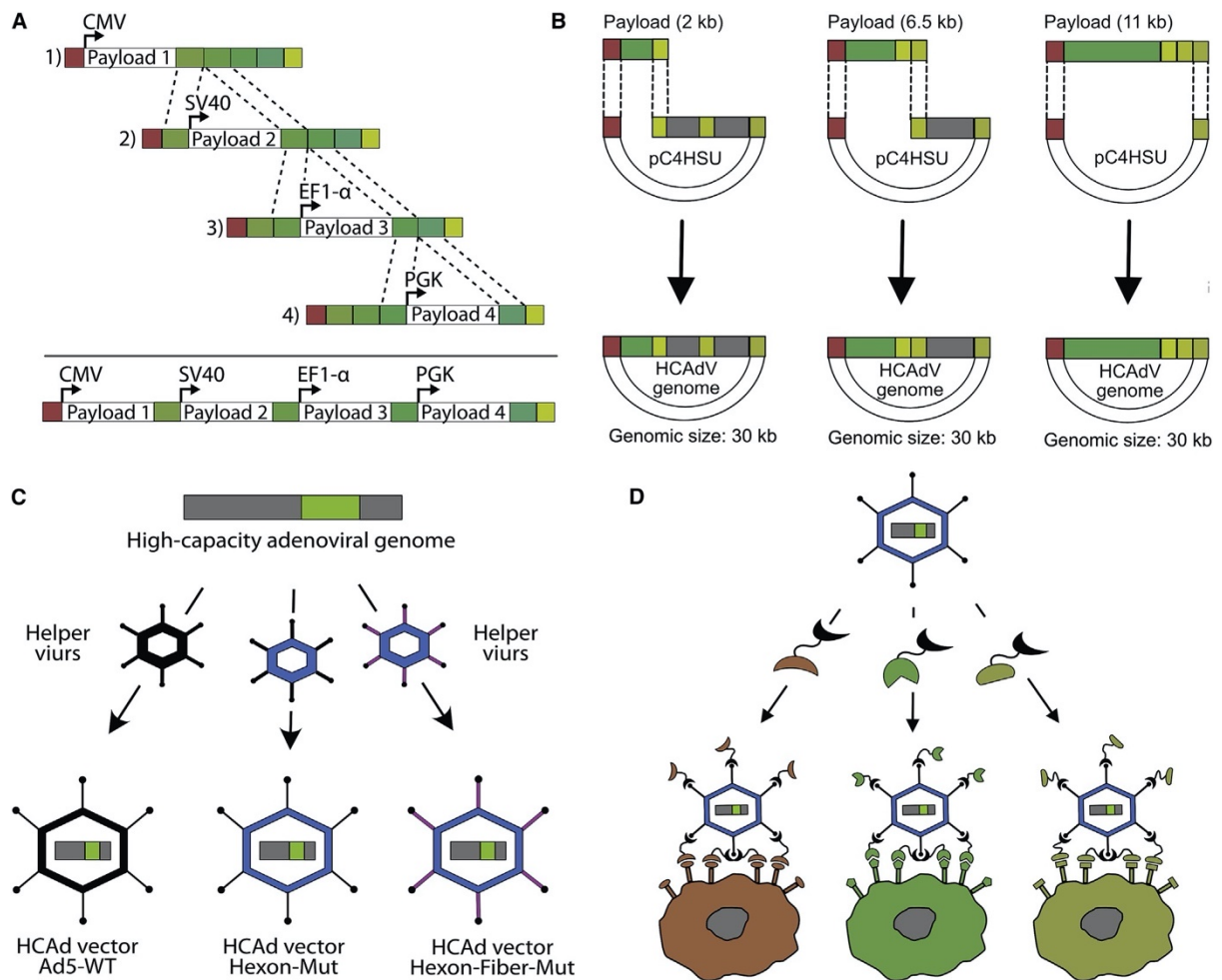


Figure 1: Schematic overview of the iMATCH platform

a) Four separate cloning plasmids (pUniversal 1-4) were constructed, each with an orthogonal expression cassette with a distinct promoter (CMV, SV40, EF1- α or PGK). Unique restriction sites and payload assembly overlaps (shades of green) enable a rapid combination of payloads encoded on different pUniversal plasmids via ligation or Gibson Assembly (dotted lines). b) Assembled payload combinations (green), released from the pUniversal plasmids using a different set of unique restriction sites (Sup. Fig. 2a-b), result in linear DNA fragments terminated by pC4HSU overlaps (red and shades of yellow). Depending on the genomic size of the payload combination and the desired genome size of the HCAAdV vector, different overlaps can be chosen (shades of yellow). Thereby, stuffer DNA (grey) of different sizes (0, 4.5 or 9 kb) is excised from the HCAAdV genome backbone plasmid (pC4HSU). The pC4HSU overlaps of the pUniversal fragments and the linearized pC4HSU plasmid (dotted lines) thus allow the efficient generation of HCAAdV genomes with defined genomic sizes via Gibson Assembly. c) HCAAdV genomes (grey, green) can be packaged into HCAAdV particles with defined capsid modifications, e.g., modification of the hexon (blue) or fiber (violet) protein by administering different HV vectors encoding the mutated capsid proteins during HCAAdV production. d) HCAAdV particles can be retargeted to defined cells via a chosen surface biomarker by using a very tight-binding retargeting adaptors that binds to the HAdV-C5 knob, here depicted as bispecific DARPin retargeting adaptors with two binding modules connected by a flexible linker: The first binder (knob binding DARPin, black) binds trivalently to the trimeric adenoviral fiber knob and simultaneously blocks HAdV-C5 from binding to its natural receptors (CAR). A new cell tropism is introduced by the second binding entity (retargeting DARPin, red, green, or yellow) that facilitates the specific binding to surface markers expressed on the cell of interest.

2.1.3.2 Rapid integration of gene combinations into a high-capacity adenoviral vector genome

Once the desired payload combination is assembled, an additional set of orthogonal restriction sites and overlaps (pC4HSU overlaps) on the pUniversal plasmids can be utilized for the integration of the payload combination into a well-characterized HCA_{AdV} backbone plasmid (pC4HSU; Flynn et al., 2010; Sandig et al., 2000) via Gibson Assembly (Fig. 1b). Depending on the payload size and the desired genome size of the HCA_{AdV}, the pUniversal plasmids can be digested with P_{meI}/P_{acl}, P_{meI}/X_{ma}I or P_{meI} (Sup. Fig. 2a). Each resulting pUniversal fragment (Sup. Fig. 2b) can be integrated into a linearized pC4HSU plasmid with compatible overlaps that was generated by A_{sc}I, A_{sc}I/NotI or A_{sc}I/S_waI restriction digest prior to assembly (Sup. Fig. 2c). Linearization of the pC4HSU plasmid releases either 0, 4.5 or 9 kb of “stuffer DNA” (Sup. Fig. 2d), which can be used to adapt the size of the resulting HCA_{AdV} vector. This enables production of HCA_{AdV} particles with the same genomic size and thus similar biophysical properties, independent of the payload size.

To increase cloning efficiency, a unique restriction site (F_spI) was introduced into the antibiotic resistance gene of the pUniversal plasmid (Sup. Fig. 2a). Backbone fragments of pUniversal plasmids that were used for payload release can lead to false positive clones due to the presence of an antibiotic resistance but a lack of payloads. For this reason, these fragments were digested with F_spI in parallel to the unique restriction enzymes required for payload release. Upon Gibson Assembly of the two fragments (linearized pUniversal and pC4HSU) and transformation of *E. coli* (Sup. Fig. 2e), cloning efficiencies of up to 85 % positive clones were obtained for a representative construct (Sup. Fig. 2f).

2.1.3.3 High-capacity adenoviral vectors with unique capsid modifications

The absence of viral genes on the HCA_{AdV} genome requires that the viral proteins are provided *in trans* by helper viruses (HV) for amplification of HCA_{AdV} vectors. We designed multiple helper viruses with different capsid modifications, including a HV with modifications in the hypervariable region 7 (HRV7) of the HAdV-C5 hexon to prevent factor X mediated liver infection (Xu et al., 2013) and a HV vector encoding the HVR7 modification with an additional deletion of the RGD motif from the HAdV-C5 penton that reduces integrin-mediated cell infection (off-target infection; Shayakhmetov et al., 2005). These different HVs readily enable the packaging of the HCA_{AdV} genome into a variety of different capsids (Fig. 1c) without the need to genetically modify the HCA_{AdV} genome. The use of different capsid modifications can be advantageous to modulate viral clearance, uptake, or to reduce off-target transduction for gene therapy approaches. (Barry et al., 2020) The desired target cell specificity of HCA_{AdV} particles with genetic capsid modifications was introduced by exogenously-added retargeting adaptors (Dreier et al., 2013);

following amplification and purification of HCA_{AdV} vectors, again without the need to modify the original HCA_{AdV} or HV vectors (Fig. 1d). Retargeted HCA_{AdV} particles were additionally covered by a shield, formed by a trimerized scFv to prevent off-target infection and HCA_{AdV} clearance by neutralizing antibodies (Schmid et al., 2018).

2.1.3.4 Generation of high-capacity adenoviral vectors with minimal helper virus contamination

HV contamination of HCA_{AdV} preparations must be kept as low as possible, due to the unavoidable viral gene expression from HV which causes an increased adaptive immune response against HC infected recipient cells (Muruve et al., 2004). On the other hand, however, HVs are required for HCA_{AdV} production (Fig. 2a), as they provide viral proteins in *trans* for the packaging of HCA_{AdV} genomes at the necessary balanced concentrations and in sufficient yields. To minimize HV contamination, we designed HVs that had minimal genomic similarity to the HCA_{AdV} vector, even including a modified encapsulation signal (Sandig et al., 2000), which in addition to reduced genetic similarity, packaged at a lower efficiency than the wildtype packaging signal of the HCA_{AdV}. Furthermore, our HV vectors were designed to have a genome size at the upper range of adenoviral packaging capacity (37.5 kb) to reduce the risk of generating fully replication-competent WT adenoviral vectors. The formation of competent WT adenoviral vectors can occur by E1/E3 recombination of HV vectors with E1 located on the chromosome of the producer cell line. The genomic size difference between the HCA_{AdV} (28-30 kb) and the HV (37.5 kb) also facilitates a sufficient separation of both vectors in subsequent CsCl density purification. Furthermore, we used the packaging cell line 116 for HCA_{AdV} vector amplification, which was specifically created to improve HCA_{AdV} vector production yield and purity (Palmer and Ng, 2003). The cell line 116 was previously selected for increased HCA_{AdV} amplification and its high levels of Cre recombinase (Sandig et al., 2000). Cre recombinase permits the removal of the loxP flanked HV packaging signal and thus renders the HV DNA non-packageable.

The combination of this HCA_{AdV} genome, HV vectors, and packaging cell line, together resulted in efficient amplification of the HCA_{AdV} vectors utilizing our platform (Sup. Fig. 3). HCA_{AdV} vectors are traditionally purified via two density gradients, a first two-step gradient (1.25 g/cm³ and 1.35 g/cm³) in which the cell lysate, cell debris and empty particles are separated from the viral particle, and a second continuous gradient (1.33 g/cm³) in which the HCA_{AdV} particles are separated from the HVs. Instead of utilizing a traditional continuous gradient (Jager et al., 2009; Palmer and Ng, 2003) as the second purification step, we employed a discontinuous four-step gradient ranging from 1.29-1.35 g/cm³ (Fig. 2b), which led to a visible separation of the desired HCA_{AdV} (30 kb) from the HV particles (37.5 kb; Fig. 2c).

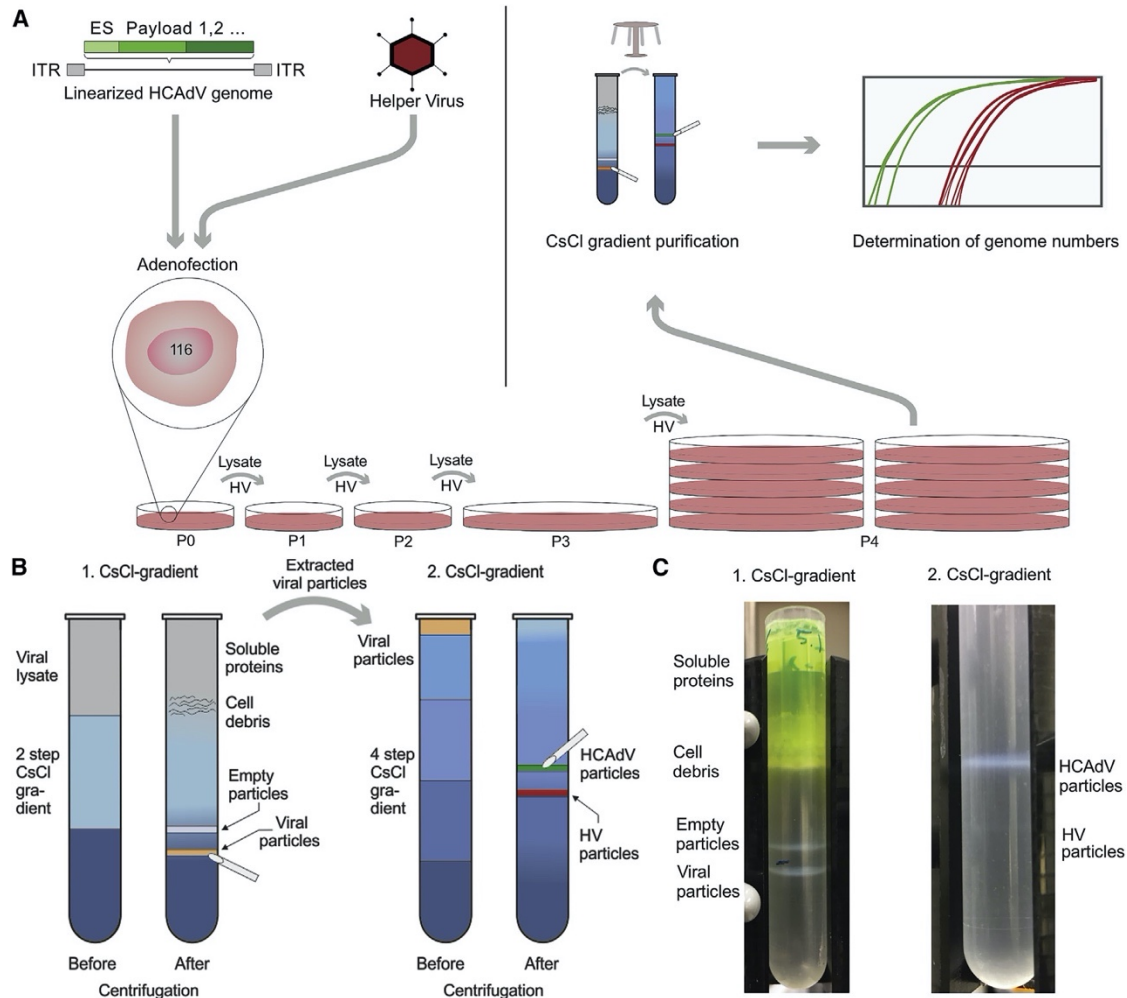


Figure 2: High-capacity adenoviral vector amplification and purification

a) HCAAdV producer cells, e.g., the cell line 116, were infected with helper virus (HV) and transfected with linearized HCAAdV genomes (adenofection) in passage 0 (P0). During HCAAdV amplification (P0-P4), HV amplification is inhibited by Cre-mediated excision of the HV packaging signal; thus, HV particles are re-administered to the cell lysate before infecting the next passage. After amplification, adenoviral particles are released from the 116 cell line and purified by two CsCl density purification steps. HCAAdV (green curve) and HV (red curve) genomes are quantified by qPCR post amplification and purification. b) Adenoviral particles (orange band) are separated from cell debris, cell lysate and empty particles on a two-step CsCl gradient (left) and subsequently applied to a four-step gradient (right) for further separation of HCAAdV particles (green band) from HV particles (red band). c) A GFP-expressing HCAAdV vector was purified. After the first centrifugation step (left), three distinct white bands are visible in the following order from top-to-bottom: cell debris, empty viral particles, and mature viral particles. Notably, the cell lysate above the CsCl gradient is colored green from the presence of soluble HCAAdV reporter (GFP). Following extraction of the band containing mature particles and application to the second CsCl gradient (right), a prominent upper band containing HCAAdV particles (30 kb) is separated from a very faint lower HV band (37.5 kb). Contribution: DB optimized the design and purification of HCAAdV and produced HCAAdV for all the following studies. DB prepared figure.

Purified HCAAdV vectors with the capsid modifications described above encoding a reporter protein (GFP) showed dose-dependent reporter expression with non-detectable HV reporter protein expression (mCherry), even under very high multiplicities of infection (MOIs; Fig. 3a-d and

Sup. Fig. 4a). Sensitive quantification of HV contamination via qPCR (Sup. Fig. 4b) revealed unprecedented low HV contaminations of 0.00001-0.00012 % or 0.1-1.2 ppm HV of HCAdV vectors generated with the iMATCH platform (Fig. 3e). Other HCAdV vector production and purification protocols typically report 0.01-0.2% HV contamination (Jager et al., 2009; Palmer and Ng, 2003), which is 2-4 orders of magnitude higher than obtained with the iMATCH platform. In addition to the high purity of the HCAdV particles, the iMATCH platform provided high yields of HCAdV vectors (Fig. 3e) sufficient for multiple *in vivo* studies (Fig. 4 and 6). On average, 2×10^{11} genomic HCAdV particles per production from 3×10^8 cells with a ratio of 24 genomic HCAdV particles per transducing unit were obtained (averaged across 11 preparations). HCAdV yields were not affected by the number of transgenes encoded on the vectors, i.e., single-payload HCAdV vectors yielded on average 1.98×10^{11} genomic HCAdV particles, similar to payload combinations vectors (e.g., RMP1-14_IL-12_IL-2) with on average 2.02×10^{11} genomic HCAdV particles. Furthermore, negative staining of purified HCAdV viral particles with electron microscopy revealed intact HCAdV particles free from AAV and other contaminants (Fig. 3f).

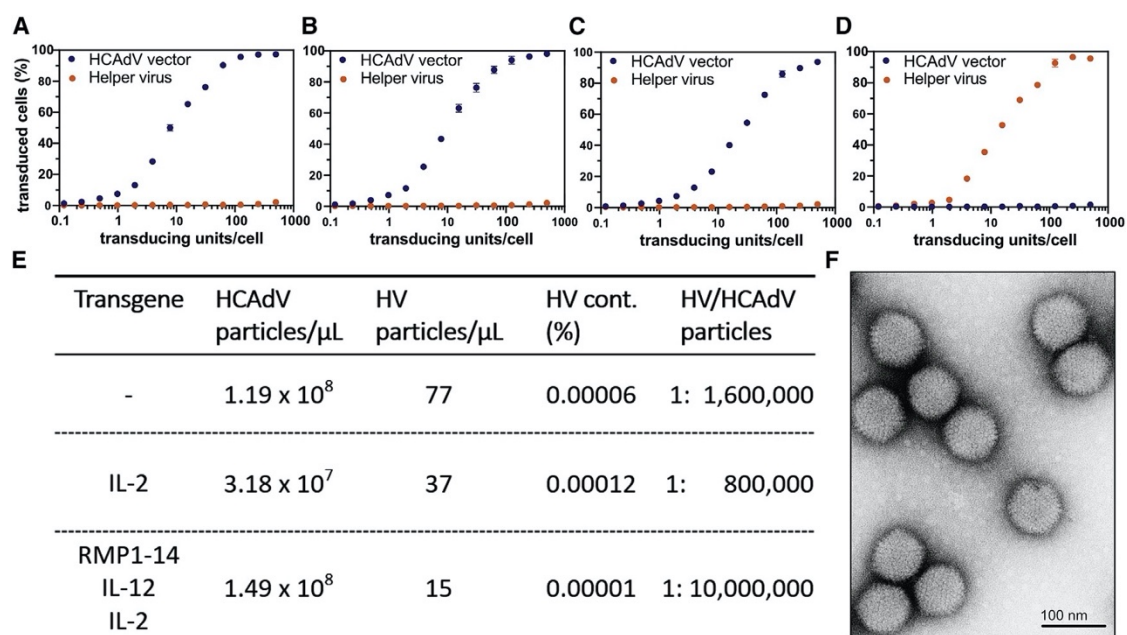


Figure 3: Production of HCAdV vectors in high purity and quantity

A549 cells were infected (a) with HCAdV vectors carrying the wild-type HAAdV-C5 capsid, (b) with a modified hexon-encoding a HVR7 mutation (Xu et al., 2013) or (c) with modified hexon and fiber proteins containing the HVR7 hexon mutation and the deletion of the RGD fiber motif. All HCAdV vectors showed titratable payload reporter (GFP) expression with no detectable helper virus reporter (mCherry) signal. As a control, (d) purified helper virus showed comparable reporter expression as HCAdV vectors. e) Quantification of HCAdV and HV genomic particles via qPCR of purified HCAdV vectors revealed unprecedented purity of produced HCAdV particles of 0.00001-0.00012 % or 0.1 - 1.2 ppm. Furthermore, HCAdV vectors were generated in high quantities of $0.3-1.5 \times 10^{11}$ genomic HCAdV particles from $2-3 \times 10^8$ cells. f) Transmission electron micrographs (TEM) analyzed with negative staining of purified HCAdV vectors showed intact HCAdV particles free from AAV and other contaminants. Contribution: DB optimized the design and purification of HCAdV and produced HCAdV for all the following studies. DB prepared figure.

2.1.3.5 Cell- and organ-specific targeting of high-capacity adenoviral vectors mediated by exogenously added shield and retargeting adaptors

In order to test whether retargeting and shielding strategies previously developed for first-generation (FG) adenoviral vectors are compatible with HCAAdV vectors generated by the iMATCH platform (Fig. 4a) we transduced EMT6 cells that express HER2 (EMT6-HER2) *in vitro* (Fig. 4b) or *in vivo* (Fig. 4c-e) with identical MOIs of HER2-retargeted and shielded FG or HCAAdV reporter vectors encoding a firefly luciferase gene. All HCAAdV and FG adenoviral vectors used in this and the following *in vitro* and *in vivo* studies contained a HVR7 modification to reduce factor X binding (Xu et al., 2013). Transgene expression was only detected from cells infected with adenoviral vectors that were incubated prior to infection with retargeting adaptors for HER2 and shield (Fig. 4b). Cells transduced with naked virus, and those transduced with virus incubated with shield and adaptors that lacked the retargeting DARPin but still contained the knob-binding DARPin (blocked vectors), showed no elevated transgene expression compared to PBS-treated cells. Notably, transgene expression mediated by the HER2-retargeted and shielded FG vector was equal in terms of transgene expression induced by the HER2-retargeted and shielded HCAAdV vector.

We further monitored gene delivery via retargeted and shielded FG and HCAAdV vectors in an immunocompetent mouse model. For this purpose, EMT6-HER2 cells were injected into the mammary gland of female BALB/c mice. Seven days later, tumor-bearing mice received an intratumoral application of virus with 3×10^8 transducing units of either HER2-retargeted and shielded FG or HCAAdV vectors (Fig. 4c). Luciferase activity was measured in live animals using *in vivo* imaging one day post injection (Fig. 4d) following intraperitoneal injection of luciferin. The luciferase signal was only detectable within tumors treated with adenovirus but not in the untreated control animals. Quantification of the *in vivo* luciferase signals revealed no significant differences between FG and HCAAdV vectors (Fig. 4e), in agreement with *in vitro* results. Following measurements in live animals, mice were sacrificed, and various tissues were harvested, lysed, and analyzed for luciferase activity. Transgene expression was indeed limited to the tumor, with no significant signal detectable in all other organs for both FG- and HCAAdV-treated mice. No significant difference in luciferase activity could be detected between FG and HCAAdV vectors in the tumor (Fig. 4f).

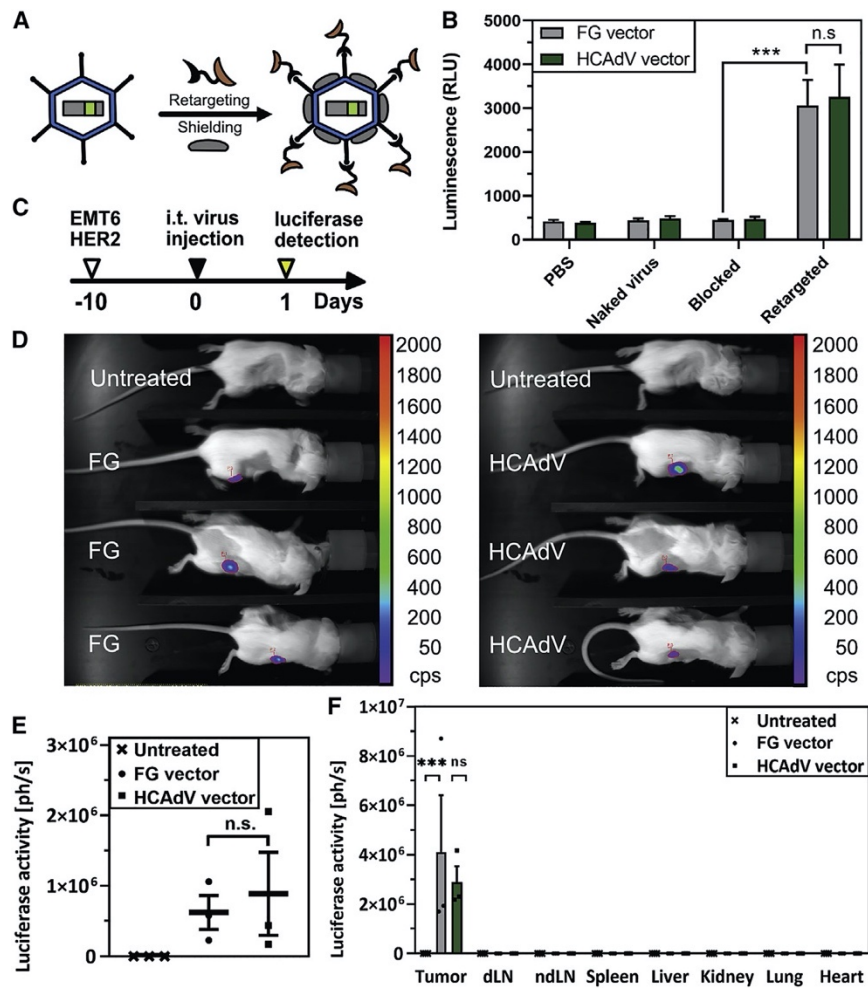


Figure 4: Retargeted and shielded HCAdV vectors showed comparable gene expression and biodistribution to FG vectors

a) First-generation (FG) and HCAdV vectors were retargeted via a trivalent knob-binding bispecific DARPIn retargeting module (black and light brown) and coated with a trimeric scFv shield (grey). b) EMT6-HER2 cells infected *in vitro* by shielded and HER2-retargeted FG or HCAdV vectors that encoded a luciferase reporter gene showed both significantly elevated levels of luciferase activity. Only background levels of luciferase activity were detected from untreated cells (PBS), cells infected with untreated HCAdV vectors (naked virus) and cells infected with HCAdV vectors which carry a blocking adapter (no HER2-retargeting DARPIn) and the shield (blocked). No significant differences between luciferase activity mediated by FG and by HCAdV vectors could be detected *in vitro*. Luciferase activity was measured from lysates of three separately transduced cell populations, which were measured in technical duplicates (n=6). c) EMT6-HER2 tumor-bearing mice were injected intratumorally with retargeted and shielded HCAdV or FG vectors and luciferase activity was measured 24 hours post infection with an *in vivo* imaging system after intraperitoneal injection of luciferin substrate. d) Vector-treated mice showed detectable luciferase activity while no luciferase signal was detected in untreated control mice. e) Quantification of the luciferase signal from d) revealed no significant differences of transgene expression mediated by retargeted and shielded vectors between the HCAdV or FG type. f) Following organ harvest and lysis, luciferase signals were measured from multiple tissues including tumor, draining lymph nodes (dLN), non-draining lymph nodes (ndLN), spleen, liver, kidney, lung, and heart as described for d). Significantly elevated levels of luciferase activity could only be detected in tumor tissues. Three mice per group were used for studies presented in d-f. Statistical analyses were done with a two-way ANOVA test, $p > 0.9$ (n.s.), $p < 0.1$ (*), $p < 0.01$ (**), and $p <$

0.001 (***) are indicated. All error bars represent SEM. Contribution: NK planned, organized, conducted and analyzed the experiment. NK and DB prepared figure.

2.1.3.6 Expression of multiple therapeutic payloads from a single high-capacity adenoviral vector

Next, we assessed payload transcription and expression from a single HCA_{AdV} vector encoding multiple therapeutic payloads and compared it to a mixture of HCA_{AdV} vectors encoding the same payloads as single payloads per vector. We generated an immunotherapeutic combination of three payloads, a murine anti-PD-1 antibody (RMP1-14) and two cytokines (IL-12 and IL-2). This combination was chosen due to the strong synergistic effects between anti-PD-1 and IL-12 and between anti-PD-1 and IL-2, as compared to single agent treatments in previous preclinical and clinical studies (Garris et al., 2018; Rafei-Shamsabadi et al., 2019). The number of total transducing viral particles was kept equal for each treatment group in the following *in vitro* and *in vivo* studies, in order to equalize the immunologic response to adenoviral particles: which was deemed a relevant factor in studies with non-human primates and human patients (Brunetti-Pierri et al., 2004).

Single payload containing HCA_{AdV} vectors (Ad_RMP1-14, Ad_IL-12 or Ad_IL-2) and a HCA_{AdV} vector encoding all three payloads (triple vector) were generated via the iMATCH platform. According to the therapeutic windows of the payload, the antibody RMP1-14 was encoded under the control of a strong CMV promoter. In contrast, the two cytokines IL-12 and IL-2, which are highly effective already at low picomolar concentrations, were encoded under the control of a weaker SV40 promoter (Fig. 5a). The payload design is described in further details in the Methods part. Due to the toxicity of IL-2 at high concentrations (Dutcher et al., 2014), IL-2 was encoded under the translational control of an encephalomyocarditis virus internal ribosomal entry site (EMCV-IRES; Mizuguchi et al., 2000) in the triple and single payload HCA_{AdV} vector.

Following infection of A549 cells, an overall correlation between transcript numbers (Fig. 5b) and protein secretion (Fig. 5c) could be observed. The triple HCA_{AdV} vector showed a small, albeit not significant, reduction of transgene transcription and expression levels for payloads encoded under the CMV promoter (RMP1-14), as compared to the single payload vector (Ad_RMP1-14) alone. The mixture of single payload vectors showed a three-fold decrease in CMV-driven RMP1-14 expression, compared to the single Ad_RMP1-14 vector, which was proportional to the reduced copy numbers of the RMP1-14 transgene in the mixture. The CMV promoter generated an average of 6.5 CMV-driven mRNAs (RMP1-14) per GAPDH mRNA, compared to 0.7 SV40-driven (IL-12) mRNA per GAPDH in the single vector condition, i.e., a roughly 9-fold difference. This indicates that the CMV promoter has an increased transcriptional activity compared to the SV40 promoter in A549 cells. A decrease of SV40-driven transgene (IL-12 and IL-2) transcription

and expression could be observed in the presence of the stronger CMV promoter in the HCAdV triple vector and in the mixture of single payload vectors. The absence of a transgene upstream of the EMCV-IRES and downstream of the SV40 promoter in the Ad_IL-2 HCAdV vector (Fig 5a) led to a decrease in IL-2 transgene transcription and expression compared to the triple HCAdV vector, which encoded IL-12 upstream of the EMCV-IRES.

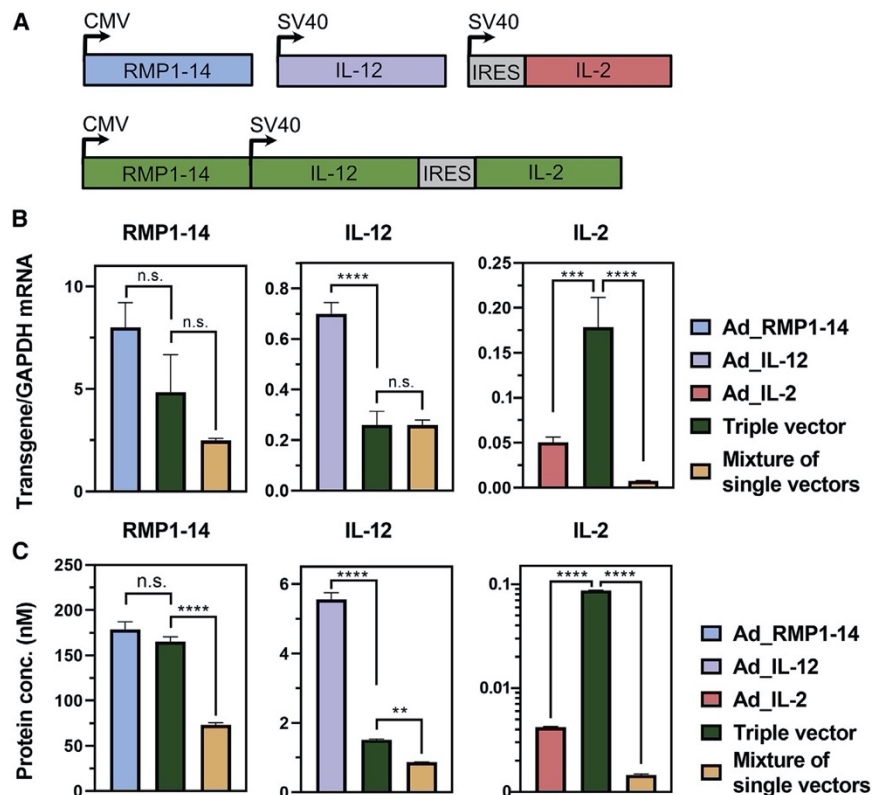


Figure 5: *In vitro* expression of a triple payload combination encoded on a triple vector or on different single payload HCAdV vectors.

a) RMP1-14 (CMV promoter), IL-12 (SV40 promoter) and IL-2 (SV40 promoter) were encoded each on a separate HCAdV vector (blue, violet, and light red) or together on a combination HCAdV triple vector (green). Transcription (b) and secretion (c) levels of RMP1-14 (left panel), IL-12 (middle panel) and IL-2 (right panel) were measured in A549 cells 72 hours post infection with 10 transducing units/cell. Cells were infected with either a single payload vector (left bar), the triple HCAdV vector (middle bar) or a mixture of single payload vectors (right bar). In all cases, the same total viral particle numbers were used. Transcription and translation levels of RMP1-14 (CMV promoter) were decreased only slightly upon co-expression of IL-12 and IL-2 from a SV40 promoter in the triple vector. In the mixture of single vectors, the gene dosage is one third, and this is reflected well in transcript and protein level. Payload transcription and expression from the weaker SV40 construct was significantly reduced by the presence of the stronger CMV promoter independent of whether both promoters were located on a combination vector (triple vector) or on different vectors (a mixture of single payload vectors). The observed reduction of SV40 derive gene expression was in both conditions over-proportional to the number of transgenes delivered (more than a threefold reduction). As an exception, IL-2 transcription and expression from the triple vector was drastically increased, compared to the single Ad_IL-2 vector due to the lack of a transgene upstream of the IRES in the single Ad_IL-2 vector. Overall, transcription and protein secretion levels of the encoded payload correlated well. *In vitro* protein secretion was determined from supernatants of three separately transduced cell populations which were measured in duplicates in an antigen capture ELISA setup. Transcription levels were determined from A549 cell lysates of three separately transduced cell populations measured in

duplicates via real time PCR. Statistical analysis was done with a two-way ANOVA test, $p > 0.9$ (n.s.), $p < 0.01$ (**), $p < 0.001$ (***) and $p < 0.0001$ (****) are indicated. All error bars represent SEM. Contribution: DB planned, organized, conducted and analyzed the experiment. DB prepared figure.

We acknowledge that absence of a gene upstream of the IRES in front of IL-2 in the single vector might impede the comparison of the combination HCAAdV vector and the mixture of single payload vectors. Therefore, we also analyzed transcription and expression of a second combination (RMP1-14 and IL-12) in the absence of IL-2 (Sup. Fig. 5a). In analogy to the triple combination, decrease of SV40 transgene (IL-12) expression in the presence of a CMV promoter was also observed in the dual combination (Sup. Fig. 5b). CMV-mediated (RMP1-14) expression was not significantly reduced in the dual combination by SV40-driven co-expression of IL-12 (Sup. Fig. 5c). Despite the small number of payloads in the tested combinations we could observe that the transgene (RMP1-14 or IL-12) expression from a combination HCAAdV vector was less reduced with increasing transgene numbers, compared to a mixture of single payload vectors (Sup. Fig. 6) provided that the total viral particle numbers are constant. In conclusion, a HCAAdV vector encoding multiple transgenes showed similar or even improved *in vitro* transgene transcription and protein secretion compared to a mixture of HCAAdV single payload vectors.

2.1.3.7 *In vivo* efficacy of high-capacity adenovirus combination immunotherapy

To determine the *in vivo* efficacy of the combination HCAAdV triple vector encoding RMP1-14, IL-12 and IL-2, we administered iMATCH vectors containing either a single payload or the combination of all three payloads intratumorally to immunocompetent C57Bl/6 mice bearing subcutaneous B16-D5-HER2 tumors (Fig. 6a). B16-D5-HER2 are highly aggressive melanoma cells that stably express HER2 and form immune-excluded tumors in C57Bl/6 mice. The triple combination led to a successful tumor rejection, while mice treated with a single payload vector only showed a delay in tumor growth (Fig. 6b). Tumor growth curves for individual mice of each treatment group are depicted in Sup. Fig. 7 and 8. The improved tumor control of the triple vector resulted in prolonged survival of these mice compared to mice treated with single payload vectors or untreated mice (Fig. 6c). IL-12 encoded on a single payload vector caused the second highest survival rate, while IL-2 as a single payload vector showed no improved survival compared to the untreated group.

Next, we compared the triple combination vector against the mixture of single payload vectors. Both groups successfully decreased tumor growth (Fig. 6d), compared to the untreated group, and showed prolonged survival (Fig. 6e). Tumor regression and prolonged survival were increased in the triple vector treatment group compared to the mixture of single payload vectors. Overall, all mice treated with payload-containing HCAAdV vectors, except for the IL-2 single payload vector, led to a significant reduction in tumor burden compared to the untreated group

(Fig. 6f). Although the treatment with the triple vector showed decreased tumor regression, it was not significantly different from tumor regression induced by IL-12 single vector treatment or treatment with a mixture of all three single payload vectors. The IL-12 single payload vector, the triple vector and the mixture of single payload vectors led to similar improved survival compared to the untreated group (Fig. 6g): There was no significant difference between triple vector treatment and treatment with a mixture of single payload vectors or IL-12 single treatment. Neither treatment lead to a significant change in the body and physical scoring of the mice (Sup. Fig. 9).

Although the single IL-2 HCA₂V vector showed no improvement in tumor control or survival, it is possible that the increased expression of IL-2 from the triple vector could positively influence the *in vivo* efficacy of the triple vector in comparison to a mixture of single payload vectors. For this reason, we performed an additional study with a dual vector encoding RMP1-14 and IL-12 and compared the dual vector with a mixture of single payload RMP1-14 and IL-12 vectors. The dual vector and the mixture of the two single payload vectors led to significantly decreased tumor growth (Sup. Fig. 5d) and improved survival (Sup. Fig. 5e) compared to the untreated group with no significant differences between the dual vector and the mixture of the single payload vectors. In conclusion, the mixtures of single payload vectors and the respective combination HCA₂V vector showed virtually identical therapeutic efficacy in tumor regression and survival *in vivo*.

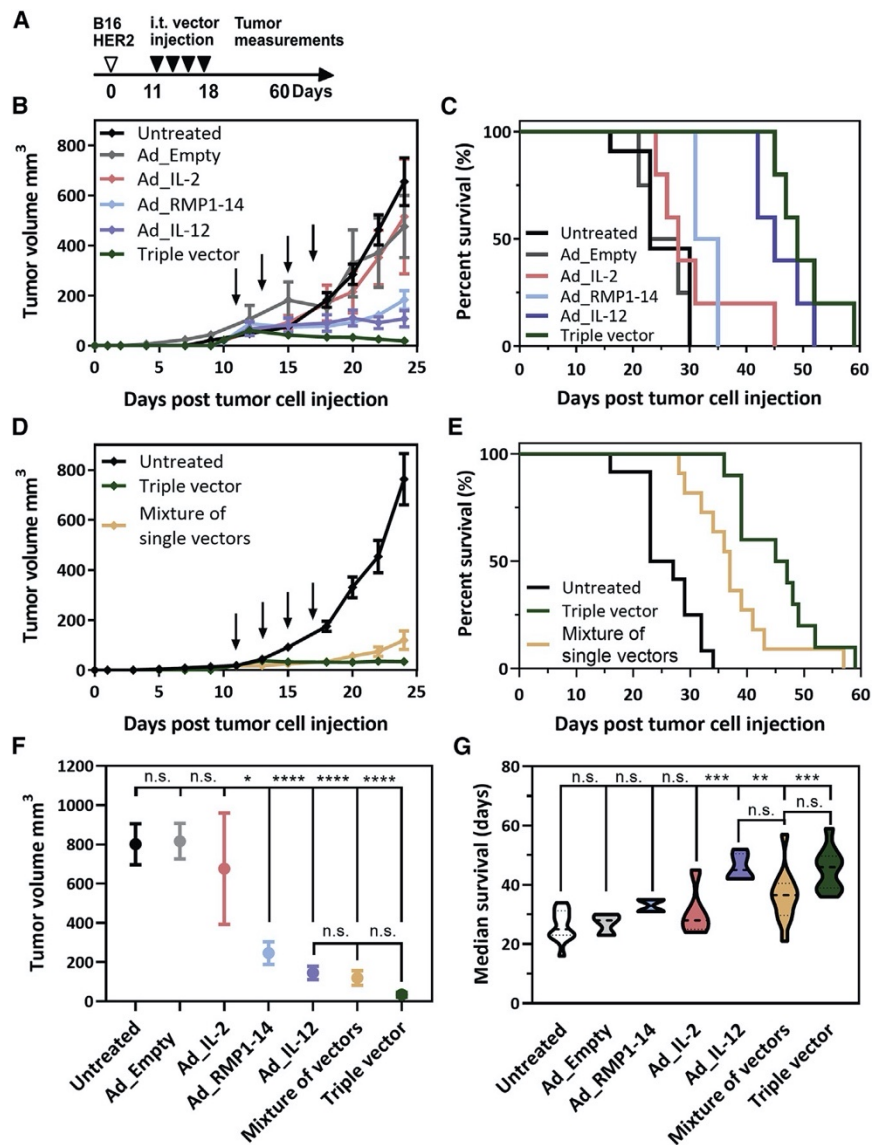


Figure 6: *In vivo* efficacy of a triple payload immunotherapy HCAAdV vector

a) Tumors were injected four times intratumorally with retargeted and shielded HCAAdV vectors ten days post injection of B16-HER2 cells at two-day intervals. All treatments were given with the same total viral particle number (3×10^8 transducing units per injection). Tumor volumes were measured for 60 days post cell injection. Mice treated with a triple vector showed improved tumor regression (b) and survival (c) compared to single payload vector treatment and compared to a mixture of single payload HCAAdV's (d-e). All payload containing vectors except of the Ad_IL2 single vector showed a significantly decrease of tumor volume with no significant differences between the triple vector and the mixture of single payload vectors 24 days post tumor cell injection (f). The average survival was significantly improved for the Ad_IL-12 vector, the triple vector and the mixture, compared to the untreated group, with no significant differences between the triple vector and the mixture (g). Treatment groups in b and c) consisted of 5 mice, except of Ad_Empty and Ad_RMP1-14 (n=4), and groups of d) and e) of 11 mice. Data of b) and d) were pooled for f) and data of c) and e) pooled for g). Statistical analysis of f) and g) was done with a two-way ANOVA test including all treatment groups. Indicated significances in f) and g) refer to the untreated control (upper lane) except for the separate comparison of the three samples: Ad_IL-12, Mixture of vectors and Triple vector (lower lane) with $p > 0.9$ (n.s.), $p < 0.1$ (*), $p < 0.001$ (***) and $p < 0.0001$ (****) indicated. Error bars represent in b), d) and f) are SEM. Contribution: NK planned, organized, conducted and analyzed the experiment. DB gave input for experimental design. NK and DB prepared figure.

2.1.4 Discussion

So far, more than a dozen different gene-therapy-based therapeutics have been approved in different countries for treating cancer, blindness, immune disorders or neurological failure, and an increasing number of preclinical and clinical gene vector trials is currently ongoing. More than 400 adenoviral gene vectors have been tested in these trials (Wold and Toth, 2014). Nonetheless, a system for the rapid and efficient generation of high-capacity adenoviral gene vectors for cell targeted gene delivery of therapeutic combinations is still missing (Goswami et al., 2019).

Here we designed the iMATCH platform, which enables the rapid assembly of multiple therapeutic genes, encoded under four different constitutive promoters (CMV, SV40, EF1- α or PGK) on a size-optimized pUniversal cloning plasmid. The cell-type-specific transcription activity of these promoters allows for a defined transgene expression tailored to the targeted cell type and the required transgene concentration (Qin et al., 2010). In this highly modular system, each of these promoters could also be exchanged to tissue-specific or otherwise regulatable promoters. Promising combinations of immunotherapeutics, vaccination agents or gene modifier can be generated with the presented modular assembly system rapidly and tested *in vitro* as plasmids, before starting time- and cost-intensive vector production. Moreover, because of the non-covalent nature of the targeting adapter, this extends to the search for the optimal surface receptor and its epitope which can also be achieved without producing a new vector. Once the most suitable combination is found, the previously laborious and time-consuming integration of therapeutic combinations into high-capacity viral vectors (HCA Δ V) can be avoided by the iMATCH system, with which cloning efficiencies of up to 85% were achieved (Lee et al., 2019).

The genomic size of adenoviral vectors can influence packaging efficiency and thus the yield of functional virions, but also their biophysical properties, for instance thermostability (Smith et al., 2009). To exclude that suboptimal vector size influences the efficacy of combinational HCA Δ V vectors, the iMATCH system was designed to generate HCA Δ V vectors with defined genomic sizes by exploring unique sets of restriction enzymes and overlaps for Gibson Assembly. Utilizing this versatile, efficient cloning system, HCA Δ V vectors with multiple therapeutic genes can be cloned, amplified, and purified from existing transgene constructs with the iMATCH system within 3 weeks. This reduces the production time for therapeutic high-capacity adenovirus vectors by half, compared to previously reported protocols (43 days) enabling a faster screening of therapeutic combinations, and allowing the production of several HCA Δ Vs in parallel (Jager et al., 2009).

HV contamination of purified HCA Δ V vectors should be minimized due to the high immunogenicity of HV particles and the potential interference with the target cells (Muruve et al., 2004). Although multiple systems have been developed to reduce HV contamination of HCA Δ V

preparations in the past (Jager et al., 2009; Palmer and Ng, 2003; Parks et al., 1996; Sandig et al., 2000), HV contamination is still a major issue in many applications, limiting the broad use of HCAAdV vectors. We achieved unprecedented low amounts of HV contamination of 0.00001-0.00012 % or 0.1-1.2 ppm HCAAdV particles, using optimized HVs and purification protocols which is an improvement of 100-2000-fold to previously published HCAAdV purification protocols, which have reported 0.2-0.01 % HV contamination (Jager et al., 2009; Palmer and Ng, 2003). We hypothesize that the residual absolute HV contamination level in our HCAAdV preparations is constant under the established conditions (<100 HV genomes per mL) and that the relative contamination therefore varies, depending on the HCAAdV yield obtained. Due to the reduced production time and the repeatedly low HV contamination of the iMATCH platform, this approach is adaptable and straightforward, and might thus be widely used to achieve HCAAdV vector production of the highest quality.

Furthermore, our results indicate that transgene combinations of interest can be systematically screened as combinations of FG or HCAAdV vectors encoding single payloads. Promising combinations can then be encoded on a single HCAAdV vector with a packaging capacity of up to 36 kb. We suggest this procedure as the most efficient strategy, based on the following findings: (1) retargeted and shielded HCAAdV and FG vectors showed similar protein expression *in vitro* and *in vivo* as well as similar biodistribution, (2) expression and transcription from a combination vector was equal or higher than from a mixture of single-payload vectors when comparing the same total particle numbers, (3) transgene expression from a combination vector decreased less drastically with increasing numbers of transgenes, compared to a mixture of single-payload vectors and (4) combination HCAAdV vectors gave rise to comparable *in vivo* tumor regression and survival than the mixture of the respective single-payload vectors, notably in an aggressive syngeneic immune-excluded tumor model (B16-HER2 in C57Bl/6 mice).

We noticed that the concentration of the most effective single payload (IL-12 encoded under a SV40 promoter) was reduced by the presence of a transcriptionally more active promoter (CMV), independent of whether the transgenes were encoded on a combination vector or administered as a mixture. The downregulation of one promoter by a second cis-encoded promoter was also previously observed for retroviral vectors (Emerman and Temin, 1984). As a consequence, we recommend adapting the choice of promoter for each of the payloads after an initial *in vitro* or *in vivo* assessment with the single payload vectors. Utilizing this procedure, it may be possible to further increase the potency of the tested, synergistic RMP1-14, IL12 and IL-2 combination. Nevertheless, we emphasize that the presented studies were designed to investigate the suitability of combination HCAAdV vectors for the delivery of complex immunotherapy

combinations, rather than establish a pre-clinical argument for the particular anti-PD1, IL-12, IL-2 combination and their promoters and expression levels.

The clinical approval of combination treatments such as in immunotherapies, in a variety of different indications, for instance in metastatic melanoma, advanced renal cell carcinoma and metastatic colorectal cancer (Rotte, 2019), emphasizes that the preclinical testing of combination HCA₂AdV vectors in multiple different cancer or disease models would be beneficial. However, the systemic administration of some of these combinations as systemically administered proteins has led to adverse side effects (Chan and Bass, 2020), highlighting the need for cell- or organ-specific production of these agents. This has been a key motivation for developing the iMATCH platform. Cell-specific transduction of adenoviral vectors can be achieved via genetic modifications (Barry et al., 2020), which requires the re-construction and re-production of the same combination HCA₂AdV vector for each disease model and can lead to virion instability and reduced production yields (Poulin et al., 2020). Furthermore, many strategies would not be able to generically target any surface receptor of choice.

For this reason, HCA₂AdV vectors generated by the iMATCH system were designed to be compatible with any exogenously added retargeting adapter for HAdV-C5 vectors. The large library of existing DARPins, the rapid selection of new DARPin adaptors against surface markers (Dreier and Plückthun, 2012) and the efficient production of DARPin-based retargeting adaptors in bacteria (Dreier et al., 2013) are advantages unique to the here presented retargeted strategy. In addition, due to the high abundance of pre-existing antibodies against HAdV-C5 (Fausther-Bovendo and Kobinger, 2014) in the population of many countries, covering of iMATCH-generated HCA₂AdV-C5 vectors with the previously described shield that has been shown to reduce neutralizing antibody binding to HAdV-C5 FG vectors would be beneficial for therapeutic uses (Schmid et al., 2018). Alternatively, high-capacity adenovirus vectors of other serotypes with a lower pre-existing immunity can now be developed for clinical purposes (Gao et al., 2019), based on the strategy described here.

In conclusion, we believe that the rapid production of HCA₂AdV combination vectors in high quantity and purity, the compatibility with established cell specific targeting strategies and the broad variety of payload molecules that can be encoded on HCA₂AdV vector make the iMATCH platform an attractive vector-developing tool for multiple research fields.

2.1.5 Materials and methods

2.1.5.1 Plasmid, cells and mice strains

The plasmid pAdEasy-1 was obtained from Agilent (Luo et al., 2007) and modified as described below. The pC4HSU plasmid was purchased from Microbix® and originally developed by (Sandig et al., 2000). The murine cell line EMT6-HER2 was generated as previously described (D'Amico et al., 2019). Briefly, murine EMT6 cells were modified for constitutive expression HER2. The B16-D5-HER2 murine cell line was kindly provided by Louis Weiner (Wang et al., 2012). A poorly immunogenic subclone of murine B16 cells, D5, was modified to constitutively produce HER2. The human cell line 116 was kindly provided by Philip Ng and cultured as recommended (Palmer and Ng, 2003). The remaining cell lines were purchased from the vendor ATCC® and cultivated according to the provider's recommendations. Cells were passaged no more than 15 times from the original stocks. C57BL/6 and BALB/c mice were bred in-house at University Hospital Basel, Switzerland. Animals were housed under specific pathogen-free conditions. All animal experiments were performed in accordance with Swiss federal regulations.

2.1.5.2 Plasmid constructions

The helper viral vector pmCherry-HV plasmid was generated by replacing the natural packaging signal of the pAdEasy-1 vector with a loxP-flanked modified encapsulation signal derived from (Sandig et al., 2000) and a mCherry reporter under the control a PGK promoter. The plasmid pmCherry-HVR7 was derived from pmCherry-HV by inserting four mutations into the hypervariable loop 7 of the hexon (I421G, T423N, E424S) as previously described (Schmid et al., 2018). Further deletion of the RGD region of the fiber protein generated the plasmid vector pmCherry-HVR7-ΔRGD. All cloning steps involving helper viral plasmids were carried out by homologous recombination as reported in previous studies (Schmid et al., 2018). The pUniversal plasmids were generated *de novo* using Gibson Assembly (Gibson et al., 2009) by combining the pUniversal backbone fragment that encodes the origin of replication and the Ampicillin resistance derived from the pcDNA3.1(+) plasmid (Invitrogen®) with gene fragments containing expression cassettes synthesized by GeneArt® (Thermo Fisher Scientific®). Each expression cassette consists of a unique pair of promoters and terminators (*e.g.*, SV40 promoter + SV40 terminator, CMV promoter + bovine growth hormone terminator, EF1- α promoter + human growth hormone terminator or PGK promoter + human β globin terminator), each with a set of unique restriction sites for payload insertion (*e.g.*, *EcoRI* and *BamHI* or *EcoRI* and *XbaI*).

2.1.5.3 Payload design

The rat IgG2ak anti-PD1 antibody, clone RMP1-14, whose sequence was identified from hybridoma sequencing (BioXCell), was converted to a chimeric mouse IgG2ak antibody with rat

variable domains. The mouse IgG2a*01 heavy chain (HC; IMGT: IGHG2A*01; AccNum: V00825) and the kappa light chain (LC; IMGT: IGKC*01; AccNum: V00807) were used as scaffolds (Giudicelli, 2006). The following mutations were included in the heavy chain: (1) the CH2 glycosylation site was mutated to alanine (N297A) to impair FcγR binding, (2) effector functions were further ablated by introducing L234A, L235A and P329G mutations to the CH2 domain (Arduin et al., 2015; Lo et al., 2017), and (3) a cloning site was added that introduces a K115S mutation into the CH1 domain. Optimized H5 and L1 leader sequences were used for heavy and light chain secretion (Haryadi et al., 2015), respectively. Chains were expressed bicistronically using an F2A (Fang et al., 2005; Simmons et al., 2008) with optimized furin site (RKRR; Fang et al., 2007) with the orientation HC-F2A-LC as described previously (Brücher et al., 2020). The murine IL-12 gene was generated from translated Genbank cDNA sequences for IL-12B/p40 (NCBI Reference: BC103608.1) and IL-12B/p35 (NCBI Reference: BC146595.1) connected by F2A peptide as above, and the murine IL-2 gene was created from the translated Genbank cDNA sequence (NCBI Reference: NM_008366.3). The cytokine genes included their native signal sequences. All payload constructs were codon-optimized for mouse expression and synthesized by GeneArt (Thermo Fisher Scientific).

2.1.5.4 High-capacity adenoviral vector generation

Helper viral vectors were generated in the human cell line HEK293 as previously described; they originate from the HV plasmids pmCherry, pmCherry-HVR7 and pmCherry-HVR7-ΔRGD (Luo et al., 2007). HCAAdV vectors were amplified as described in detail by Ehrke-Schulz et al. (2016). Following three wash steps with PBS, the collected cells from 15 x 15 cm dishes were lysed by three freeze-thaw cycles using a 37°C water bath and liquid nitrogen. The cell lysate was cleared by 8 min. centrifugation at 500 *g*, 4°C. The cell supernatant was applied on the first CsCl gradient consisting of two steps, 1.25 g/cm³ and 1.25 g/cm³ CsCl. The remaining cell pellet was washed with 2 ml PBS and the supernatant additionally applied on the first CsCl gradient. The lower viral band of the first CsCl gradient was extracted after 2 hours of centrifugation at 12°C, 226,000 *g* with a syringe and transferred to a second, four-step CsCl gradient, consisting of four steps ranging from 1.29 to 1,35 g/cm³. The lower-density HCAAdV particles formed an upper band and were extracted from the second gradient after 18-24 h of centrifugation at 12°C, 226,000 *g*. Following dialysis in dialysis buffer of 20 mM HEPES pH 8.1, 150 mM NaCl and 1 mM MgCl₂, glycerol was supplied to the viral solution reaching a final concentration of 10% prior to viral storage at -80°C.

2.1.5.5 Genomic and transducing particle determination

For transducing particle determination, 0.5×10^5 A549 cells per well were seeded in a 24-well plate 24 hours prior to infection. Cells were transduced with 3 μ L of purified HCA Δ V vectors and incubated for 2 hours at 37°C. The infection medium was aspirated, and the cells were washed with 0.5 ml PBS. Following trypsin digest, detached cells were washed once with 1 ml PBS, 1000 g, 5 min, 4°C. For viral genome quantification during HCA Δ V amplification, viral genomes were extracted from collected cells using a DNA isolation kit (Genekam® SB0071), following the manufacturer's protocol. Viral genomes of purified HCA Δ V samples were quantified directly from the viral solution following a 5 min inactivation step at 80°C. HCA Δ V genomes were quantified by quantitative polymerase chain reaction (qPCR) with specific primers (5'-TCTGCTGGTTCACAACTGG-3', 5'-TCCTCCCTTCTGTCCAAATG-3') and a specific probe (5'-CGCCTTCTCCAGCATCCCGA-3') in a multiplex reaction with helper virus specific primers (5'-GAATAACAAGTTTAGAAACCCACGGTGG-3', 5'-GTTTGACCTTCGACACCTATTTGAATACCC-3') and probe (5'-TGACATCCGCGGCGTGCTGGACAGG-3'). All reactions were performed using PrimeTime Gene Expression Master Mix (IDT, 105571) and HCA Δ V and HV signals were normalized to the passive dye rhodamine-X (ROX). All qPCR primer and probes were generated with the double quench technology by IDT. The qPCR reaction was performed and analyzed as described previously (Ehrke-Schulz et al., 2016).

2.1.5.6 Reporter quantification in HEK293 cells

HEK293 cells were seeded with 10,000 cells per well in a 96-well plate, 24 hours prior to infection. Cells were infected with a defined number of viral particles and harvested 72 hours post infection. Following three wash steps with 1xPBS, fluorescence protein expression was quantified at a BD LSRFortessa™ cytometer. The Alexa 488 channel was used for detecting GFP expression and the PE-Texas Red channel for detecting tdTomato expression after gating on single cells.

2.1.5.7 Electron microscopy analyzed with negative staining of high-capacity adenoviral particles

Purified HCA Δ V vector (encoding no transgene) was diluted to a concentration of 1 μ g/ μ L. Next, 10 μ L droplets HCA Δ V vector samples were spotted on copper grids (300 mesh, glow-discharged) for 30 seconds, then overlaid with 10 μ L droplets of 2% uranyl acetate for 1 min. The excess uranyl acetate was removed with filter paper. A CM100 transmission electron microscope (Thermo Fisher Scientific) with an acceleration voltage of 80 kV and an Orius 1000 digital camera (Gatan) were used to examine the grids.

2.1.5.8 *In vitro* retargeting of adenoviral vectors

EMT6-HER2 cells were seeded with 1×10^5 cells per well of a 24 well plate, 24 hours prior to infection. First-generation adenovirus or HCAAdV vectors encoding firefly luciferase under the control of a CMV promoter were incubated either with a retargeting G3 adaptor (Dreier et al., 2013) containing human HER2 specificity and a shield (termed "retargeted"), or a blocking adaptor that only contained the knob-binding DARPin but no retargeting DARPin and a shield ("blocked"), or without any retargeting adaptor or shield ("naked virus") for 1 hour at 4°C. The ratio of viral knobs to retargeting adaptor and shield to hexon was 1:5 as previously described (Schmid et al., 2018) with a multiplicity of infection (MOI) of 10 transducing units per cell (tp/cell). Viral particle containing supernatants were removed 3 hours post infection and replaced by fresh culture medium. Luciferase activity was determined by a Luciferase assay (E1500, Promega) according to the manufacturer's instruction 72 hours post infection.

2.1.5.9 *In vivo* biodistribution study (EMT6-HER2 model)

1×10^6 EMT6-HER2 cells, suspended in phenol red-free DMEM (without supplements), were injected into the mammary gland of 8-12 weeks old BALB/c wt mice. Once the tumors reached an average volume of 40-60 mm³, luciferase-encoding retargeted and shielded HCAAdV or FG viruses (3×10^8 transducing units per mouse) were injected intratumorally. The luciferase signal was determined in live animals one day after virus injection and 10 minutes after intraperitoneal injection of 150 mg/kg D-luciferin (PerkinElmer) using the *in vivo* imaging system NightOWL II LB 983 (Berthold). Following live imaging, luciferase activity was determined in isolated tumors and organs (draining and non-draining lymph node, spleen, liver, kidney, lung, and heart). The overlay of the real image and the luminescence representation allowed the localization and measurement of luminescence emitted from xenografts. The signal intensities from manually derived regions of interest (ROI) were obtained and data were expressed as photon flux (photon/s). All measurements were performed under the same conditions, including camera settings, exposure time (60 s), distance from lenses to the animals and ROI size.

2.1.5.10 *In vitro* quantification of payload expression

For quantification of payload expression, A549 cells were infected 24 hours post seeding (1×10^5 cells per well of a 24-well plate) at a MOI of 10 tp/cell for single- and triple-payload containing viruses. A549 cells infected with a mixture of viruses were infected with the same total MOI of 10 tp/cell, *i.e.*, a MOI of 3.33 tp/cell per single-payload vector. Infected cells and cell supernatant were harvested 72 hours post infection. Infected cells were stored at -80°C before mRNA levels were quantified (see below). Cytokine secretion was determined from supernatants using a mouse IL-12- p70 sandwich ELISA assay (Invitrogen; 88-7121) for IL-12 and a mouse IL-2

sandwich ELISA kit (Invitrogen; 88-7024) for IL-2, following the manufacturer's instruction. RMP1-14 expression was quantified via an antigen capture ELISA. A protein-binding 96-well plate (Thermo Fisher scientific; 44-2404-21) was coated with a 20 nM murine PD-1 (amsbio; AMS.PD1-M82F4-25UG) solution at 4°C overnight (100 uL/well). Following blocking with 1x casein (Merck; B6429), the cell supernatant or a standard of recombinantly produced and purified RMP1-14 antibody were applied. Following three wash steps with PBS + 0.1 % Tween-20, an alkaline phosphatase-coupled anti-mouse κ -light chain detection antibody (Southern Biotech; 1050-04) was added. Post wash, para-nitrophenylphosphate (p-NPP) was used as a substrate and absorbance at 406 nm was measured with an Infinite M1000 microplate reader (Tecan). Antibody concentrations were determined from a standard curve of recombinantly produced RMP1-14 protein using a sigmoidal four parameter fit.

2.1.5.11 mRNA quantification by reverse transcription polymerase chain reaction

To quantify mRNA levels of the expressed payloads by quantitative reverse transcription polymerase chain reaction (RT-PCR), RNA was extracted from cells used for quantification of payload expression, according to the manufacturer's instructions (Zymo Research; R1054). 500 ng of extracted RNA was reverse-transcribed into cDNA using a QuantiTect Reverse Transcription kit (Qiagen; 205311) with the supplied mix of oligo-dT and random primers. Following RT-PCR cDNA samples were analyzed by qPCR using specific primers for RMP1-14 (5'-CGCTTCTGTCGTGTGCTTCC-3', 5'-TTGTGGGTAGCCTCGCATGT-3'), IL-12 (5'-CCTGGCGAGACAGTGAACCT-3', 5'-CCGCCCTTGTGACAGGTGTA-3'), IL-2 (5'-GCCACCGAGCTGAAGGATCT-3', 5'-ATGCTCTGGCAGAAGGCGAT-3') and GAPDH (5'-AGCCACATCGCTCAGACAC-3', 5'-GCCCAATACGACCAAATCC-3') in single reactions with a SYBR Green dye for quantification (Applied Biosystems; ANF00117457).

2.1.5.12 *In vivo* efficacy study (B16-HER2 model)

C57BL/6N wt mice were injected subcutaneously into the right flank with 5×10^5 syngeneic B16-D5-HER2 cells suspended in phenol red-free DMEM (without additives). Mice bearing palpable B16-HER2 tumors (average volume of 20-30 mm³) received intra-tumoral injection of 3×10^8 transducing units of HER2-targeted and shielded HCAVs, coding for the indicated payloads, on days 11, 13, 15 and 18 post tumor challenge. The tumor volume was calculated according to the formula: $V = \frac{1}{2} \{D \text{ (mm)} \times [d \text{ (mm)}]^2\}$, with D and d being the longest and shortest tumor diameter in mm, respectively. Bodyweight and score including appearance, behavior, and respiration was monitored during the whole experiment to detect signs of toxicity.

2.1.6 Acknowledgments

We acknowledge Prof. Dr. Anja Ehrhardt (University of Witten/Herdecke) and Dr. Maren Schiwon (University of Witten/Herdecke) for providing fruitful help and discussions in establishing the HCA_ΔV system in our group. Furthermore, we want to thank Dr. Philip Ng (Baylor college of Medicine) for providing the cell line 116, Dr. Louis Weiner for providing the cell lines B16-HER2, Dr. Annemarie Honegger (University of Zurich) for assisting in antibody design, Dr. Abhishek Kashyap (Boehringer Ingelheim) and Karen Patricia Hartmann (University of Zurich) for valuable input, Lea Flühler (University of Zurich) for assistance in FG-HV genomic assembly and Polina Zaytseva for providing shield protein. This research is supported by the SNF Sinergia grant 170929 (to AP, AZ and UG), National Cancer Institute of the National Institutes of Health under Award number F32CA189372 (to SNS), and the University of Zurich Forschungskredit 2017 ID 3761 (to DB).

2.1.7 Authors contributions

D.B., A.P., M.S. and S.N.S. designed the project. S.N.S. designed antibody and cytokine constructs; D.B., C.K., J.S. and N.S. designed, cloned and generated all pUniversal plasmid and HCA_ΔV genomes; D.B., J.S. and N.S. generated and characterized all HCA_ΔV vectors; D.B., M.S., P.C.F. and J.K. generated all FG vectors; P.F. and S.N.S. generated shield protein; S.N.S. generated retargeted adaptors; D.B., J.K. and F.W. performed qPCR and RT-PCR analysis; N.K. performed all *in vivo* experiments; D.B., A.P. and A.Z. coordinated the project; D.B., N.K., S.N.S. and A.P. wrote the paper.

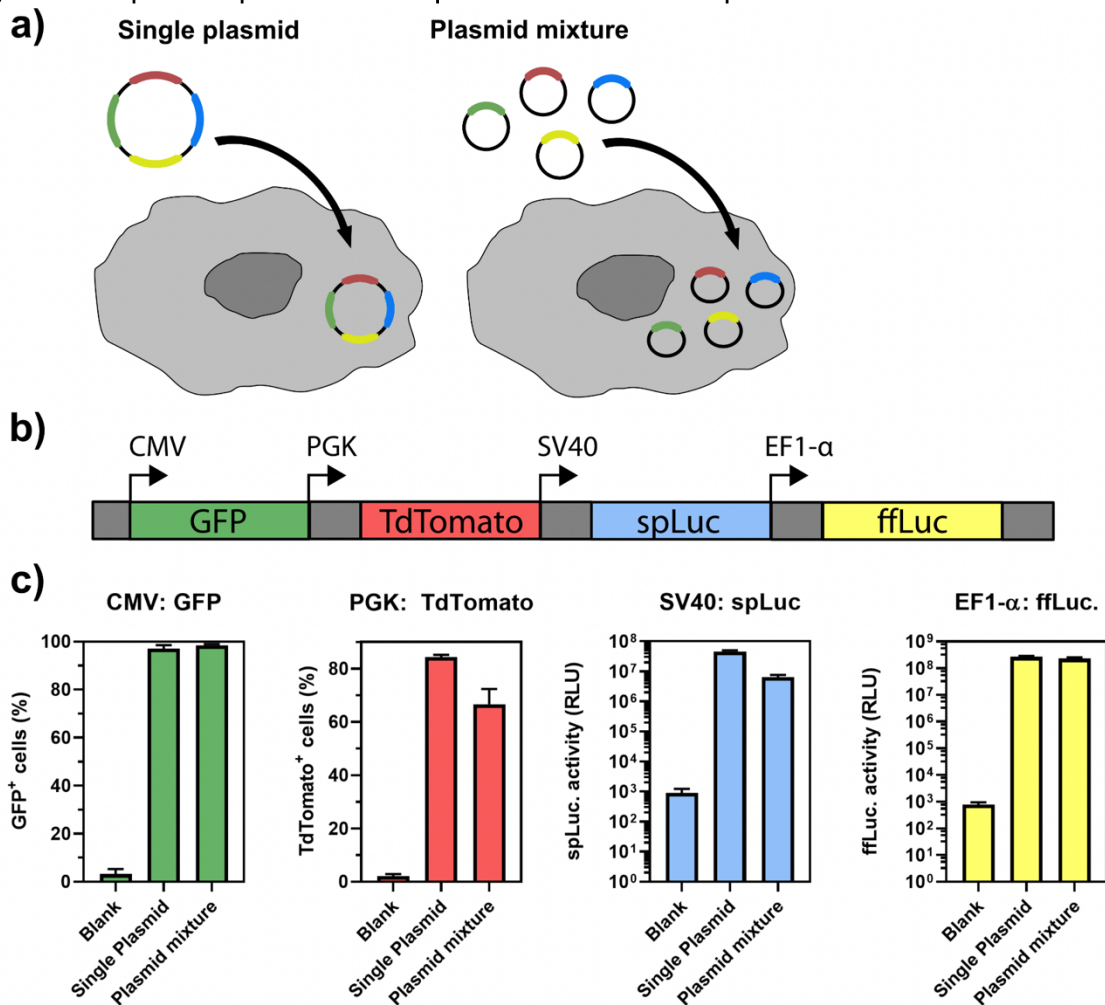
2.1.8 Conflict of interest

The authors have no known competing financial interests or personal relationships that could have appeared to influence the work reported here.

2.1.9 Supplemental information

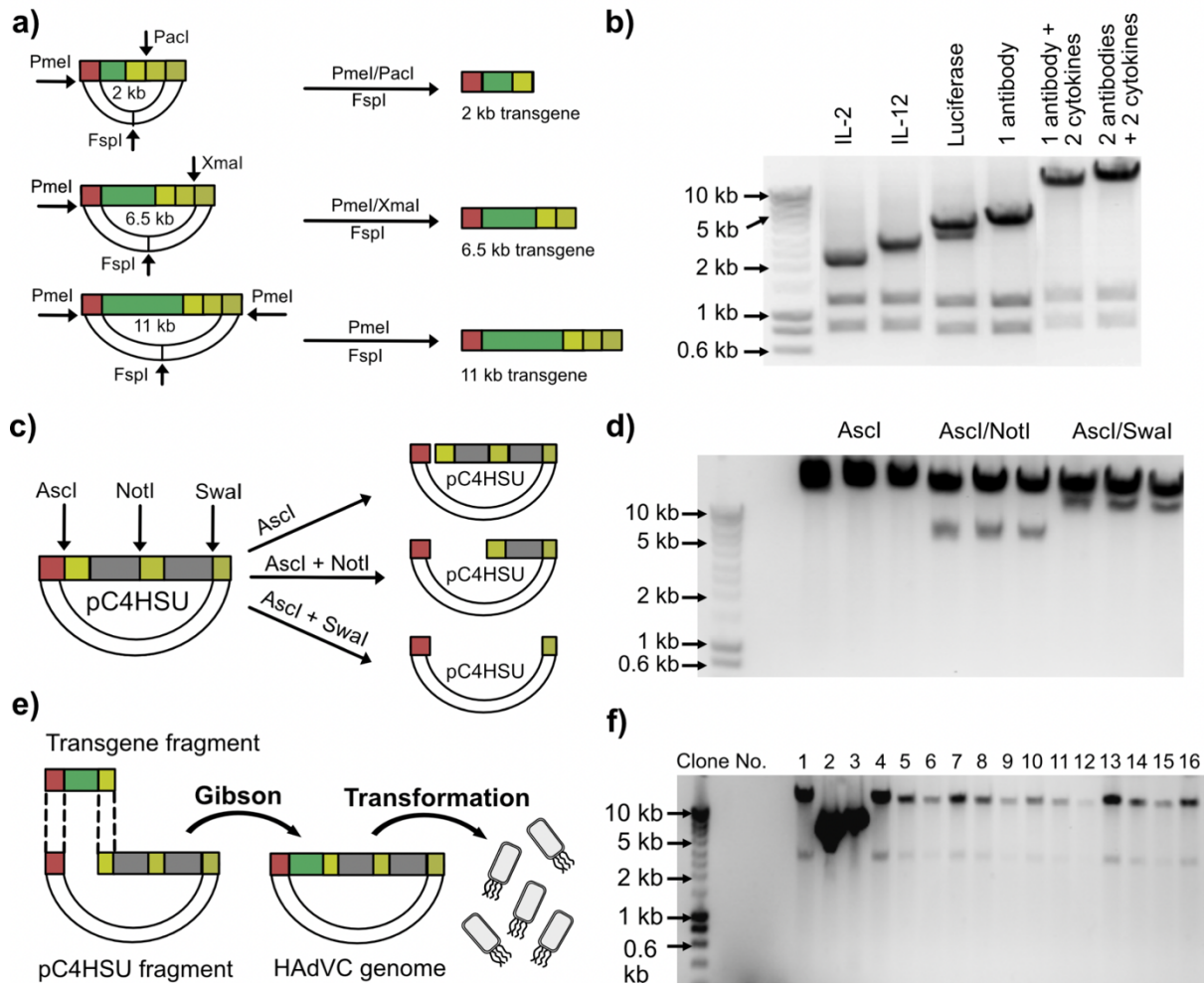
2.1.9.1 Supplementary figures

Figure S1. Reporter expression from a pUniversal combination plasmid:



(a) Reporter proteins (red, blue, yellow or green) were encoded either on a single quadruple- expression plasmid (left) or on four separate plasmids each containing only a single reporter gene. HEK293 cells (grey) were transfected with a single plasmid encoding all four reporters (left) or with the mixture of single reporter plasmids, each at the same concentration as the single plasmid (right). (b) Schematic depiction of a single plasmid encoding GFP (green), TdTomato (red), sea pansy luciferase (spLuc, blue) and firefly luciferase (ffLuc, yellow) under the control of the CMV, PGK, SV40 and EF1- α promoter, respectively. (c) Reporter expression from each promoter was determined by transfection of HEK293 cells followed by subsequent analysis with flow cytometry for GFP (CMV promoter, green) and TdTomato (PGK promoter, red) or via luciferase activity for sea pansy luciferase (SV40 promoter, blue) or firefly luciferase (EF1- α promoter, yellow). Reporter expression from a single plasmid encoding all four- reporters showed similar or increased reporter expression, compared to the mixture of single reporter plasmids. Fluorescent protein expression and luciferase activity were quantified from three separately transfected cell populations and measured in duplicates. All error bars represent SEM. Contribution: DB planned, organized, conducted and analyzed the experiment. DB prepared figure.

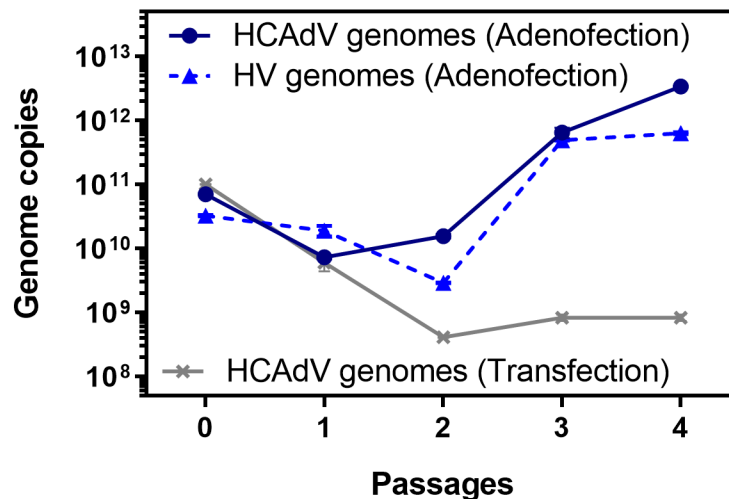
Figure S2. High-capacity adenoviral genome assembly:



(a) pUniversal plasmids can be digested via PmeI/PacI, PmeI/XmaI or PmeI to release payload- containing fragments with defined overlaps, consisting of a fixed N-terminal overlap (red) and one of several C-terminal overlaps (shades of yellow). The optimal choice of the latter overlaps depends on the genomic size of the transgene (green). An FspI digest inactivates the ampicillin resistance located on the pUniversal plasmid backbone, and thus reduces false positive clones due to residual starting plasmid during ampicillin selection, following HCAv genome assembly, which carries an ampicillin resistance without FspI site. (b) Agarose gel image of DNA fragments encoding single payloads or combinations of payloads (upper band) released from the pUniversal plasmid by digestion with enzyme pairs depicted in (a). Single transgenes or transgene combinations are indicated above each lane. The two lower bands (1.2 and 0.8 kb) represent the FspI-digested pUniversal backbone. (c) Restriction enzyme digestion of the (HCAv) backbone plasmid pC4HSU with either Ascl, Ascl/NotI or Ascl/SwaI results in a linearized HCAv backbone genome with terminal overlaps (red and shades of yellow) compatible with payload fragments generated from pUniversal plasmids. Depending on the genomic size of the payload fragment, different restriction enzymes can be used to remove either 0, 4.5 or 9 kb of stuffer DNA (grey) from the HCAv backbone. (d) Agarose gel image of digested pC4HSU plasmids as depicted in (c) in triplicate. Restriction enzymes used are depicted above the lanes. The upper band represents the pC4HSU backbone while the lower bands represent cut-out stuffer DNA of either 4.5 or 9 kb. (e) Digested and purified pUniversal and pC4HSU fragments with compatible overlaps can be combined via Gibson Assembly and used afterwards to transform *E. coli* cells. (f) An example test digest with PmeI of 16 different colonies obtained after Gibson Assembly of a HCAv vector encoding IL-2 under the control of a SV40 promoter revealed 14 correctly assembled HCAv genomes, indicated by the genomic size of detected bands. The upper band represents the HCAv with

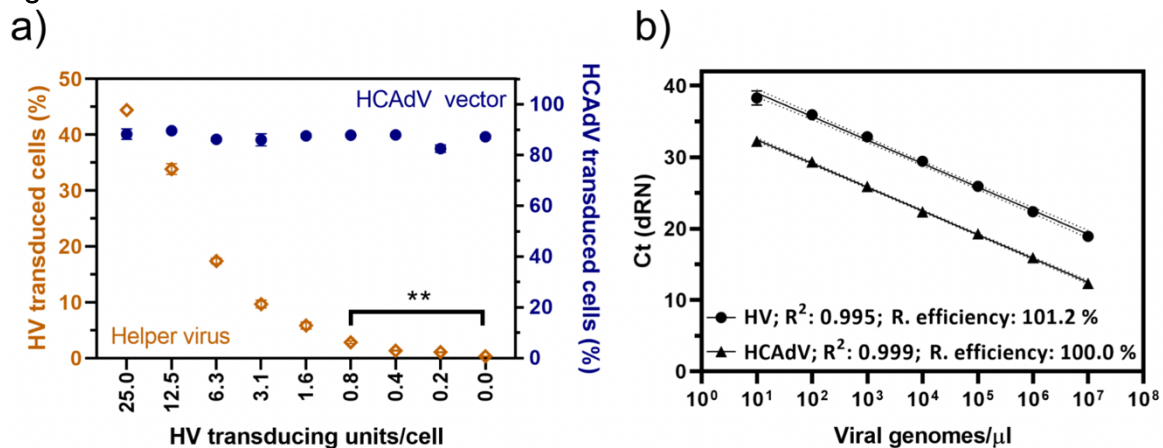
inserted transgene (here, IL-2). The lower band represents the part of the HCA Δ V genomic plasmid required for bacterial cloning. Plasmids indicated as correctly assembled via the test digest were later sequence-verified. The two plasmids represented by clone two and three which were not positive showed internal homologous recombination and thus a smaller plasmid size of lower than 8 kb instead of the expected 30 kb. Overall, we were able to achieve cloning efficiencies of up to 85 %. Contribution: DB planned, organized, conducted and analyzed the experiment. DB prepared figure.

Figure S3. High-capacity adenoviral vector (HCA Δ V) amplification monitored by qPCR:



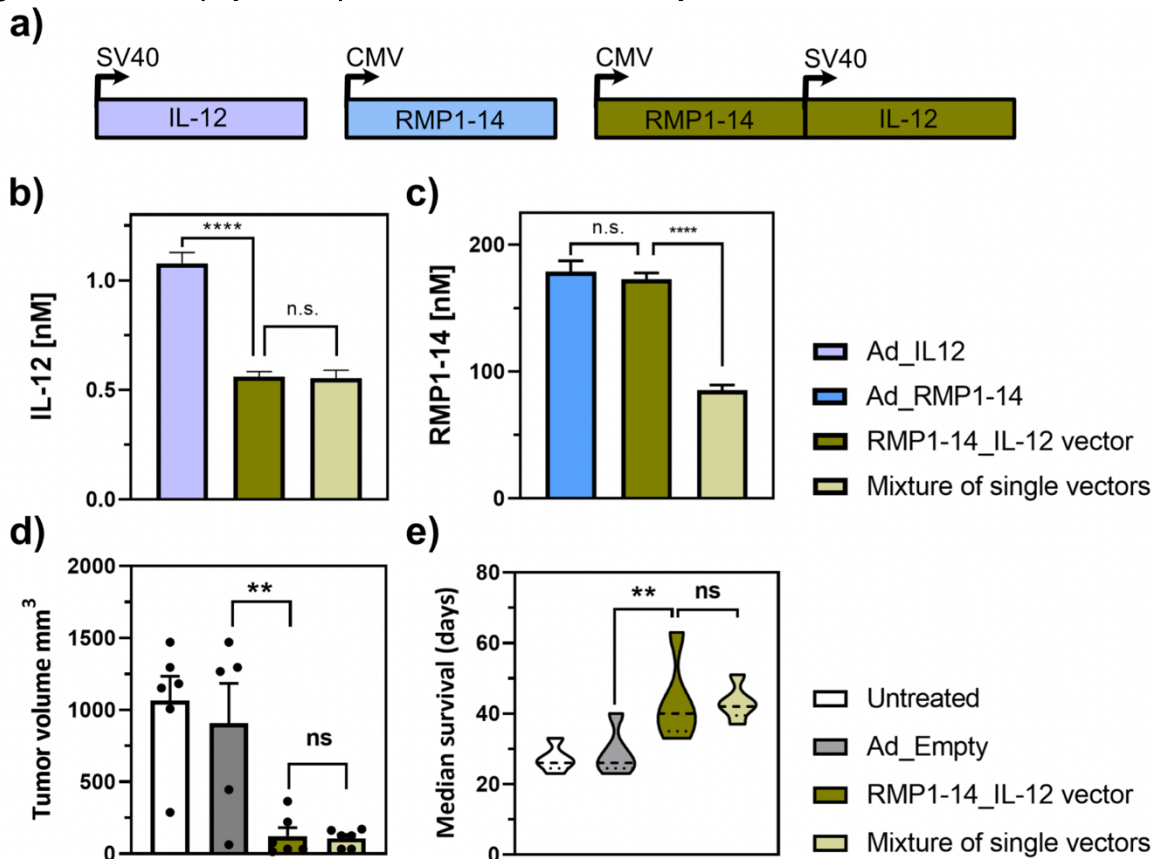
HCA Δ V (straight line) and helper virus (dotted line) genomes were detected with specific primers for HCA Δ V vector encoding RMP1-14 under the control of a CMV promoter over 5 passages (P0-4) via qPCR. Cells were adenofected in P0 by transfection with HCA Δ V DNA and co-infection with helper virus (blue lines) and showed an increase in HCA Δ V genomes during amplification, as compared to cells transfected with HCA Δ V DNA alone (grey line) which lacked viral protein provided in *trans* from a helper virus. The total number of HCA Δ V genomes of the transfection control increased slightly from P2-3 due to the increased number of cells per passage. The measured concentrations of HCA Δ V genomes in the transfection control reached the lower qPCR detection limit in P3-4. Total HCA Δ V genome numbers surpassed HV genome numbers after passage 3 in the adenofection group. 2 x 10⁶ cells (P0-2), 2 x 10⁷ cells (P3) and 2 x 10⁸ cells (P4) were used for HCA Δ V amplification. Error bars represent SEM. Extracted genomes were measured in duplicates (n=2) in qPCR analysis. Contribution: DB planned, organized, conducted and analyzed the experiment. DB prepared figure.

Figure S4. Quantitative determination of HV contamination levels:



(a) A549 cells were co-infected with HCAdV and HV vectors. HCAdV concentration was kept constant at 100 transducing units per cell, while HV concentration was spiked in, ranging from 25 to 0 transducing units per cell. The wildtype HAAdV-C5 high capacity vector shown here encodes the fluorescence marker GFP (right Y axis) while the HV encodes mCherry as a fluorescence reporter (left Y axis). Protein expression from HV vectors was titratable with a detection limit of 0.8 transducing HV units per cell, which is the equivalent of a HV contamination of 0.8 % in this experiment. (b) A standard curve with viral genomes ranging over six magnitudes (10 to 1 x 10⁷ HV or HCAdV genomes per μl) could be measured accurately via qPCR. For comparison, at the lowest detectable concentration of 10 genomes/μl only 100 molecules of viral genomes are present per measured qPCR sample. This sensitivity is required to determine the low HV contamination of HCAdV vectors achieved here. Error bars represent SEM. Protein expression was measured from three separate transduced cell populations and analyzed by a two-way ANOVA test $p < 0.01$ (**). qPCR samples were measured in duplicates for HV and HCAdV vectors. Contribution: DB planned, organized, conducted and analyzed the experiment. DB prepared figure.

Figure S5. *In vitro* payload expression and *in vivo* efficacy of a RMP1-14_IL-12 combination:



(a) Schematic depiction of a dual combination HCAdV vector RMP1-14_IL12 (olive) and two single payload vectors, Ad_IL12 (violet) and Ad_RMP1-14 (blue). Secretion of IL-12 (b) and RMP1-14 (c) from A549 cells was measured as the triple combination (RMP1-14, IL-12 and IL-2) in Fig 5. As with the triple combination, the dual combination of RMP1-14 and IL-12 also showed a reduction in expression of the SV40-driven payload (IL-12), independent of whether IL-12 was encoded on the same (RMP1-14_IL-12 vector) or separate (mixture of single vectors) vectors. The CMV-driven payload (RMP1-14) level was only influenced by the number of present transgenes, and it was thus reduced in the mixture of vectors that contained only half the transgene copy numbers but not by the co-expression of a SV40-driven transgene (IL-12). *In vivo* experiments (d and e) of the dual combination were performed as described for the triple combination (Fig. 6) in a B16-hHER2 tumor model. Mice treated with the dual HCAdV vector or a mixture of single payload vectors showed significantly reduced tumor burden 30 days post cell injection (d) and significantly increased survival (e) compared to mice treated with a HCAdV vector encoding no therapeutics (Ad_Empty) or untreated mice. Furthermore, no significant differences between the mixture and the dual combination HCAdV vector could be detected in terms of tumor reduction or survival. *In vitro* protein secretion (a-b) was determined from supernatants of three separately transduced cell populations which were measured in duplicates via an antigen capture ELISA. *In vivo* data (d and e) were obtained from five mice per group. Error bars represent SEM. Data comparison was done with a two-way ANOVA test, $p > 0.9$ (n.s.), $p < 0.01$ (**) and $p < 0.0001$ (****) are indicated. Contribution: NK planned, organized, conducted and analyzed the experiment. DB gave input for experimental design. NK and DB prepared figure.

Figure S6. Correlation between transgene numbers and single transgene expression:

a)

Relative amount of single transgenes per total vector genome

Transgenes	Combination vector	Mixture of vectors
1	1.0	1.0
2	1.0	0.5
3	1.0	0.3

b)

Relative RMP1-14 expression (%)

Transgenes	Combination vector	Mixture of vectors
1	100.0	100.0
2	96.5	48.0
3	92.5	41.0

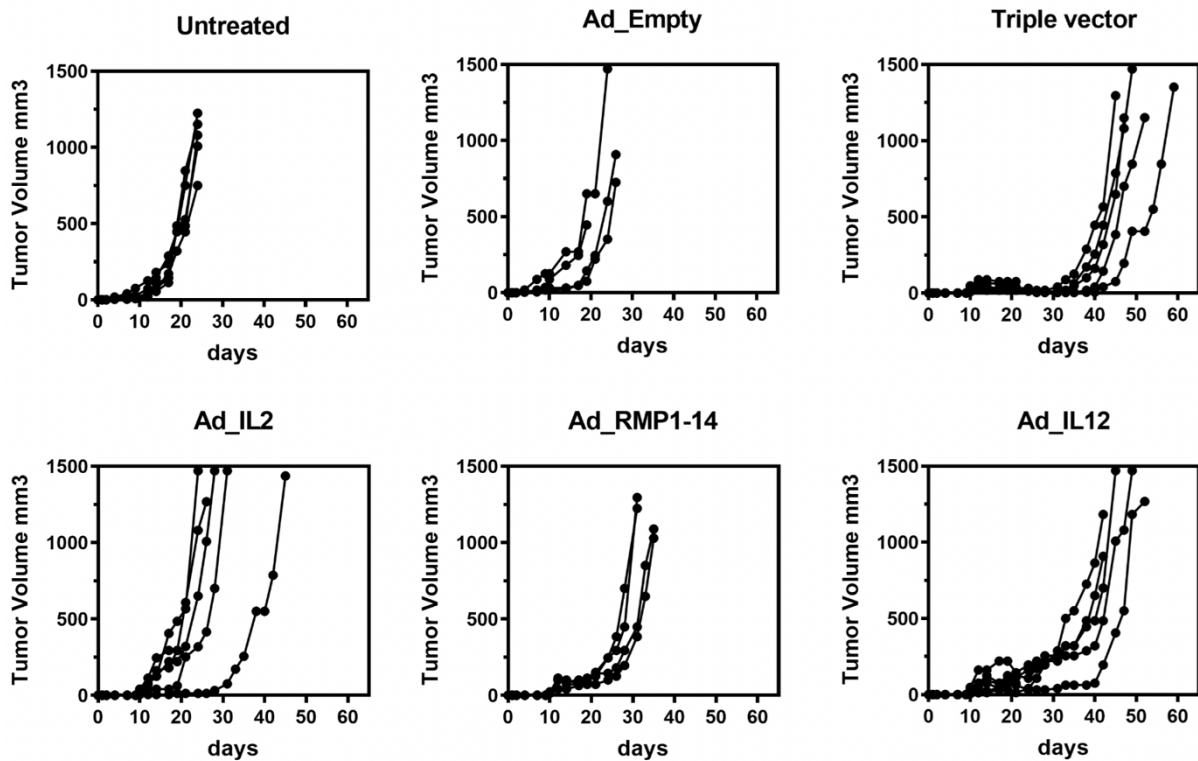
c)

Relative IL-12 expression (%)

Transgenes	Combination vector	Mixture of vectors
1	100.0	100.0
2	51.2	50.6
3	27.5	15.8

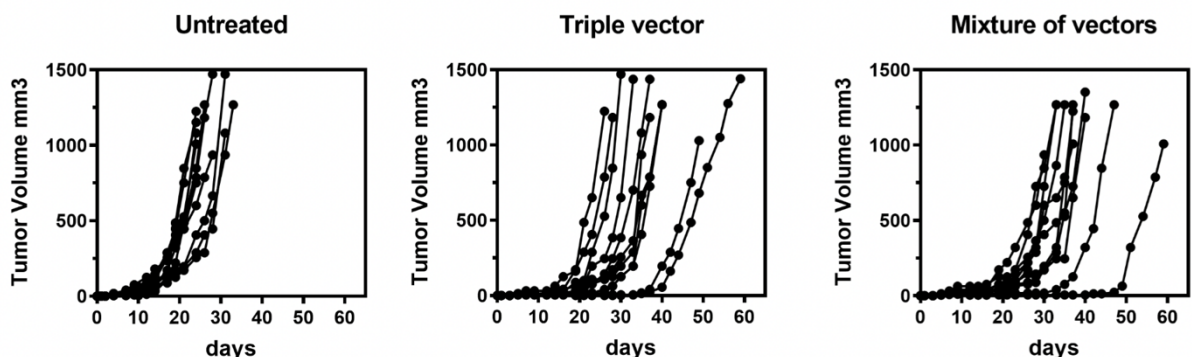
(a) Provided that the total viral particle number is constant, the single transgene number is decreasing in a mixture of vectors encoding only a single transgene, and inverse proportional to the number of delivered transgenes. In contrast, the transgene copy numbers stay constant with increasing number of transgenes for a single vector encoding all transgene — defined here as a combination vector. Secretion of therapeutics from A549 cells was measured for (b) RMP1-14 and (c) IL-12 for combinations with two (RMP1-14 and IL-12) and three (RMP1-14, IL-12 and IL-2) transgenes. Experimental data were obtained as described in Fig. 5c and Sup. Fig. 5b-c. Transgene expression from a combination HCAAdV vector or from a mixture of HCAAdV single transgene vectors were normalized to transgene expression in the absence of addition transgenes, *i.e.*, to RMP1-14 expression from Ad_RMP1-14 or to IL-12 expression from Ad_IL-12. A stronger decrease of transgene expression with increasing transgene numbers could be detected for a mixture of HCAAdV vectors, compared to the HCAAdV combination vectors, for both transgenes, (b) RMP1-14 and (c) IL-12. Protein secretion was determined from supernatants of three separately transduced cell populations, which were measured in duplicates via an antigen capture ELISA setup. Contribution: DB planned, organized, conducted and analyzed the experiment. DB prepared figure.

Figure S7. Tumor outgrowth curves of mice treated with single payload HCAAdVs and the triple HCAAdV vector:



Averaged data are shown in Fig. 6b. Treatment groups are indicated above each graph. Tumor volumes were measured for 60 days post tumor cell injection or until a mouse reached euthanasia criteria (> 1500 mm³). A drastically delayed tumor growth was observed for the triple combination vector and the Ad_IL12 vector. A moderate tumor outgrowth was detected for the Ad_RMP1-14 single vector. Each treatment group consisted of five mice, except for the Ad_Empty and RMP1-14 group (n=4). Contribution: NK planned, organized, conducted and analyzed the experiment. DB gave input for experimental design. NK and DB prepared figure.

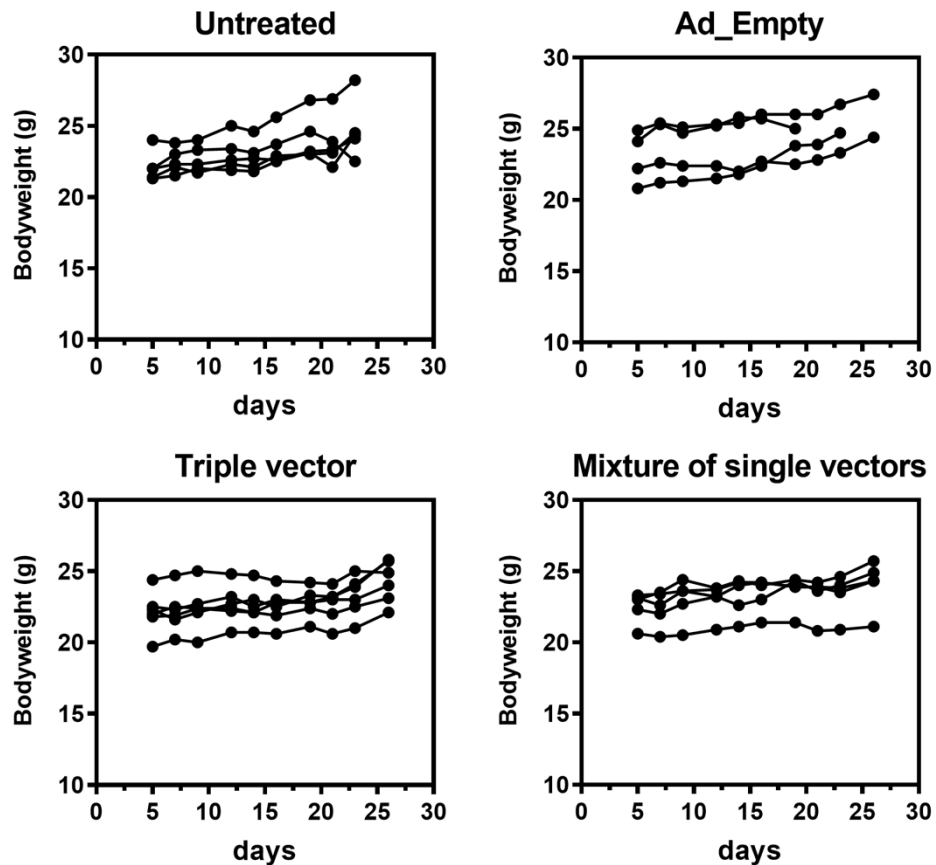
Figure S8. Tumor outgrowth curves of mice treated with the triple HCAAdV vector and a mixture of single payload vectors:



Averaged data are shown in Fig. 6d. Treatment groups are indicated above each graph. Tumor volumes were measured for 60 days post tumor cell injection or until a mouse reached euthanasia criteria (> 1500 mm³). A drastically delayed tumor growth was observed for the triple HCAAdV vector (middle) and the

mixture of single payload HCAAdV vectors (right) compared to the untreated group (left). Each treatment group consisted of 11 mice. Contribution: NK planned, organized, conducted and analyzed the experiment. DB gave input for experimental design. NK and DB prepared figure.

Figure S9. Acute toxicity monitored by body weight:



The body weight of mice treated with PBS (untreated), empty vector (Ad_Empty), triple vector or a mixture of single payload vectors of Ad_RMP1-14, Ad_IL12 and Ad_IL2 were measured. No significant loss of body weight in treated mice during (day 10 to 18) or post (> day 18) treatment was observed. Each treatment group consisted of four mice, except for the triple vector group (n=5). Contribution: NK planned, organized, conducted and analyzed the experiment. DB gave input for experimental design. NK and DB prepared figure.

2.1.9.2 Supplementary methods

Reporter quantification in HEK293 cells

2 x 10⁵ HEK293 cells were transfected with 1.5 µg polyethyleneimine (PEI) and 0.5 µg single plasmid or 2 µg plasmid mixture per single well in a 24-well plate. Cells were harvested 48 hours post transfection. Following three wash steps with 1xPBS, fluorescent protein expression was measured with a BD LSRFortessa™ cytometer. The Alexa 488 channel (500- 560 nm) was used for GFP detection and the PE-Texas Red (655-735 nm) channel for tdTomato detection. Luciferase activity was detected from lysed cells via a dual luciferase kit (Promega, E1910), following the manufacturer's protocol.

2.2 Targeting intra-tumoral crosstalk between adaptive and innate immunity enhances cancer immune control

Nicole Kirchhammer^{1, 13}, Marcel P Trefny¹, Marina Natoli¹, Dominik Brücher², Sheena N Smith², Franziska Werner^{1, 3}, Victoria Koch¹, David Schreiner⁴, Ewelina Bartoszek⁵, Mélanie Buchi¹, Markus Schmid^{2, 6}, Daniel Breu⁷, K. Patricia Hartmann², Polina Zaytseva⁸, Daniela S Thommen⁹, Heinz Läubli¹², Michal A Stanczak^{1, 10}, Abhishek S Kashyap^{1, 11}, Andreas Plückthun², Alfred Zippelius^{1, 10, 13}

¹ Cancer Immunology, Department of Biomedicine, University Hospital Basel, 4031 Basel, Switzerland

² Department of Biochemistry, University of Zurich, 8057 Zurich, Switzerland

³ Present address: Molecular Dermato-Oncology and Tumor Immunology, Department of Dermatology, General Hospital Vienna, 1090 Vienna, Austria

⁴ Immune Cell Biology, Department of Biomedicine, University Hospital Basel, 4031 Basel, Switzerland

⁵ Microscopy Core Facility, Department of Biomedicine, University Hospital Basel, 4031 Basel, Switzerland

⁶ Present address: Roche Diagnostics GmbH, 82377 Penzberg, Germany

⁷ Department of Immunology, University Hospital Zurich, 8091 Zurich, Switzerland

⁸ Institute for regenerative medicine, University of Zurich, 8952 Schlieren, Switzerland

⁹ Division of Molecular Oncology and Immunology, The Netherlands Cancer Institute, 1066 Amsterdam, The Netherland

¹⁰ Present address: Department of Immunometabolism, Max Planck Institute of Immunobiology and Epigenetics, 79108 Freiburg, Germany

¹¹ Present address: Boehringer Ingelheim Pharmaceuticals, Inc., 6877 Ridgefield, USA

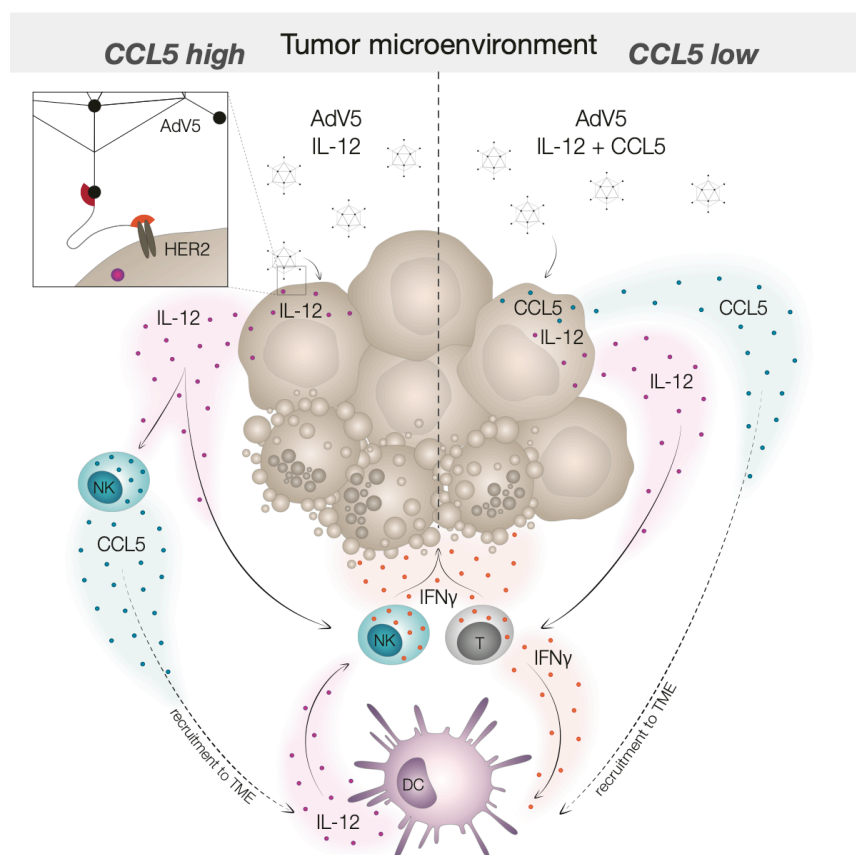
¹² Medical Oncology, University Hospital Basel, 4031 Basel, Switzerland

¹³ Corresponding authors

Manuscript in preparation. This work is presented with an extended, overall discussion and will be modified and shortened before the submission to a peer-reviewed scientific journal.

2.2.1 Abstract

Targeting T cells for cancer immunotherapy only occasionally generates robust tumor control. Harnessing additional orchestrators of the immune response against tumors may enhance and broaden the clinical benefit. Here, we demonstrate that therapeutic targeting of the IFN γ -IL-12 pathways efficiently amplify anti-tumoral T cell-NK cell-DC crosstalk for successful tumor rejection. Utilizing an engineered adenoviral platform for paracrine delivery in the tumor microenvironment, we show that IL-12 enhances a functional DC-CD8 interaction to generate profound anti-tumor immunity. This effect was dependent on the abundance of intra-tumoral NK cells, particularly their capacity to produce the DC chemoattractant CCL5. Treatment failure in response to IL-12 and other IFN γ -inducing therapies such as immune checkpoint blockade could be overcome by intra-tumoral therapeutic delivery of CCL5 and subsequent recruitment of cDC1s. Our findings reveal new therapeutic avenues that enhance T cell-NK cell-DC crosstalk and thereby enforce tumor-eliminating positive feedback mechanisms to promote anti-tumor immunity and overcome resistance.



2.2.2 Introduction

Cancer immunotherapy including blockade of immune checkpoints offers great potential to induce durable anti-tumor responses and long-term remission of cancer patients (Hegde and Chen, 2020; Ribas and Wolchok, 2018; Wolchok et al., 2017). However, multiple mechanisms by which tumors evade immune-mediated detection and destruction have been identified, and these mechanisms result in the observed primary or acquired resistance to immune checkpoints (Kalbasi and Ribas, 2020). Significant effort is currently directed to introduce combinatorial immunotherapies with the goal to improve therapeutic benefit, either by concomitantly enhancing immune functions or by targeting other immunoregulatory mechanisms within the tumor microenvironment (Galon and Bruni, 2019; Hellmann et al., 2019; Motzer et al., 2018). However, despite the numerous combination strategies that have been investigated, only few have thus far translated into clinical benefit.

The clinical success of immune checkpoint blockade has initially kept the scientific focus predominantly on factors regulating T cell activity and activation (Waldman et al., 2020). It is, however, increasingly acknowledged that a diverse range of immune cells, including components of innate immunity such as dendritic cells (DCs) and natural killer (NK) cells, must function in a coordinated and synergistic manner to successfully achieve immune-mediated tumor rejection (Barry et al., 2018; Gardner et al., 2020; Huntington et al., 2020). The interferon γ (IFN γ)-Interleukin 12 (IL-12) axis plays a central role in connecting innate and adaptive cancer immunity (Garris et al., 2018). Mainly produced by DCs in the tumor microenvironment, IL-12 stimulates cytotoxicity and cytokine-secretion in T cells and NK cells (Tugues et al., 2015). In a positive IL-12-IFN γ feedback loop, T and NK cell-derived IFN γ in turn activates and induces IL-12 expression in DCs. Moreover, IFN γ enhances antigen (cross-) presentation by antigen presenting cells (APCs) and induces secretion of chemokines, thereby further potentiating the cytotoxic activity of CD8 T cells (Garris et al., 2018; Ruffell et al., 2014). The importance of this immune signaling cascade in cancer is emphasized by the fact that gene expression signatures reflecting cellular components of this axis — NK cells, DCs and CD8 T cells —, and the signature of IFN γ signaling, are predictive of improved patient survival and response to immune checkpoint inhibition in multiple cancer types (Ayers et al., 2017; Böttcher et al., 2018; Cursons, 2019; Lee, 2019; Zhao et al., 2019).

Here, we hypothesize that combining therapeutic strategies that enhance NK cell-DC-T cell crosstalk is essential to accommodate successful anti-tumor responses and to overcome resistance. We show that the described IFN γ -IL-12 axis can be directly utilized and translated into therapeutic approaches by paracrine delivery of IL-12 in the tumor microenvironment. To this end, we used an adenoviral delivery platform as a tool for intra-tumoral immunotherapy to

reduce the systemic spread of the therapeutic agent and to consequently avoid systemic side effects (Smith *et al.*, in press). To ensure tumor-specificity, human adenovirus serotype 5 (HAdV-C5 or AdV5) was targeted to the human epidermal growth factor receptor 2 (HER2; Dreier *et al.*, 2013). Due to the high abundance of pre-existing antibodies against AdV5, we made use of a shield based on a hexon-binding humanized single-chain variable fragment (scFv), fully covering the virion (Schmid *et al.*, 2018). The efficacy of AdV5-IL12 was dependent on the intra-tumoral abundance of NK cells and their ability to prime the immune microenvironment by enhancing DC-CD8 interaction. In tumors with dampened NK cell function, resistance to IL-12 could be rescued by induced expression of CCL5, leading to increased infiltration of conventional dendritic cells type 1 (cDC1s) which then set the anti-tumorigenic NK cell-DC-T cell positive feedback loop in motion. Similarly, resistance to other IFN γ -mediated treatments, such as anti-PD-1 checkpoint blockade, could also be overcome by treatment with CCL5. Our data highlight the importance of the intra-tumoral NK cell-DC-T cell axis for successful cancer immunotherapy. In particular, we show how this crosstalk can be improved by the combination of IFN γ -inducing therapies such as tumor-targeted delivery of IL-12 or anti-PD-1 antibodies with DC attractants such as CCL5.

2.2.3 Results

2.2.3.1 AdV5-IL12 stimulates anti-tumor T and NK cell responses in immunogenic murine tumors

First, we sought to characterize the pharmacokinetic profile of HER2-targeted and shielded AdV5 in immune-competent human HER2-expressing mouse tumor models. To monitor payload expression, luciferase-encoding virus (AdV5-Luciferase) was peritumorally injected into B16-HER2 and EMT6-HER2 bearing mice (Figure S1A). In both tumor models, payload was expressed exclusively in the tumor for up to 10 days with a peak expression on day 1 (Figure S1B-D).

To evaluate the efficacy of AdV5 encoding IL-12 (AdV5-IL12) in a syngeneic, orthotopic mouse breast cancer model, we treated EMT6-HER2 bearing mice with four injections of 1.5×10^8 PFU AdV5-IL12. Empty virus (AdV5-control) served as a control (Figure 1A). Treatment with AdV5-IL12 resulted in strong tumor growth inhibition, enhanced survival and complete tumor regression in 70% of the treated mice, while AdV5-control showed only moderate effects. AdV5-IL12 induced a protective immune memory response against the rejected tumor cell line as mice surviving primary EMT6-HER2 engraftment following AdV5-IL12 treatment remained tumor-free after re-challenge with EMT6-HER2 (Figure 1B). Tumors from mice simultaneously inoculated

with EMT6 wt cells on the lateral flank were equally rejected suggesting broad memory formation towards shared antigens expressed in EMT6 cells (Figure 1B).

To decipher the role of defined immune cell populations in mediating the therapeutic effect of AdV5-IL12, we performed antibody-mediated depletion studies (Figure 1C). The efficacy of AdV5-IL12 was fully abrogated by the depletion of CD8 T cells and dampened by depletion of NK cells (anti-AsialoGM1 antibody). As IL-12 is a known driver of IFN γ production in CD8 T cells and NK cells (Tugues et al., 2015), we assessed the contribution of IFN γ to the activity of AdV5-IL12. IFN γ -neutralized mice failed to control EMT6-HER2 tumors treated with AdV5-IL12 (Figure 1D). This indicates that AdV5-IL12 treatment requires sufficient NK and CD8 T cell responses and is dependent on IFN γ .

Next, we investigated the contribution of pre-existing intra-tumoral lymphocytes in the response to AdV5-IL12. Blocking lymphocyte recirculation with the trafficking inhibitor FTY720 (Morris et al., 2005) prior to tumor inoculation fully abrogated tumor control, while blocking trafficking during AdV5-IL12 treatment allowed initial tumor control, but did not result in complete tumor regression (Figure 1E). This suggests that the latter requires both pre-existing and actively recruited infiltrating lymphocytes.

To assess the systemic effect of peritumorally administered AdV5-IL12, we injected EMT6 wt cells on the contra-lateral side of the EMT6-HER2 tumor (Figure 1F). While IL-12 was not detectable in the serum (Figure S1E), we observed reduced tumor growth in the contra-lateral tumor and complete regression in 50% of the AdV5-IL12 treated animals (Figure 1G). This indicates potent systemic immune effects upon local, peri-tumoral administration of AdV5-IL12.

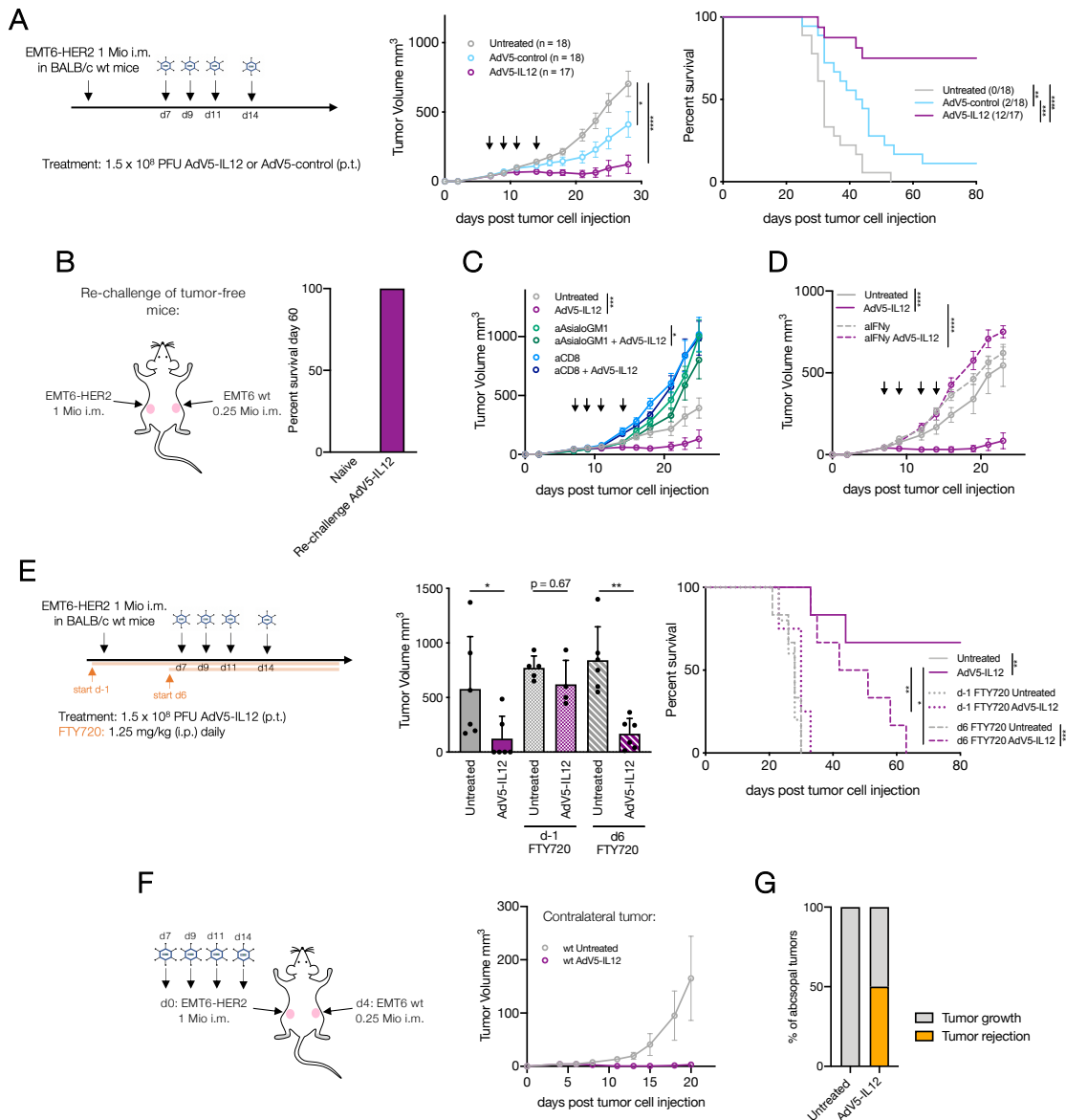


Figure 1: AdV5-IL12 stimulates anti-tumor T and NK cell responses in immunogenic murine tumors

A: Wildtype (WT) mice were engrafted with 1 mio EMT6-HER2 intramammarily (i.m.). From day 7 (tumor size 30–70 mm^3), mice were treated with 1.5×10^8 PFU of HER2-targeted and shielded adenoviral vectors (peritumorally, p.t.) encoding for IL-12 or an empty control cassette (AdV5-control) on days 7, 9, 11 and 14 p.t. Tumor growth and Kaplan-Meier survival curves are shown with the number of mice indicated. Black arrows denote days of treatment. **B:** Mice which rejected tumors after AdV5-IL12 treatment were re-challenged (60d after tumor rejection) with 1 mio EMT6-HER2 i.m. and 0.25 mio EMT6 wt cells (no HER2 transgene) on each flank. Percentage of survival 60d post re-challenge is shown. $n = 12$, naive mice served as a control. **C-D:** For depletion and neutralization studies, mice were injected i.p. with anti-CD8, anti-AsialoGM1 or anti-IFN γ , starting one day before adenoviral treatment. Tumor growth curves after depletion or neutralization are shown. Black arrows denote days of treatment. $n = 6$ mice. **E:** 1 mio EMT6-HER2 cells were injected in WT mice (i.m.). Starting from day 7 (tumor size 30–70 mm^3), mice were treated with 1.5×10^8 PFU of HER2-targeted and shielded adenoviral vectors (peritumorally) encoding for IL-12 on day 7, 9, 11 and 14. Lymphocyte trafficking was inhibited using FTY720 as indicated (orange arrow and line). Tumor volume on day 23 post tumor inoculation and Kaplan-Meier survival curves are shown. **F-G:**

Wildtype (WT) mice were engrafted with 1 mio EMT6-HER2 (i.m.) and with 4 days delay with 0.25 mio EMT6 wt cells on the contralateral flank. EMT6-HER2 tumors were peritumorally treated with Adv5-IL12. Tumor growth of contralateral tumor (EMT6 wt) was measured. Tumor growth curve and percentage of rejected contralateral tumors are shown. n = 6 mice per group.

*p < 0.05, **p < 0.01, ***p < 0.001, ****p < 0.0001. Error bar values represent SD or SEM (tumor growth curves). For comparisons between three or more groups, one-way ANOVA with multiple comparisons was used. For survival analysis, p values were computed using the Log Rank test. Two-way ANOVA was used to compare tumor growth curves. See also Figure S1. Contribution: NK planned, organized, conducted and analyzed the experiments and prepared figure.

2.2.3.2 Adv5-IL12 enhances tumor attack by NK and CD8 T cells and stimulates T cell-DC interaction

We next investigated cellular changes in EMT6-HER2 tumors upon treatment with Adv5-IL12 by multiparameter flow cytometry (Figure 2A). Consistent with the depletion experiments, Adv5-IL12 primarily induced changes in NK and T cell phenotypes (Figure 2B-C and S2). A higher frequency of NK cells in Adv5-IL12 compared to the empty vector control was accompanied by enhanced functionality (CD25⁺ and PD-1⁺) and proliferation (Ki67⁺, Figure 2D). Moreover, Adv5-IL12 resulted in a higher frequency of tumor antigen-experienced (CD39⁺), functional (granzyme B⁺; GzmB) and proliferating (Ki67⁺) CD8 T cells (Figure 2E). Durable immunotherapeutic anti-cancer responses require sufficient functionality of CD8 T cells, which can arise from a memory-like CD8 T cell precursor population that expresses TCF7 and PD-1 (Tim3^{low}). This precursor subset, which has characteristics of both progenitor cells and memory cells, can not only give rise to effector cells, but as well to terminally differentiated exhausted T cells (PD-1^{hi} Tim3^{hi}) with limited anti-cancer capacity (Brummelman, 2018; Jeannet, 2010; Kurtulus, 2019; Sade-Feldman, 2018; Siddiqui, 2019). In tumors treated with Adv5-IL12, the proportion of PD-1^{hi} Tim3^{lo} was increased whereas the proportion of double-positive CD8 T cells was unchanged (Figure 2F). Ultimately, this resulted in an enhanced proportion of TCF7⁺ PD-1^{hi} Tim3^{lo} precursor subset upon Adv5-IL12 treatment.

Next, we assessed the capability of NK and CD8 T cells to directly interact and attack cancer cells using a highly multiplexed cytometric imaging approach, termed co-detection by indexing (CODEX; Goltsev *et al.*, 2018). Adv5-IL12 led to pronounced accumulation of CD45⁺ immune cells (Figure S3A-B). Spatial proximity (defined as a distance of <50 μ m) of NK and CD8 T cells with tumor cells was increased upon Adv5-IL12 treatment (Figure 2G and S3C). Of note, this effect was specific for IL-12, as Adv5-control vector treatment did not increase the interactions between these cell populations. To confirm biological interactions and tumor lysis by NK and CD8 T cells, we analyzed the expression of the effector marker granzyme B in cells with close contact (<50 μ m) to tumor cells (CD45⁻ CD31⁻). In both NK and CD8 T cells, the number of granzyme B⁺ cells was increased in proximity to tumor cells (Figure 2H). Besides the increased

interaction with tumor cells upon AdV5-IL12 treatment, spatial proximity of CD8 T cells with DCs was enhanced after AdV5-IL12 treatment compared to both control groups (Figure 2G). Moreover, the co-stimulatory molecules, CD40, CD80 and MHCII, as well as PD-L1 on DCs in close proximity to CD8 T cells were specifically increased after AdV5-IL12 treatment, indicating an enhanced functional interaction between DCs and CD8 T cells induced by IL-12 (Figure 2I). In line with the FTY720 experiment, we could determine significantly more CD8 and NK cells in close proximity to endothelial cells (Figure 2G and J) which may indicate a potential influx of these cells from the blood vessels.

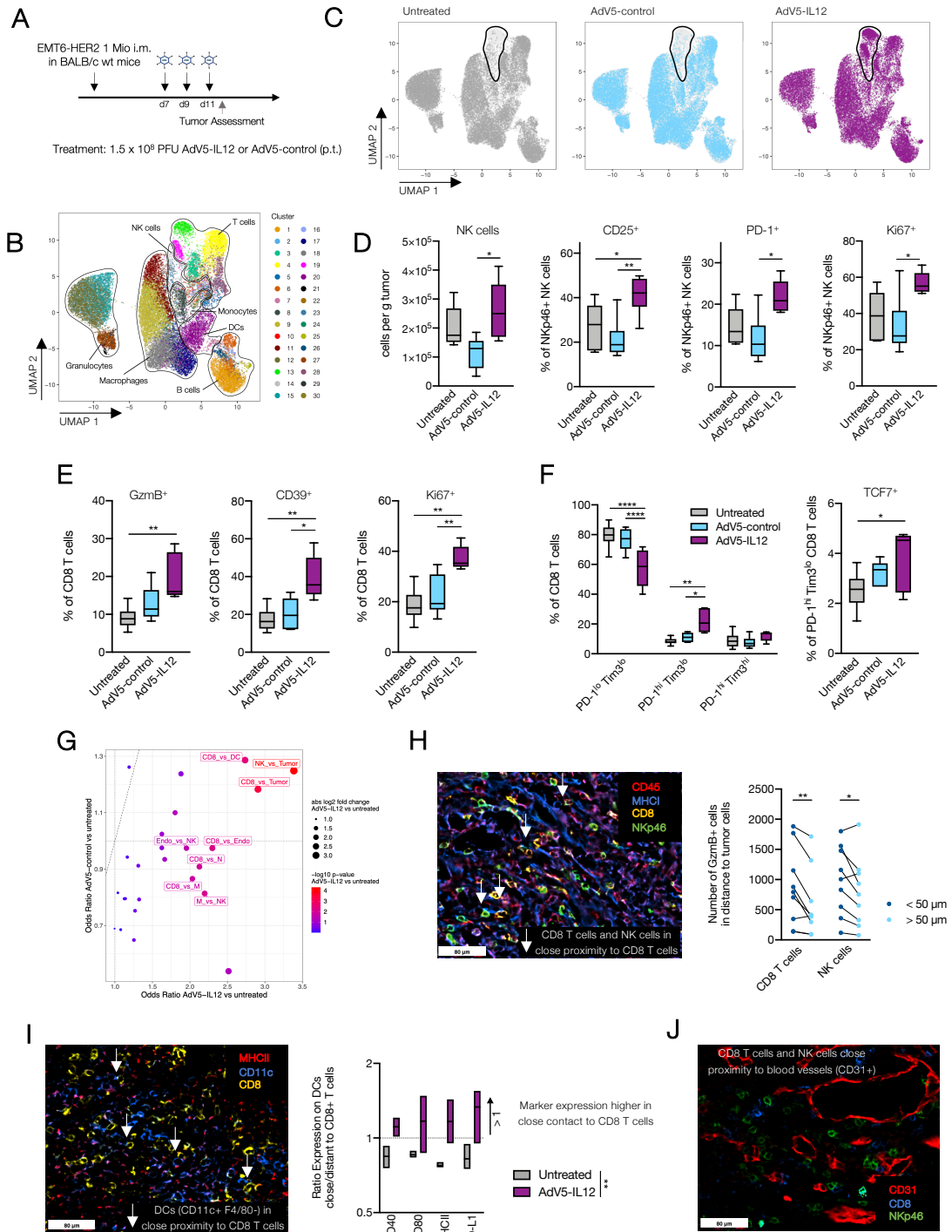


Figure 2: Adv5-IL12 enhances tumor attack by NK and CD8 T cells and stimulates T cell-DC interaction

A-F: Wildtype (WT) mice were engrafted with 1 mio EMT6-HER2 intramammarily (i.m.). Starting from day 7 (tumor size 30–70 mm³), mice were treated with 1.5×10^8 PFU of HER2-targeted and shielded adenoviral vectors (p.t.) encoding for IL-12 or empty control cassette (Adv5-control) on day 7, 9 and 11. On day 12 post inoculation, tumors were isolated and single cell suspensions were analyzed by flow cytometry. **B:** UMAP projection is depicting the alive CD45+ tumor infiltrating lymphocytes colored by cluster. **C:** UMAP projection is showing distribution of cells colored by treatment condition (dark grey: untreated; blue: Adv5-control; magenta: Adv5-IL12). **D:** Quantification of NK cells (NKp46+, CD3-, Ly6G-, CD19-, F4/80-) per

gram tumor and proportion of CD25+, PD-1+ or Ki67+ of NK cells between the different treatment conditions. **E-F:** Proportion of granzyme B+ (GzmB+), CD39+ or Ki67+ of CD8 T cells (CD3+, CD4-, NKp46-, CD19-) between the different treatment conditions. Proportion of PD-1^{lo}TIM3^{lo}, PD-1^{hi}TIM3^{lo} or PD-1^{hi}TIM3^{hi} intra-tumoral CD8 T cells in each treatment group. **A-F:** n = 5-6 mice per group. *p < 0.05, **p < 0.01, ***p < 0.001, ****p < 0.0001. Error bar values represent SD. For comparisons between three or more groups, one-way ANOVA with multiple comparisons was used. **G-J:** Wildtype (WT) mice were engrafted with 1 mio EMT6-HER2 (i.m.). Starting from day 7 (tumor size 30–70 mm³), mice were treated with 1.5x10⁹ PFU of HER2-targeted and shielded adenoviral vectors (p.t.) encoding for IL-12 or empty control cassette (Adv5-control) on day 7, 9 and 11. On day 12 post inoculation, tumors were isolated, embedded in OCT and analyzed by multiparameter immuno-fluorescence microscopy. **G:** Visualization of odds ratios and p values for changes in cell-cell type interactions between experimental conditions focusing on interaction including CD8 T cells and NK cells. **H:** Representative IF pictures are showing Adv5-IL12 treated tumors (CD45: red, MHCII: blue, CD8: yellow, NKp46: green). White arrows are showing CD8 T cells (CD45+, MHCII+, CD8+) or NK cells (CD45+, MHCII+, NKp46+) neighboring tumor cells (CD45-, MHCII+). Quantification of GzmB+ CD8 T cells and NK cells in close proximity (<50 µm) to tumor cells in comparison to more distant (>50 µm) proximity. Each dot represents the count in one acquired tumor. Treatment conditions were pooled in this analysis. **I:** Representative IF pictures are showing Adv5-IL12 treated tumors (MHCII: red, CD11c: blue, CD8: yellow). White arrows are showing CD8 T cells (CD45+, CD8+) neighboring DCs (CD45+, CD11c+, F4/80-). Ratio of CD40, CD80, MHCII and PD-L1 expression on the DC cluster in close (<50 µm) or distant (>50 µm) proximity to CD8 T cell cluster comparing untreated and Adv5-IL12 treated tumors. **J:** Representative IF pictures showing CD8 T cells and NK cells in close proximity to blood vessels in Adv5-IL12 treated tumors (CD31: red, CD8: blue, NKp46: green). **G-J:** n = 3 mice per group. *p < 0.05, **p < 0.01, ***p < 0.001, ****p < 0.0001. For comparisons between three or more groups, one-way ANOVA with multiple comparisons was used. See also Figure **S2** and **S3**. Contribution: NK planned, organized, conducted and analyzed the experiments and prepared figure. DS conducted clustering of multi-dimensional flow cytometry analysis. MPT and EB assisted to analyze multi-dimensional microscopy analysis. FW established CODEX methodology under the supervision of NK.

2.2.3.3 AdV5-IL12 response relies on sufficient CCL5 induction by NK cells

In addition to direct cytotoxicity against tumor cells, NK cells were shown to drive immune cell infiltration and intrinsic inflammation within tumors (Barry et al., 2018; Böttcher et al., 2018). To define how this dual role of NK cells contributes to the efficacy of Adv5-IL12, we depleted NK cells throughout the Adv5-IL12 treatment and assessed immune cell fate and infiltration in the tumor (Figure 3A). NK cell depletion led to a reduced number of MHCII+ CD103+ cDC1s (CD11c+ F4/80-; Figure 3B). Furthermore, NK depletion was associated with reduced granzyme B expression in CD8 T cells, suggesting an important role of NK cells in facilitating optimal anti-tumor CD8 T cells responses (Figure 3C). While the number of macrophages (CD11b+ F4/80+) in the tumor was unchanged, depletion of NK cells skewed the polarization towards an immunosuppressive M2 (CD206+ MHCII-) phenotype (Figure 3D). In summary, we confirmed that during Adv5-IL12 treatment, NK cells orchestrate the recruitment and priming of other cell subsets including cDC1s and activated CD8 T cells to enhance tumor killing.

To confirm the importance of NK cells in mediating clinical benefit to IL-12 treatment, we correlated tumor immune signatures derived from pre-treatment tumor biopsies with therapeutic

responses to intra-tumoral IL-12 therapy of melanoma patients (NCT01502293; Algazi *et al.*, 2019). In addition to increased CD8 T cell scores, patients with partial response (PR), but not with progressive disease (PD) showed higher NK cell scores (Figure 3E). The latter were highly correlated with CCL5 and its receptor CCR5, suggesting a potential role in guiding immune cell recruitment (Figure 3F). Accordingly, CCL5 was significantly upregulated in patients with clinical benefit (CB = PR+SD, Figure 3G). Together, these results indicate that NK cells and the CCL5 axis play a role in facilitating IL-12 responsiveness in melanoma patients.

We next investigated whether NK cell-mediated CCL5 contributes to Adv5-IL12 efficacy in EMT6-HER2 tumors. We first showed that CCL5 concentration was dramatically reduced in tumor lysates after NK cell depletion which confirms NK cells were the main producers of CCL5 in this model (Figure 3H). In line with the clinical data (Figure 3G), we could show that CCL5 production was upregulated in NK cells by Adv5-IL12 treatment (Figure 3I). We then depleted CCL5 using antibodies during Adv5-IL12 treatment (Figure 3J). Neutralizing CCL5 starting one day before tumor inoculation fully abrogated IL-12 efficacy, while CCL5 neutralization starting one day before Adv5-IL12 treatment partially inhibited efficacy (Figure 3K). Therefore, we concluded that CCL5 produced by NK cells plays a dual role in the efficacy of IL-12. While CCL5 at steady state permits responsiveness to Adv5-IL12 treatment, further induction of CCL5 by the latter Adv5-IL12 treatment may attract immune cells to improve anti-tumor immunity.

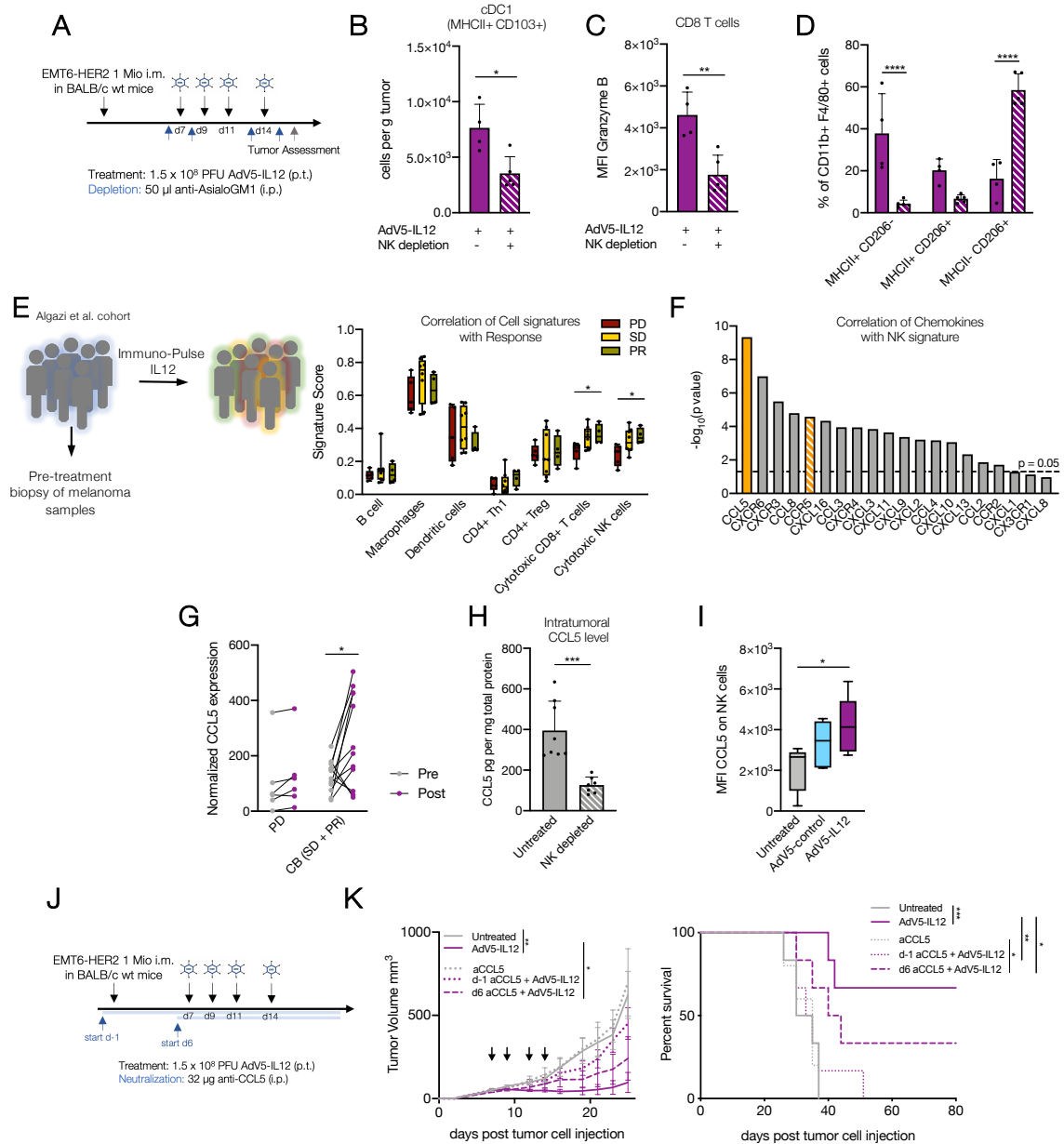


Figure 3: AdV5-IL12 response relies on sufficient CCL5 induction by NK cells

A-D: 1 mio EMT6-HER2 cells were injected in WT mice (i.m.). Starting from day 7 (tumor size 30–70 mm³), mice were treated with 1.5x10⁸ PFU of HER2-targeted and shielded adenoviral vectors (p.t.) encoding for IL-12 on day 7, 9, 11 and 14. NK cells were depleted using 50 µl anti-AsialoGM1 antibody (i.p.) as indicated (blue arrow). Tumors were isolated and single cell suspensions of tumors digest were analyzed using flow cytometry on day 16. **B:** Intra-tumoral cDC1s (CD11c+, F4/80-, Ly-6G-, MHCII+, CD103+, CD11blow) were quantified after AdV5-IL12 treatment +/- NK depletion. **C:** Mean fluorescence intensity (MFI) of granzyme B on CD8 T cells (CD3+, CD8+, NKp46-, CD19-, Ly-6G-). **D:** Polarization of macrophages (CD11b+ F4/80+) after AdV5-IL12 treatment comparing NK depletion versus non-depleted. A-D: n = 4-5 mice per group. *p < 0.05, **p < 0.01, ***p < 0.001, ****p < 0.0001. Error bar values represent SD. 2-tailed Student's t tests were used. For comparisons between grouped data sets, two-way ANOVA with multiple comparisons was used. **E-G:** Cell signature scores measured by Nanostring in skin tumor biopsies from 19 melanoma patients before intra-tumoral treatment with ImmunoPulse IL-12 were correlated with clinical response (PD: progressive disease, SD: stable disease, PR: partial response; Algazi et al., 2019). **F:** -log₁₀(p value) of chemokines and their receptors which are correlating with NK signature are shown. **G:**

Normalized CCL5 expression of patients with no-response (NR: PD) versus response (R: SD + PR) before and after intra-tumoral treatment with ImmunoPulse IL-12. E-G: * $p < 0.05$, ** $p < 0.01$, *** $p < 0.001$, **** $p < 0.0001$. Error bar values represent SD. **H-I:** Wildtype (WT) mice were engrafted with 1 mio EMT6-HER2 (i.m.). **H:** NK cells were depleted using 50 μ l anti-AsialoGM1 antibody (i.p) every 3-4 days. On day 7 post inoculation (tumor size 30–70 mm³), tumors were isolated and lysed. CCL5 expression was determined by ELISA and normalized to total protein measured by BCA. $n = 6$ per condition. 2-tailed Student's t test was used. **I:** Starting from day 7 (tumor size 30–70 mm³), mice were treated with 1.5×10^8 PFU of HER2-targeted and shielded adenoviral vectors (p.t.) encoding for IL-12 or empty control cassette (AdV5-control) on day 7, 9 and 11. On day 12 tumors were isolated and CCL5 expression (MFI) was analyzed on NK cells. $n = 6$ mice per condition. One-way ANOVA with multiple comparisons was used. **J-K:** Wildtype (WT) mice were engrafted with 1 mio EMT6-HER2 (i.m.). Mice were treated with AdV5-IL12 following the indicated schedule. Starting one day prior tumor inoculation or one day prior adenoviral therapy, CCL5 was neutralized using antibodies every 3-4 days. Tumor growth and Kaplan-Meier survival curves are shown. Black arrows denote days of treatment. * $p < 0.05$, ** $p < 0.01$, *** $p < 0.001$, **** $p < 0.0001$. Error bar values represent SEM. For survival analysis, p values were computed using the Log Rank test. Two-way ANOVA was used to compare tumor growth curves. Contribution: NK planned, organized, conducted and analyzed the experiments and prepared figure. MPT re-analyzed RNA Seq data.

2.2.3.4 AdV5-CCL5 boosts AdV5-IL12 response in tumor models with dampened NK cell function

To analyze the contribution of CCL5 to NK cell-mediated tumor rejection upon AdV5-IL12 treatment, we combined paracrine delivery of IL12 with that of CCL5, both using our adenoviral platform (AdV5-IL12 + AdV5-CCL5) during NK cell depletion (Figure 4A). As already shown above (Figure 1C), the NK cell depletion abrogated the efficacy of AdV5-IL12. While AdV5-CCL5 alone did not reinstate anti-tumor control after NK cell depletion, the combination with AdV5-IL12 delayed tumor growth, yet did not lead to full tumor rejection (Figure 4B). This suggests that CCL5 partially rescues the AdV5-IL12 response in an NK cell-depleted murine tumor model.

Next, we asked whether AdV5-CCL5 can further boost AdV5-IL12 efficacy in tumor models with dampened anti-tumor NK cell function. To this end, we depleted NK cells in B16-HER2, a well-known immune-excluded aggressive tumor model. Unlike in EMT6-HER2, NK cell depletion in B16-HER2 did not increase tumor growth in neither untreated nor AdV5-IL12 treated tumors (Figure 1C and 4C). Similarly, as we have shown that NK cells are driving immune cell infiltration after AdV5-IL12 treatment in EMT6-HER2 tumors (Figure 3A), AdV5-IL12 response in B16-HER2 tumors was not altered by FTY720, suggesting that trafficking of immune cells does not contribute to therapeutic efficacy in this model (Figure 4D). Additionally, the lower impact of NK cell depletion in B16-HER2 tumors was accompanied by lower levels of CCL5, as expected (Figure 4E).

In order to test if reduced NK cell-derived CCL5 could be therapeutically substituted, we combined AdV5-IL12 and AdV5-CCL5 therapy also in B16-HER2 bearing mice (Figure 4F). The combination further delayed tumor growth and increased survival compared to single treatments (Figure 4G). Taken together, these data suggest that in tumor models with low CCL5 levels,

presumably through dampened NK cell function, IL-12 responses can be boosted by paracrine delivery of CCL5 in the tumor.

To show the potential of our adenoviral vector as a platform for combinatorial approaches, we then designed adenoviral vectors expressing both, IL-12 and CCL5 (Figure S4A). To avoid gene deletion of IL-12 or CCL5 from the adenoviral vectors by homologous recombination, we encoded both transgenes under the control of the orthogonal promoters, CMV or SV40, in the combination approach. We were able to demonstrate similar therapeutic efficacy by expressing both payloads within one viral vector, independent of the promoter choice, despite the fact that we thereby decreased the viral load per injection (Figure S4B-C).

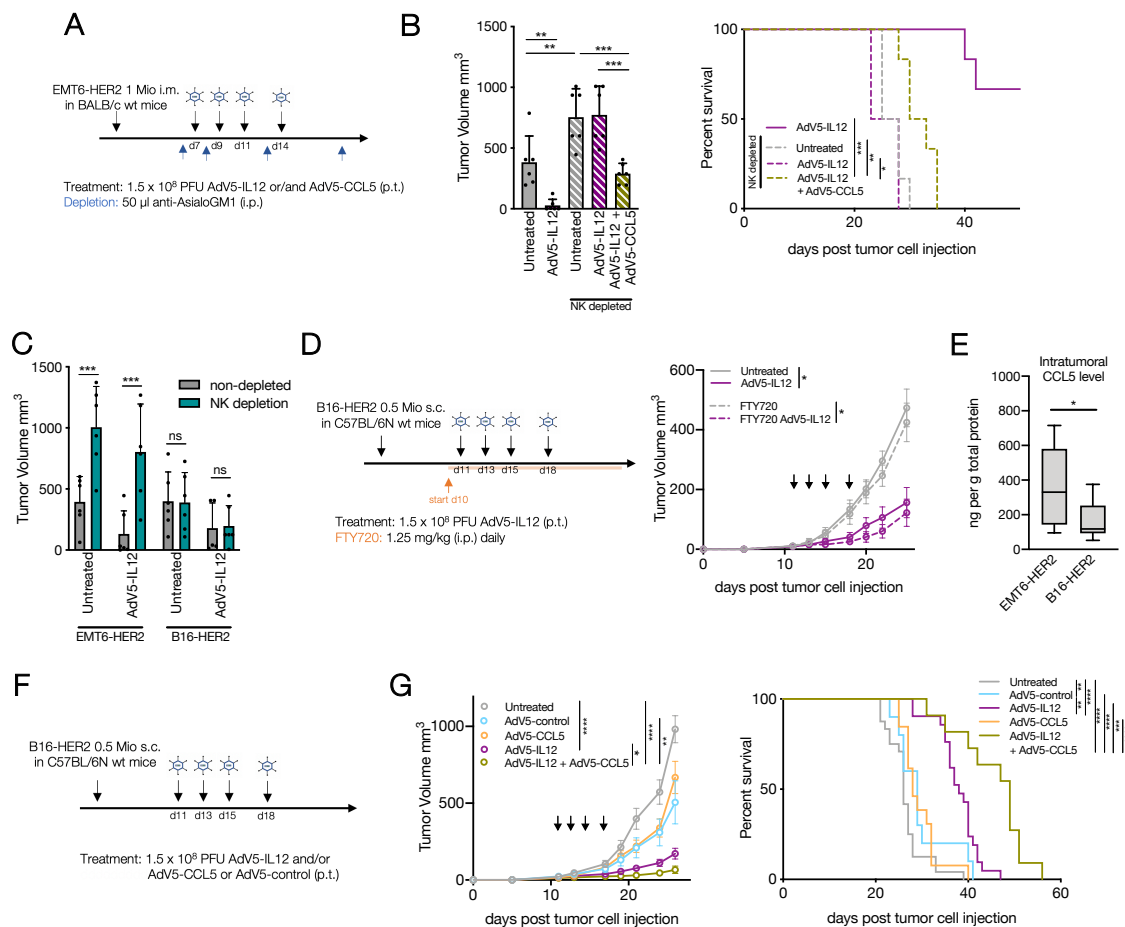


Figure 4: AdV5-CCL5 boosts AdV5-IL12 response in tumor model with dampened NK cell function

A: Wildtype (WT) mice were engrafted with 1 mio EMT6-HER2 (i.m.). Mice were treated with AdV5-IL12 and AdV5-CCL5 following the indicated schedule. Starting one day prior adenoviral therapy, NK cells were depleted using anti-AsialoGM1 antibody as indicated (blue arrow). **B:** Tumor volume on day 23 post tumor inoculation and Kaplan-Meier survival curve are shown. **C:** Wildtype (WT) mice were engrafted with 1 mio EMT6-HER2 (i.m.) or 0.5 mio B16-HER2 (s.c.). Mice were treated with AdV5-IL12 on day 7, 9, 11 and 14 or day 11, 13, 15 and 18 (tumor size 30–70 mm^3), respectively. NK cells were depleted using anti-AsialoGM1 and anti-NK1.1 antibody every 4-5 days starting one day prior adenoviral therapy. Tumor volume on day 25 post tumor inoculation is shown. **D:** Wildtype (WT) mice were engrafted with 0.5 mio

B16-HER2 (s.c.). Mice were treated with AdV5-IL12 on day 11, 13, 15 and 18 (tumor size 30–70 mm³). Lymphocyte trafficking was inhibited using FTY720 as indicated (orange arrow and line). Tumor growth curves are shown. **E:** Intra-tumoral CCL5 concentration was determined by ELISA and normalized to total protein in EMT6-HER2 and B16-HER2 tumor lysates. **F-G:** Mice were treated with AdV5-IL12 and AdV5-CCL5 on day 11, 13, 15 and 18 (tumor size 30–70 mm³) after B16-HER2 inoculation as indicated: Tumor growth and Kaplan-Meier survival curves are shown (n > 15 mice per condition). **A-G:** n = at least 6 mice per group. *p < 0.05, **p < 0.01, ***p < 0.001, ****p < 0.0001. Error bar values represent SD or SEM (tumor growth curves). For comparisons between three or more groups, one-way ANOVA with multiple comparisons was used. For survival analysis, p values were computed using the Log Rank test. Two-way ANOVA was used to compare tumor growth curves. See also Figure **S4**. Contribution: NK planned, organized, conducted and analyzed the experiments and prepared figure.

2.2.3.5 AdV5-CCL5 improves IL-12 efficacy by inducing cDC1 recruitment

We next investigated the role of CCL5-mediated lymphocyte trafficking on the therapeutic synergy of AdV5-CCL5 on AdV5-IL12 (Figure 5A). FTY720 treatment diminished the benefit of the combination compared to AdV5-IL12 single treatment, suggesting that CCL5 predominantly acts by mechanisms depending on cell migration (Figure 5B). To further understand the intra-tumoral cellular network, we performed multiparameter flow cytometry analysis upon treatment with the combination of AdV5-IL12 and AdV5-CCL5. We could show that AdV5-IL12 increased the CD8/Treg ratio, which is known to be associated with improved anti-tumor responses (Müller *et al.*, 2015, Figure 5C-D). This effect could not be further increased when combining AdV5-IL12 with AdV5-CCL5 (Figure 5D). Similarly, the combinatorial approach enhanced the expression of granzyme B in both CD8 T cells and NK cells, compared to untreated tumors, with no significant increase compared to AdV5-IL12 (Figure 5E).

CCL5 produced by NK cells has been shown to induce cDC1 recruitment into the tumor (Böttcher *et al.*, 2018). In agreement with this finding, we were able to detect increased numbers of cDC1s in the tumor after AdV5-CCL5 single treatment or in combination with AdV5-IL12 compared to untreated controls, and importantly, compared to single AdV5-IL12 treatment (Figure 5F). We also found an increased number of cDC1s expressing CD80 and PD-L1 in response to the combination of AdV5-IL12 and AdV5-CCL5, suggesting enhanced activation through increased IFN γ levels exclusively by the combination treatment in the tumor (Figure 5G). To further understand the contribution of cDC1s to the therapeutic efficacy of the AdV5-IL12-AdV5-CCL5 combination we used Batf3 KO mice, which lack cDC1s (Hildner *et al.*, 2008). Strikingly, the beneficial effect of AdV5-IL12 +/- AdV5-CCL5 on tumor control and survival were lost in Batf3 KO mice (Figure 5H). Taken together, these data suggest that cDC1s attracted by CCL5 are essential for IL-12-mediated therapeutic benefit.

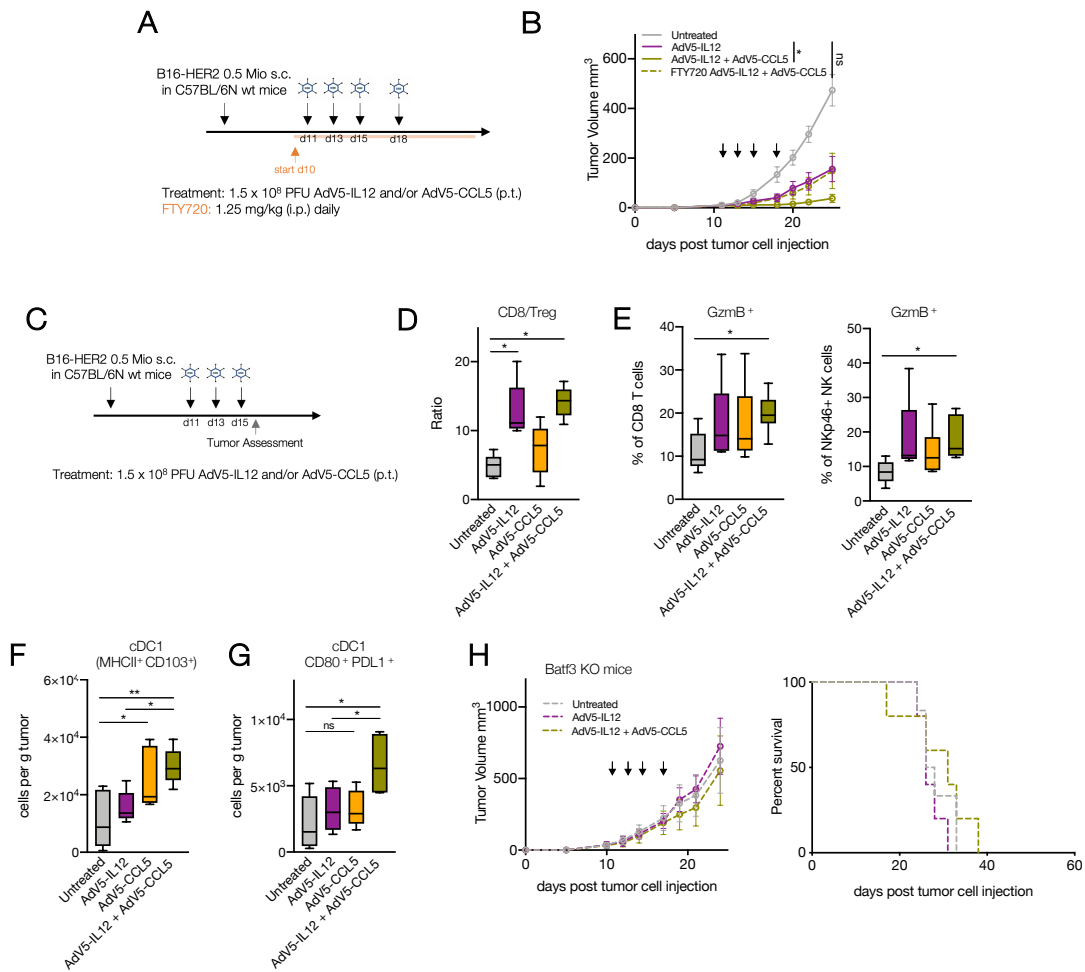


Figure 5: AdV5-CCL5 improves IL-12 response by inducing cDC1 recruitment

A: Mice were treated with AdV5-IL12 and AdV5-CCL5 on day 11, 13, 15 and 18 (tumor size 30–70 mm^3) after B16-HER2 inoculation. Lymphocyte trafficking was inhibited using FTY720 as indicated (orange arrow and line). Tumor growth curves are shown. Black arrows denote days of treatment. **B:** Wildtype (WT) mice were engrafted with 0.5 mio B16-HER2 (s.c.). Mice were treated with AdV5-IL12 and/or AdV5-CCL5 on day 11, 13 and 15 (tumor size 30–70 mm^3). On day 16 post inoculation, tumors were isolated and single cell suspensions were analyzed by flow cytometry. **D:** Ratio of CD8 T cells (CD8) versus regulatory T cells (Treg) (CD8: CD3⁺, CD4⁻, NKp46⁻ CD19⁻; Treg: CD3⁺, CD4⁺, FOXP3⁺, CD25⁺, NKp46⁻, CD19⁻). **E:** Proportion of granzyme B⁺ of CD8 T cells (CD3⁺, CD4⁻, NKp46⁻ CD19⁻) and NK cells (NKp46⁺, CD3⁻, Ly6G⁻, CD19⁻, F4/80⁻). **F-G:** Number of cDC1s (CD11c⁺, F4/80⁻, Ly-6G⁻, MHCII⁺, CD103⁺, CD11b^{low}) and PD-L1 and CD80 expressing cDC1s, respectively. **H:** Batf3 knockout mice (lacking cDC1s) were engrafted with 0.5 mio B16-HER2 (s.c.). Mice were treated with AdV5-IL12 and/or AdV5-CCL5 as indicated (black arrows). Tumor growth and Kaplan-Meier survival curves are shown. **A-H:** n = 5-6 mice per group. *p < 0.05, **p < 0.01, ***p < 0.001, ****p < 0.0001. Error bar values represent SD or SEM (tumor growth curves). For comparisons between three or more groups, one-way ANOVA with multiple comparisons was used. For survival analysis, p values were computed using the Log Rank test. Two-way ANOVA was used to compare tumor growth curves. Contribution: NK planned, organized, conducted and analyzed the experiments and prepared figure.

2.2.3.6 AdV5-huIL-12 induces CCL5 expression in patient-derived tumor cultures

To test whether AdV5-IL12 can induce anti-tumorigenic effects in a human *ex vivo* system, we co-cultured primary tumor suspensions, including tumor infiltrating lymphocytes (TILs) from non-small cell lung cancer patients (Figure 6A) or peripheral blood mononuclear cells of healthy donors (HD PBMCs, Figure S5) with a HER2-expressing ovarian cancer cell line (OVCAR3), which was transduced with human IL-12-encoding HER2-targeted and shielded adenoviral vector (Figure 6A-E). This co-culture induces an allogeneic immune response and has been shown to activate primary human lymphocyte subsets and trigger human cancer cell killing in response to PD-1/PD-L1 blockade (Natoli et al., 2020). Within patient-derived TILs and OVCAR3 co-cultures, AdV5-IL12 significantly reduced OVCAR3 viability due to enhanced tumor cell killing (Figure 6B). This was similarly achieved when PBMCs were co-cultured with OVCAR3 (Figure S5A). This effect was accompanied by an increase in IFN γ secretion (Figure 6C, Figure S5B) and induction of IFN γ -expressing patient-derived or healthy-donor CD8 T cells and NK cells (Figure 6D, Figure S5C, respectively). In line with our murine data, CCL5 was upregulated by IL-12, an effect that was NK cell-dependent (Figure 6E, S5D).

Next, we assessed AdV5-IL12 functionality using a patient-derived tumor fragment platform, a human *ex vivo* model that preserves the tumor microenvironment and architecture, but enables *ex vivo* perturbation by checkpoint blockade (Figure 6F; Voabil et al., submitted). Tumor fragments of HER2-expressing ovarian cancer samples were embedded in Matrigel (Figure 6G), transduced with HER2-retargeted IL-12-encoding adenoviral vector and cultured for 48 hours. In all four tested patients, we could see an upregulation of IFN γ in CD8 T cells, as well as upregulation of CCL5 in NK cells (Figure 6H). The latter was confirmed in the supernatant by ELISA (Figure 6I).

Collectively, these experiments with primary human patient material recapitulate our observations in mice that IL-12 can directly stimulate tumor-infiltrating T cell antitumor activity and induce CCL5 upregulation by NK cells.

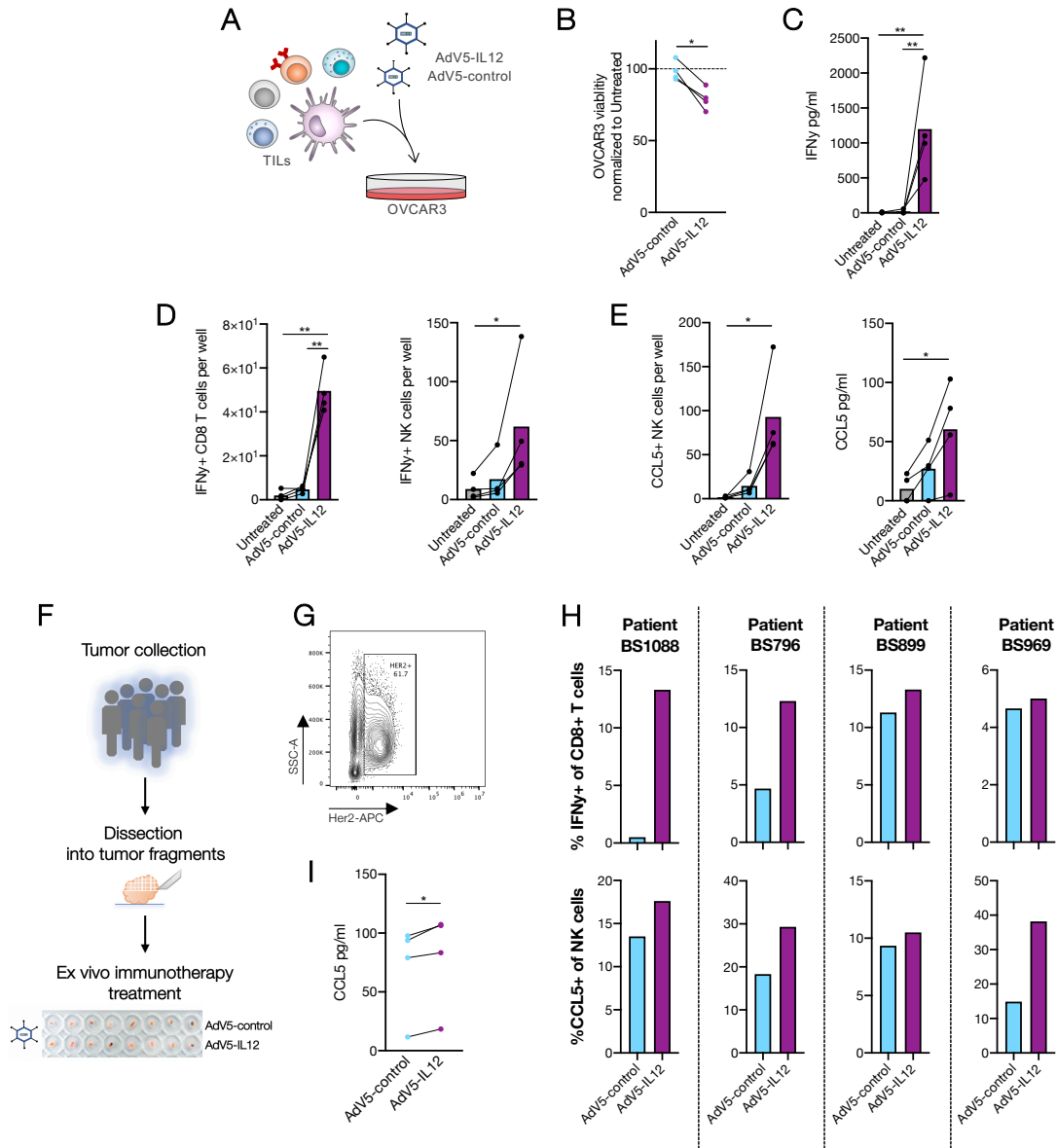


Figure 6: AdV5-hu-IL12 induces CCL5 expression in patient-derived tumor cultures

A-E: Tumor digests of NSCLC patients were co-cultured with OVCAR-3 cells which were transduced with HER2-targeted AdV5 encoding human IL-12 or control virus. **B:** Quantification of OVCAR-3 viability normalized to untreated co-cultures after 96 h. **C:** IFN γ expression was determined in supernatants after 5d. **D:** Cell count of IFN γ + CD8 T cells (CD3+, CD56-) and NK cells (CD56+, CD3-) per well after 96 h. **E:** Cell count of CCL5+ NK cells (CD56+, CD3-) after 96 h and CCL5 expression in supernatants after 5d. **F-G:** HER2+ ovarian cancer samples were dissected into tumor fragments and cultivated embedded in matrigel. Tumor fragments were treated with HER2-targeted AdV5 encoding human IL-12 for 48 h (8-12 fragments per condition). **G:** Representative dot plot of HER2 expression analyzed by flow cytometry. **H:** After treatment tumor fragments per condition were pooled and analyzed by flow cytometry. Quantification of IFN γ + CD8 T cells (CD3+, CD56-) and NK cells (CD56+, CD3-) after treatment. **I:** CCL5 concentration in supernatant was analyzed by ELISA. **A-G:** n = each 4 patients. *p < 0.05, **p < 0.01, ***p < 0.001, ****p < 0.0001. 2-tailed paired Student's t test was used. For comparisons between three or more groups,

paired one-way ANOVA with multiple comparisons was used. Contribution: NK and MN planned, organized and conducted experiments. NK analyzed data and prepared figure.

2.2.3.7 CCL5 expression is beneficial for anti-PD-1 efficacy

It has been demonstrated that IL-12-producing DCs, activated by IFN γ -secreting CD8 T cells, are involved in successful responses to anti-PD-1 treatments (Garris et al., 2018). This led us to investigate whether the DC attractant CCL5 is associated with efficient tumor responses to anti-PD-1 therapy.

In melanoma patients undergoing nivolumab treatment (Riaz et al., 2017), we compared CCL5 induction during treatment between patients with progressive disease (PD) and clinical benefit (CB, SD+PR+CR; Figure 7A). Indeed, CCL5 upregulation was significantly associated with response in the tested cohort (Figure 7B). Using an NK cell signature as a surrogate of NK cell abundance, we found a significant positive correlation between the NK signature and CCL5 expression, consistent with intra-tumoral NK cells in patients being a source of CCL5 (Figure 7C; Böttcher *et al.*, 2018). Furthermore, using gene signatures for cDC1s to estimate cellular abundance, we also found a positive correlation between levels of CCL5 and cDC1s in treated melanoma patients (Figure 7D), consistent with observed cDC1 recruitment by CCL5 in our tumor mouse model (Figure 5F).

Utilizing the patient-derived tumor fragment platform, we recently demonstrated that the clinical response of patients to PD-1 blockade correlates with the capacity of intra-tumoral immune cells to be reactivated by anti-PD-1 *ex vivo* (Voabil *et al.*, *submitted*). We therefore analyzed IFN γ and CCL5 expression in the supernatant of tumor fragments of cancer patients exposed to anti-PD-1 (nivolumab, Figure 7E). In line with the clinical data (Figure 7B), we found an upregulation of CCL5 in responding fragments (IFN γ upregulation) after anti-PD-1 blockade (Figure 7G).

Consequently, we asked whether CCL5 can further boost anti-PD-1 therapy in our tumor model with low endogenous CCL5 level. We combined anti-PD-1 therapy with our adenoviral vector encoding CCL5 in B16-HER2 bearing mice (Figure 7H). While Adv5-CCL5 single treatment did not show any therapeutic efficacy, we observed synergistic therapeutic effects when combined with anti-PD-1 treatment.

Taken together, these data demonstrate that CCL5 exerts promising therapeutic potential through the induction of cDC1 infiltration; thus, the IL-12-IFN γ -CCL5 axis we have herein revealed presents a tangible opportunity to improve PD-1 checkpoint blockade therapy.

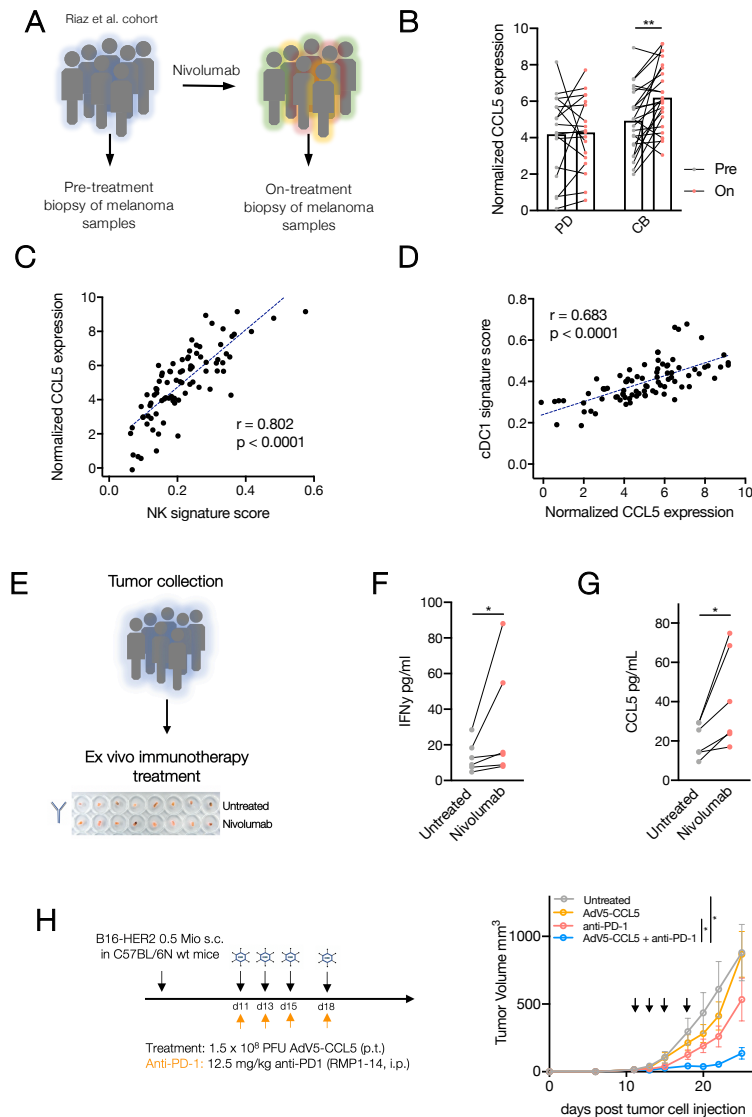


Figure 7: CCL5 expression is beneficial for anti-PD-1 efficacy

A-D: CCL5 expression in tumor biopsies of melanoma patients ($n = 42$) was analyzed pre and on nivolumab treatment (Riaz et al., 2017). **B** Comparison of CCL5 expression pre and on nivolumab treatment between patients with progressive disease (PD) or clinical benefit (CB = SD+PR+CR). **C:** Correlation between CCL5 expression and NK signature score. **D:** Correlation between CCL5 expression and cDC1 signature score. **E-G:** Cancer samples were dissected into tumor fragments and cultivated embedded in Matrigel. Tumor fragments were treated with nivolumab for 48 h (6-8 fragments per condition). IFN γ and CCL5 were determined in the supernatant. $n = 6$ tumor samples. **H:** WT mice were engrafted with 0.5 mio B16-HER2 (s.c.). Mice were treated with AdV5-CCL5 (p.t.) and/or anti-PD-1 (i.p.) antibodies on day 11, 13, 15 and 18 (tumor size 30–70 mm 3) as indicated. Tumor growth curves are shown. $n = 6$ mice per condition. **A-F:** * $p < 0.05$, ** $p < 0.01$, *** $p < 0.001$, **** $p < 0.0001$. Error bar values represent SEM. For comparisons between grouped data sets, two-way ANOVA with multiple comparisons was used. 2-tailed paired Student's t test was used. Two-way ANOVA was used to compare tumor growth curves. Contribution: MPT re-analyzed RNASeq data. NK planned, organized, conducted and analyzed the experiments and prepared figure. DST conducted and analyzed experiments (E-G).

2.2.4 Extended discussion

Combination immunotherapy has become a cornerstone in the therapeutic management of patients with different cancer types (Meric-Bernstam et al., 2020; Mokhtari et al., 2017; Sun et al., 2017). Although extensively investigated in clinical trials, multiple combination strategies have failed to show clinical benefit and have been discarded due to futility and/or toxicity (Day and Siu, 2016; DiMasi and Grabowski, 2007; Larkin et al., 2019; Long et al., 2019). Here, we propose a novel mechanism-driven combinatorial approach which improves therapeutic outcomes by exploiting key cellular components and their crosstalk to amplify anti-tumor immunity. Specifically, using a retargeted and shielded adenoviral vector platform, we were able to show responses upon paracrine delivery of IL-12 in immune-infiltrated tumors. We demonstrate that IL-12 enhances anti-tumorigenic DC-CD8 interactions which relied on NK cell-specific induction of CCL5. Consequently, in tumor models with dampened NK function and thus low CCL5 levels, only moderate IL-12 responses were observed, which, however, could be boosted by combination with a CCL5-encoding adenoviral vector that induced cDC1 infiltration after infecting tumor cells and converting them into CCL5 production sites. Due to the unique role of cDC1s in the initiation of T cell responses, both *de novo* and upon anti-PD-1 checkpoint inhibition, we subsequently observed synergistic efficacy of the AdV5-CCL5-anti-PD-1 combination. These findings suggest that intra-tumoral delivery of therapeutics using an adenoviral vector platform provides an attractive opportunity to improve immunotherapy through rational drug combinations adjusted to the pre-existing tumor microenvironment; mechanistically, this is mediated by enhancing the crosstalk between lymphoid and myeloid immune compartments.

Viral vectors have been shown to be a suitable tool for local immunotherapy, reducing the systemic spread of therapeutic agents and consequently avoiding systemic side effects (Riley et al., 2019). Recently, the development of high-capacity, helper-dependent AdVs (HCAVs) has enabled the expression of transgenes of up to 36 kilobase pairs, making these vectors ideal candidates for combinatorial approaches (Ricobaraza et al., 2020). However, a system for the rapid assembly and production with low helper virus contamination has so far been missing. For this reason, we developed the iMATCH platform which is presented here. This platform allows to integrate four unique expression cassettes, enabling a broad combination of therapeutic payloads. Moreover, the number of payloads encoded by these vectors is not necessarily restricted to the number of expression cassettes as those can be extended using multi-cistronic protein expression motives such as 2A binding sites and internal ribosomal entry sites (Kim et al., 2011; Licursi et al., 2011). In order to test potential combinations, single payload HCAVs or even commercially available first-generation AdVs can be used. We here show that these vectors,

when retargeted and shielded, have similar biodistribution profiles, as well as similar efficacies both when given as a mixture of single vectors or encoded by a single combinatorial HCA_{AdV}.

Our adenoviral platform utilizes exogenously added retargeting adaptors consisting of DARPins (Dreier et al., 2013). This strategy has unique advantages, compared to targeting by genetic modifications, including the large existing library of DARPins and the rapid selection of new DARPins against any given surface protein (Dreier and Plückthun, 2012; Plückthun, 2015). We targeted the human tumor antigen HER2 which is overexpressed in different cancer types (Yan et al., 2014). To further broaden the clinical applicability, DARPins may be selected to specifically recognize targets on cells other than tumor cells, such as fibroblast activation protein (FAP) on tumor-associated fibroblasts (Kakarla et al., 2012; Trüb et al., 2020).

We were previously able to show that the combination of targeting and shielding drastically improves the intratumoral accumulation of the expressed payloads in immune-deficient mice, not only when administered intratumorally, but also intravenously. Systemic administration, however, led to a lower total level of payload expression in the tumor (Schmid et al., 2018). In the current study, focusing on the immunological mechanism and efficacy of treatment with an IL-12 and CCL5 encoding viral vector, we have used the intratumoral route to maximize production levels. However, we have tested the systemic route of administration in immune-competent mice, which resulted in significantly reduced production of payload in the tumor compared to immune-deficient mice. Nevertheless, we could observe increased accumulation using our retargeting and shielding approach. The reduction in targeting efficiency in immune-competent mice compared to immune-deficient mice could be explained by the observed downregulation of the immunogenic HER2 on tumor cells in immune-competent mice, or by the development of anti-human shield antibodies against the humanized shield after repetitive administration.

An immediate clinical development might therefore be delayed by insufficient tumor-targeting which prevents the use in broader applications, such as treatment of non-superficial tumors and disseminated metastases. Strategies to further enhance transduction efficiencies and reduce off-target binding of systemically administered virus include the incorporation of additional capsid protein mutations that reduce transduction via secondary receptors (e.g. Δ RGD), combination with angiogenesis inhibitors (e.g. bevacizumab) in order to increase tumor perfusion and targeting of different, easily accessible cell types such as tumor-associated endothelial cells (e.g. via VEGFR2 targeting; Akbari et al., 2019; El-Kenawi and El-Remessy, 2013; Mizuguchi et al., 2002). To prevent neutralization of adenoviral vectors by pre-existing antibodies, vectors of other serotypes with lower or no immunogenicity in humans can be used alternatively, such as AdV2 or non-human adenoviruses, e.g. chimpanzee AdVs. In the case of HCA_{AdVs}, this can easily be achieved by exchanging the helper virus for a different serotype (Bots and Hoeben, 2020;

Coughlan, 2020). However, cell specificity and tropism need to be taken into consideration, as these are dictated by the capsid provided by the helper virus. In order to use our described retargeting adapters, the fiber knob of the desired serotype would therefore need to be replaced with the AdV5 fiber knob, which would enable interchangeable cell-targeting independent of the capsid serotype. Utilizing this strategy, repeated injections of therapeutic adenoviral vectors of different serotypes could be achieved which have been shown to result in lower vector neutralization, longer maximal treatment duration, and higher payload expression (Jung et al., 2018; Parks et al., 1999). In addition to a high and tumor-specific transduction, the clinical applicability of adenoviral vectors for future cancer therapies will depend on overcoming manufacturing challenges such as insufficient production efficiency (van der Loo and Wright, 2016). The latter mainly results from the strict regulatory requirements and costs when these vectors are produced under good manufacturing practice (GMP) conditions.

The efficacy of immunotherapy is dependent on a variety of factors and cell types in the tumor microenvironment, and untangling these complex interactions is critical to understand and improve therapeutic responses. Dendritic cells play a key role in orchestrating anti-tumor immunity. Although typically rare, they include distinct subsets with non-overlapping functions that can be harnessed for cancer immunotherapy (Zilionis et al., 2019). Intra-tumoral presence of DCs and their production of IL-12 has been associated with improved survival in various cancer types and is positively correlated with clinical outcome to anti-PD-1 therapy (Barry et al., 2018). Consequently, IL-12 has been extensively investigated for use in cancer immunotherapy. However, many previous attempts to develop IL-12-based therapies for use in humans resulted in severe toxicities, likely due to their systemic routes of administration (Hurteau et al., 2001; Motzer et al., 2001). Utilizing the AdV5 platform, our data demonstrate the potential of IL-12 to bridge innate and adaptive immunity to successfully improve tumor immunity. IL-12 produced by tumor cells after treatment with AdV5-IL12 increased activation and cytotoxic potential of murine and human CD8 T cells. Although we could show that early tumor growth control is achieved by the steady state of lymphocytes present within the tumor, our results suggest that lymphocyte and antigen trafficking to draining lymph nodes is needed for long-term tumor rejection. In agreement, we observed enhanced numbers of NK cells and CD8 T cells in close proximity to blood vessels which may indicate an increased trafficking from the periphery to the tumor. This may be induced by the observed CCL5 secretion by NK cells or other IFN γ -induced chemokines such as CXCL9 and CXCL10. The fact that cDC1s have been described as the main source of CXCL9 and CXCL10 (Spranger et al., 2017) could explain the increased interactions between DCs and CD8 T cells and therefore increased T cell immunity after AdV5-IL12 treatment. Consequently, we demonstrated that AdV5-IL12 not only improves lymphocyte homing and

activation in the primary tumor, but also promotes abscopal anti-tumor effects at distant tumor sites.

NK cells contribute to various immune functions during cancer initiation and progression, including the recognition of cells undergoing stress or early transformation and the direct killing of sensitive cells (Huntington et al., 2020). In addition to rapid degranulation upon target recognition, NK cells are powerful producers of a broad variety of pro-inflammatory cytokines and chemokines shaping the inflammatory milieu of tumors (Barry et al., 2018; Böttcher et al., 2018). Several preclinical models have confirmed that NK cells are required for optimal anti-tumor CD8 T cell responses by inducing the recruitment of cDC1s and subsequently CD8 T cells (Huntington et al., 2020). Consistent with these models, there is growing evidence that the magnitude of NK cell infiltration has a strong prognostic value in various cancers, and it predicts clinical outcome to immune checkpoint blockade in different tumors (Prat et al., 2017). In our study, NK cells and their induction of CCL5 expression was essential for the efficacy of Adv5-IL12 and was significantly correlating with the response to anti-PD-1 therapy in human melanoma. These data confirm the crucial role of NK cells in priming the tumor immune microenvironment and provide direct evidence that lack of intra-tumoral cDC1 recruitment triggered by NK cells represents a major barrier of T cell-based therapies. However, further work needs to identify tumor-derived factors that mediate resistance by limiting accumulation, survival, and function of these cells within the tumor microenvironment. Such factors may serve as predictive markers for T cell-focused therapies and therefore define the need for potential combinations with therapeutics providing signals for cDC1 attraction. With regard to the latter, we here identified CCL5, which we could show to improve the efficacy of IFN γ -inducing therapies, such as checkpoint inhibition or IL12 in tumors with dampened NK function.

Some controversy exists regarding the role of CCL5 in cancer. Some studies suggest CCL5 has potential tumor-promoting effects, either by directly affecting tumor growth (Murooka et al., 2009), fostering an immunosuppressive tumor microenvironment (Casagrande et al., 2019), enhancing tumor cell migration (Karnoub et al., 2007), or expanding cancer stem cells (Jiao et al., 2018). On the contrary, other studies show delayed tumor growth and prolonged survival in mouse models with CCL5-expressing tumor cells (Debré et al., 2021). In our models, Adv5-CCL5 did not exhibit any tumor-promoting properties, but also failed to show therapeutic benefits as a single treatment. Notably, in agreement with previous work (Böttcher et al., 2018), Adv5-CCL5 single treatment induced cDC1 recruitment. Only the combination with Adv5-IL12, however, led to higher co-stimulatory potential (i.e., CD80 upregulation) and subsequently increased tumor-reactive T cells, presumably by triggering the IFN γ -IL-12 forward loop. Besides CCL5, XCL1 has been described to have similar capacities in recruiting cDC1s to the tumor bed

while not being reported to have tumor-promoting capacities (Böttcher et al., 2018). On this note, XCL1 might be an intuitive alternative payload to guide cDC1 into tumors to improve anti-tumor immunity.

Taken together, our data may inform novel combination strategies utilizing viral vector platforms as an approach to further potentiate the NK cell-DC-T cell crosstalk. Our data highlight a relevant tumor-eliminating positive feedback mechanism to be prioritized for clinical development, particularly in patients with immune-excluded and/or resistant tumors.

2.2.5 Methods

2.2.5.1 Redesign of AdV5 shuttle vector

The pShuttle vector from the AdEasy™ Adenoviral Vector System (Agilent Technologies; Luo *et al.*, 2007) was redesigned to allow for the rapid generation and exchange of modular expression cassettes encoding a variety of payloads. The multiple cloning site (MCS) of the pShuttle vector was replaced with synthetic MCS modules, called MCS1 or MCS2, via Gibson Assembly (New England Biolabs). The synthetic MCS1 module contained, from 5' to 3', the CMV promoter, *NheI* restriction site, *XhoI* restriction site and the polyA site from BGH as previously described (Smith *et al.*, in press). The MCS2 module contained, from 5' to 3', the SV40 promoter, *SpeI* restriction site, *Sall* restriction site and the polyA site from SV40. MCS modules were synthesized by GeneArt (Life Technologies Europe BV) containing the N-terminal flanking DNA 5'- GAA TAA GAG GAA GTG AAA TCT GAA TAA TTT TGT GTT ACT CAT AGC GCG TAA -3,' and C-terminal flanking DNA 5'- TAA GGG TGG GAA AGA ATA TAT AAG GTG GGG GTC -3' for Gibson Assembly into pShuttle to generate the plasmids pShuttle-MCS1 or pShuttle-MCS2. Additionally, a plasmid called pShuttle-MCS1-MCS2 was constructed where both the MCS1 and MCS2 modules were inserted in tandem into the same pShuttle construct.

2.2.5.2 Construction of payload construct

Murine and human IL-12 constructs were generated from translated Genbank cDNA sequences for the IL-12B/p40 (NCBI Reference: BC103608.1 or BC074723.2, respectively) and IL-12A/p35 (NCBI Reference: BC146595.1 or BC104984.1, respectively) connected by a F2A peptide as previously described (Brücher *et al.*, 2021). The murine CCL5 gene was generated from Uniprot sequence P30882. Cytokines included their native signal sequences, were codon-optimized for human or mouse expression, respectively, and synthesized by GeneArt (Thermo Fisher Scientific). For reporter assays, a firefly luciferase reporter was synthesized from GenBank: BAL46512.1. Payload constructs were inserted into redesigned pShuttle vectors by Gibson assembly or standard ligation cloning to generate pShuttle-MCS1 including the payload. The pShuttle-MCS1 backbone (without payload) was used to generate the AdV5-control vector. In general, pShuttle-MCS1-IL12 (AdV5-IL12), pShuttle-MCS1-CCL5 (AdV5-CCL5) and pShuttle-MCS1-Luciferase (AdV5-Luc) were used to generate immunotherapeutic vectors. For the combinatorial approach optimization (Figure S4), pShuttle-MCS2-CCL5 (AdV5-SV40-CCL5) and pShuttle-MCS2-IL12 (AdV5-SV40-IL12), pShuttle-MCS1-IL12-MCS2-CCL5 (AdV5-CMV-IL12-SV40-CCL5) and pShuttle-MCS1-CCL5-MCS2-IL12 (AdV5-CMV-CCL5-SV40-IL12) were used.

2.2.5.3 Virus production

The plasmid containing the adenoviral genome, pAdEasy-1, from the AdEasy™ Adenoviral Vector System (Agilent Technologies; He *et al.*, 1998; Luo *et al.*, 2007) was previously modified to include a mutation to the hypervariable loop 7 (HVR7) of the hexon, which prevents blood factor X binding to virions and thus reduces liver infection (Schmid *et al.*, 2018). To generate viral constructs, the modified pAdEasy-1_HVR7 plasmid was co-transformed with the pShuttle-MCS variants listed above into *recA*-proficient *E. coli* BJ5183 cells, from which the desired recombinants, obtained by homologous recombination, could be isolated for virus production. Packaging and amplification of adenoviral particles was performed by Vector Biolabs (Malvern, PA, USA) and they were purified on two consecutive cesium chloride density gradients and provided directly in PBS with 5% glycerol.

2.2.5.4 Protein purification of adenoviral shield and retargeting adaptor

The human HER2 adenoviral retargeting adapter (G3_1D3nc_SHP1) was expressed and purified as previously described (Dreier *et al.*, 2013; Schmid *et al.*, 2018). Endotoxin was removed from purified adapters using the Endotrap® HD Endotoxin Removal System (Hyglos GmbH) and adapters were stored at -80°C in endotoxin-free Dulbecco's PBS (Millipore TMS-012-A). The adenoviral shield was purified in *Sf9* insect cells as previously described (Schmid *et al.*, 2018).

2.2.5.5 Mice

C57BL/6 and Balb/c mice were bred in-house at University Hospital Basel, Switzerland. Batf3 KO (B6.129S(C)-Batf3<tm1Kmm>/J) mice were obtained from the Jackson laboratory, USA. Animals were housed under specific pathogen-free conditions. All animal experiments were performed in accordance with Swiss federal regulations. Sex-matched littermates at 8-12 weeks of age at the start of experiments were used.

2.2.5.6 Tumor models

C57BL/6 and Batf3KO mice were injected subcutaneously into the right flank with 0.5 mio syngeneic murine B16 D5 melanoma cells expressing HER2 (kindly provided by Dr. L. Weiner, Georgetown University, Washington, DC) suspended in phenol red-free DMEM (without additives). EMT6 murine breast cancer cells expressing HER2 (1 mio; D'Amico *et al.*, 2019) were injected into the mammary gland of female Balb/c mice. Cell lines were tested for mycoplasma contamination before injection. Tumor volume was calculated according to the formula: $D/2 \times d \times d$, with D and d being the longest and shortest tumor diameter in mm, respectively.

2.2.5.7 Immunotherapy treatments

Tumor bearing mice, with a tumor size of approximately 30-70 mm³, were treated with each 1.5x10⁸ PFU of HER2-targeted and shielded adenoviral vectors in 50 µl of PBS (peritumorally), and/or 12.5 mg/kg mouse anti-PD-1 (RPM1-14, BioXCell) or left untreated. For depletion studies, CD8 T cells were depleted by administering anti-CD8a (53-6.72, BioXCell) at 10mg/kg (i.p.) once per week. NK depletion was performed by administering anti-Asialo-GM1 (Poly21460, Biolegend) 50 µl (i.p.) in Balb/c mice or anti-NK1.1 (PK136, BioXCell) 10 mg/kg (i.p.) in C57BL/6 mice every 4-5 days. IFN γ neutralization was performed using anti-IFN γ antibody (XMG1.2, BioXcell) at 25 mg/kg in 200 µl PBS injected every 2-3 days. To neutralize CCL5, we injected 32 µg anti-CCL5 antibody (500-P118, Peprotech) in 200 µl PBS per mouse intraperitoneally. Depletion and neutralization schedules were started the day before immunotherapy treatment unless stated otherwise.

2.2.5.8 Bilateral tumor models

Balb/c mice were inoculated with 1 mio EMT6-HER2 tumor cells (i.m.) in the right flank. Four days later, 0.25 mio EMT6 wt cells were injected in the contralateral site (i.m.). On day 7, 9, 11 and 13 post first tumor inoculation, EMT6-HER2 tumors were treated with each 1.5x10⁸ PFU of HER2-targeted and shielded adenoviral vector encoding IL-12 in 50 µl of PBS (peritumorally). Tumor volumes of contralateral (EMT6 wt) tumors were measured.

2.2.5.9 Tumor re-challenge

Long-term surviving mice from AdV5-IL12 therapy were re-challenged with EMT6 wt and EMT6-HER2 tumors in each flank 60 days after primary tumor rejection. EMT6 wt and EMT6-HER2 re-challenge doses were 0.25 mio cells and 1 mio cells, respectively. As a control, naive Balb/c mice were implanted alongside re-challenged mice.

2.2.5.10 FTY720 treatments

Mice were implanted with EMT6-HER2 or B16-HER2 tumors intramammarily or subcutaneously, respectively. Mice were treated or not with 1.25 mg/kg of FTY720 (Cayman Chemical) i.p. daily throughout the duration of the experiment. Injections were started one day before tumor inoculation or the day before adenoviral treatment.

2.2.5.11 *In vivo* pharmacokinetic experiments

Mice were implanted with EMT6-HER2 or B16-HER2 tumors intramammarily or subcutaneously, respectively. Once the tumors reached an average volume of 30-70 mm³, luciferase-encoding retargeted and shielded AdV5 (1.5x10⁸ PFU per mouse; AdV5-Luc) were injected peritumorally. The luciferase signal was determined in live animals one day after virus injection and 10 minutes

after intraperitoneal injection of 150 mg/kg D-luciferin (PerkinElmer) using the *in vivo* imaging system NightOWL II LB 983 (Berthold) over two weeks. Following live imaging, luciferase activity was determined in isolated tumors and organs (draining and non-draining lymph nodes, spleen, liver, kidney, lung and heart). The overlay of the real image and the luminescence representation allowed the localization and measurement of luminescence emitted from xenografts. The signal intensities from manually derived regions of interest (ROI) were obtained and data were expressed as photon flux (photon/s). All measurements were performed under the same conditions, including camera settings, exposure time (60 s), distance from lenses to the animals and ROI size.

2.2.5.12 Multiparameter flow cytometry

Tumor tissue was isolated from mice, weighed and minced using razor blades. Tissue was then digested using accutase (PAA), collagenase IV (Worthington), hyaluronidase (Sigma), and DNase type IV (Sigma) for 60 min at 37°C with constant shaking. The cell suspensions were filtered using a cell strainer (70 µm). Precision Counting beads (Biolegend) were added before staining to quantify the number of cells per gram tumor. Single cell suspensions were blocked with rat anti-mouse FcγIII/II receptor (CD16/CD32) blocking antibodies (“Fc-Block”) and stained with live/dead cell-exclusion dye (Zombie UV dye; Biolegend). The cells were then incubated with fluorophore-conjugated antibodies directed against cell surface antigens, washed and resuspended in FACS buffer (PBS + 2% FBS; Table 1). For intracellular/intranuclear antigens, cells stained with cell surface antibodies were fixed and permeabilized using Foxp3/transcription factor staining buffer set (eBioscience) prior to incubation with antibodies directed against intracellular antigens. Cell populations were analyzed on a Cytex Aurora and Cytotflex.

Fluorophore	Marker	Clone	Company	Cat#
BUV395	CD45	30-F11	BD Biosciences	564279
BUV496	CD4	GK1.5	BD Biosciences	612952
BUV563	Ly-6G	1A8	BD Biosciences	612921
BUV661	CD56	NCAM16	BD Biosciences	750478
BUV661	NKp46	29A14	BD Biosciences	741678
BUV737	CXCR3	CXCR3-173	BD Biosciences	741895
BUV805	CD8	RPA-T8	BD Biosciences	749366
BUV805	CD3	145-2C11	BD Biosciences	741895
BV421	PD-L1	10F.9G2	BioLegend	124315
eFluor 450	CD8	53-6.7	Thermo Fisher Scientific	eBio 48-0081-82
BV510	MHCII	M5/114.15.2	BioLegend	107636
BV570	CCR5	C34-3448	BD Biosciences	746501
BV605	CD3	SK7	BioLegend	344836

BV605	CD80	16-10A1	BioLegend	104792
BV650	CD103	2E7	BD Biosciences	748256
BV711	CD206	C068C2	BioLegend	141727
BV785	CD56	5.1H11	BioLegend	362550
BV785	PD-1	29F.1A12	BioLegend	135225
BB515	CD19	1D3	BD Biosciences	564509
FITC	IFN γ	C4.B3	Thermo Fisher Scientific	11-7319-82
FITC	CD11c	N418	BioLegend	117306
AF532	CD45	HI30	Thermo Fisher Scientific	58-0459-41
AF532	Ki67	SolA15	Thermo Fisher Scientific	58-5698-82
PerCP	Ly-6C	HK1.4	BioLegend	128028
BB700	IFN γ	B27	BD Biosciences	566395
BB700	Tim-3	5D12/TIM-3	BD Biosciences	747619
PerCP-Cy5.5	CD45	2D1	Thermo Fisher Scientific	9045-9459-120
PE	CD39	24DMS1	Thermo Fisher Scientific	eBio 12-0391-82
PE	CCL5	VL1	BioLegend	515504
PE-eFluor610	GzmB	NGZB	Thermo Fisher Scientific	61-8898-82
PE-Cy5.5	CD25	PC61.5	Thermo Fisher Scientific	35-0251-82
PE-Cy7	CD8	SK1	Thermo Fisher Scientific	9025-0087-120
PE-Cy7	CCL5	2E9/CCL5	BioLegend	149105
APC	FoxP3	FJK-16s	Thermo Fisher Scientific	17-5773-82
AF647	F4/80	BM8	BioLegend	123122
AF700	TCF-7	# 812145	R&D Systems	FAB8224N
APC-H7	CD3	SK7	BD Biosciences	560275
APC-Cy7	CD11b	M1/70	BioLegend	101226

Table 1: Murine and human antibodies used for flow cytometry.

2.2.5.13 Bioinformatic analysis of flow cytometry data

FCS files containing pre-gated alive CD45+ single cells were read into R using the flowCore package (*flowCore: flowCore: Basic structures for flow cytometry data version 2.2.0 from Bioconductor*). A logicle transform was performed per channel, with parameters calculated from aggregated data from all samples. CD45 low cells with a transformed value of < 2.5 were removed from further analysis (threshold set on left side of trough of density plot of transformed CD45 values from all samples). The measurements were randomly subsampled to 1.5×10^5 cells per condition to expedite downstream operations. Principal Component Analysis (PCA) was performed using all markers except for CD45, Live-Dead, FSC* and SSC*. Uniform Manifold Approximation and Projection (UMAP) was performed for visualization using the CATALYST module's runDR function (*CATALYST: Cytometry dATa anALYSIS Tools version 1.14.0 from Bioconductor*). Clustering was performed using Rphenograph (0.99.1), an R implementation of PhenoGraph (*GitHub - JinmiaoChenLab/Rphenograph: Rphenograph: R implementation of the*

PhenoGraph algorithm; Levine *et al.*, 2015). Five clusters with universally high expression across all markers were removed, and steps starting with PCA were repeated. Three resulting clusters were again removed and the process iterated once more to yield the final clustering, UMAP and heatmaps ([CSL STYLE ERROR: reference with no printed form.]). Supplemental UMAP visualization of scaled marker expression done with CATALYST's plotDR function. Main cell types were assigned by marker expression. To confirm certain assignments, cell populations were gated using FlowJo (10.6.2) and compared to assigned populations (e.g. NK cells: NKp46+, CD3-, CD19- Ly-6G-, F4/80-).

2.2.5.14 Multiparameter fluorescence microscopy

Tumors embedded in OCT were sectioned into 7 μm -thick slices and attached to poly-L-lysine coated square coverslips. Sections were analyzed using CODEX® (Akoya Biosciences), a highly multiplexed imaging platform, which allows the staining of solid tissue sections with a panel of up to 40 antibodies at once (Goltsev *et al.*, 2018). In brief, CODEX uses a unique DNA barcode system to label each antibody clone individually. These barcodes can be detected by reversible hybridization to its corresponding reporter. The respective reporters, which are conjugated with the fluorophores AF488, Atto550 or Cy5, are applied onto the tissue sections, imaged and removed in a multicycle experiment. For this purpose, the manufacturer's protocol "CODEX User Manual Rev A.0" (provided by AKOYA Biosciences) was followed.

The antibody panel was composed of commercially available AKOYA-conjugated antibodies (Table 2) and self-conjugated custom antibodies (CODEX Conjugation Kit, AKOYA Biosciences; Table 3). Tissue staining was performed with the CODEX Staining Kit (AKOYA Biosciences). Briefly, the tissue was thawed with drierite beads, fixed with acetone, rehydrated and fixed with 1.6% paraformaldehyde (PFA). After blocking, the tissue was stained with the established antibody panel consisting of 33 barcoded antibodies at the same time. The bound antibodies were fixed to the tissue with 1.6% PFA, ice-cold methanol and a fixative solution (AKOYA Biosciences).

The inverse microscope DMI8 (Leica) was used for acquisition (20x magnification, xyz acquisition mode 14 Z-stacks each 14.99 μm , "Best Focus" autofocus with default settings). The generated fluorescence data were formatted with the Akoya CodexDriver V2 and subsequently processed using CODEX Processor (Version v1.5.0.48b). The processing steps included 1) XY Processing with tile registration and shading correction; 2) Z-Stack Processing with deconvolution, drift compensation, overlap cropping, background subtraction (min-min mode) and best focus detection; 3) Stitching with best focus interpolation and tile overlap of 10% and 4) Cell segmentation on the nuclear stain with the radius 8.

The processed and segmented data were analyzed with the CODEX Multiple Analysis Viewer (Version 1.2.0.297). Manual gating was performed to distinguish between CD45+ cells (immune cells) and CD45- cells (tumor and stroma cells). Clustering was performed with VORTEX using unbiased hierarchical X-shift clustering (K = 55 resulting in 81 immune clusters; Samusik *et al.*, 2016). Clusters were manually verified and assigned to main immune cell populations using CODEX Multiple Analysis Viewer. Subsequently, mean marker expression and interaction counts between cellular main populations (cells with <50 μm proximity) were determined.

Antigen	Clone	Supplier	Cat#	Barcode	Reporter	Cat#
GzmB	GB11	invitrogen	MA1-80734	BX036	Cy5	5350007
CXCL9	MIG-2F5.5	BioLegend	515602	BX033	Cy5	5350006
CD40	1C10	BioLegend	102802	BX027	Cy5	5350004
PD1	29F.1A12	BioLegend	135202	BX045	Cy5	5350009
FOXP3	FJK-16s	eBioscience	14-5773-82	BX042	Cy5	5350008
CD80	16-10A1	BioLegend	104702	BX015	Cy5	5350001
IFN γ	H22	BioLegend	513202	BX022	AF488	5150003
H-2K ^d	34-1-2S	ThermoFisher	MA5-18008	BX016	AF488	5150001
Tbet	O4-46	BD Bioscience	561263	BX043	AF488	5150010
Tim-3	RMT2-23	BioLegend	119702	BX040	AF488	5150009
CD62L	95218	R&D	MAB5761	BX049	AF488	5150012
NKp46	29A1.4	BioLegend	137602	BX037	AF488	5150008
CD25	PC61	BioLegend	102002	BX034	AF488	5150007
F4/80	BM8	BioLegend	123102	BX031	AF488	5150006
CD86	GL-1	BioLegend	105002	BX046	AF488	5150011
Ly-6C	HK1.4	BioLegend	128002	BX019	AF488	5150002
IL12	C15.6	BioLegend	505202	BX032	Atto550	5250006
CD103	2.00E+07	BioLegend	121402	BX041	Atto550	5250008
PD-L1	10F.9G2	BioLegend	124302	BX017	Atto550	5250001
CD107a	1D4B	BioLegend	121602	BX035	Atto550	5250007
CD206	C068C2	BioLegend	141702	BX023	Atto550	5250003

Table 2: List of antibodies provided conjugated by AKOYA.

Antigen	Clone	Supplier	Barcode	Reporter	Cat#
CD11c	N418	BioLegend	BX030	Cy5	4350013
CD3	17A2	BioLegend	BX021	Cy5	4350014
Ly6G	1A8	BioLegend	BX024	Cy5	4350015
CD45	30-F11	BioLegend	BX007	AF488	4150002
CD11b	M1/70	BioLegend	BX025	AF488	4150015
CD31	MEC13.3	BioLegend	BX002	Atto550	4250001
CD44	IM7	BioLegend	BX005	Atto550	4250002

MHCII	M5/114.15.2	BioLegend	BX014	Atto550	4250003
CD19	6D5	BioLegend	BX020	Atto550	4250014
CD4	RM4-5	BioLegend	BX026	Atto550	4250016
CD8a	53-6.7	BioLegend	BX029	Atto550	4250017
Ki67	B56	BD Biosciences	BX047	Atto550	4250019

Table 3: List of self-conjugated antibodies.

2.2.5.15 Interaction analysis

Interaction counts between main cell populations (contact defined as <50 µm proximity) were used for further analysis. The cluster “L” containing lymph vessels was excluded from further analysis, because of the very distinct localization of its cells as small vessels. Expected interaction counts for each cell-cell interaction pair were calculated as:

$$expectedInteractions_{CellA_CellB} = interactions_{allCells} * frequency_{CellA} * frequency_{CellB}$$

Next a negative-binomial generalized linear model for the interaction counts with an offset of $\log(expectedInteractions)$ was generated in R 4.0.2. The mathematical interaction terms between cell-cell type comparison (e.g. DC_vs_CD8) and experimental condition (untreated, AdV5-empty, AdV5-IL12) were used to calculate odds ratios and p-values for changes in cell-cell type interactions between experimental conditions. Odds ratios for different subsets of immune cells were plotted using ggplot2.

2.2.5.16 Intra-tumoral and systemic cytokine measurements

Serum was collected in EDTA containing tubes (Sarstedt) and IL-12 levels were determined using the IL-12 p70 Mouse Uncoated ELISA Kit (Invitrogen). Isolated tumors were snap-frozen on dry ice. Before thawing, a 5 mm metal bead and 1 ml of lysis buffer (20 mM Tris HCl (pH 7.5), 0.5% Tween 20, 150 mM NaCl, Sigma protease inhibitors 1:100) were added to the tubes. Tumors were lysed using a TissueLyser (Qiagen) for 5 min at 25 Hz. After centrifugation, protein concentrations were determined with the Pierce BCA Protein Assay Kit (Thermo Scientific). CCL5 concentration in the tumor lysates were analyzed by ELISA (Mouse RANTES Uncoated ELISA Kit Invitrogen) and normalized to the determined total protein concentrations.

2.2.5.17 Patients and sample preparation

Surgical specimens were mechanically dissociated, digested with accutase (PAA Laboratories), collagenase IV (Worthington), hyaluronidase (MilliporeSigma), and DNase type I (MilliporeSigma), filtered, washed and frozen as single cell suspension for future use. For human *ex vivo* tumor cultures, surgical specimens were dissected into tumor fragments and frozen for future use.

Human PBMCs were isolated by density gradient centrifugation using Histopaque-1077 (MilliporeSigma) from buffy coats obtained from healthy blood donors (Blood Bank, University Hospital Basel). PBMCs were frozen for later use in liquid nitrogen. Ethics approval was obtained from the local ethical committee to analyze the tissue and blood samples (Ethikkommission Nordwestschweiz) and written informed consent was obtained from all patients prior to sample collection.

2.2.5.18 *Ex vivo* human immune cells and tumor co-culture experiments

Healthy donor PBMCs or tumor digest samples, processed as described above, were co-cultured with OVCAR3 human ovarian cancer cell line, similarly to as described in Natoli *et al.* 2020. Briefly, 6000 OVCAR3 cells were seeded on the wells of a flat-bottom 96-well plate in RPMI containing L-glutamine (R8758, Sigma-Aldrich), supplemented with penicillin/streptomycin (100 ng/ml, Sigma-Aldrich) and 10% FBS (Sigma-Aldrich). After 2 hours, the medium was replaced with fully supplemented RPMI containing AdV5-hu-IL12 or empty vector control (AdV5-control) at a PFU of 1000/cell. Additional control wells were left untreated. After 2 hours of incubation, the medium was replaced to remove the virus and the tumor cells were incubated for 2 days at 37°C, 5% CO₂. 300,000 healthy donor PBMCs or single cells from tumor digest samples were then added to the wells of the 96-well plate in a final volume of 200 µl per well. Tumor cell (OVCAR3) viability was assessed by an MTT assay and flow cytometry was conducted on the suspension cells (PBMCs, TILs) after 3 days of co-culture. The supernatant was collected after 6 days of co-culture to assess IFN γ and CCL5 levels using a Human IFN γ ELISA Set (BD OptEIA, 555142) and ELISA MAXTM Deluxe Set Human CCL5 (Biolegend, 440804), respectively, according to the manufacturers' instructions.

2.2.5.19 *Ex vivo* tumor fragment culture

Tumor fragment cultures were prepared as described in Voabli *et al.* in press. Briefly, frozen patient tumor fragments were slowly thawed at 37°C and extensively washed in PBS and warm RPMI medium containing L-glutamine (R8758, Sigma-Aldrich), supplemented with penicillin/streptomycin (100 ng/ml, Sigma-Aldrich), 10% FBS (Sigma-Aldrich), 1x MEM Non-Essential Amino Acids (Gibco) and 1 mM sodium pyruvate (Sigma-Aldrich).

Single tumor fragments were then embedded in a total of 80 µl of an artificial extracellular matrix within the wells of a flat-bottom 96-well plate. The extracellular matrix was prepared by mixing ice-cold sodium bicarbonate (Sigma; 1.1% final concentration), collagen I (Corning; 1 mg/ml final concentration) and fully supplemented RPMI with ice-cold matrigel (Matrix High Concentration, Phenol Red-Free, BD Biosciences; 4 mg/ml final concentration). 40 µl of matrix was solidified by incubation at 37°C for 20-30 min. One tumor fragment per well was placed on top of the pre-

solidified matrix, after which a second layer of 40 µl matrix was added. Plates were then placed in a 37°C incubator for further 20-30 min. 110 µl of fully supplemented RPMI was added on top of the matrix. 1 mio PFU of Adv5-hu-IL12 or control Adv5-control or nivolumab (10 µg/ml final concentration) were added to each well containing individual tumor fragments. Between 6-12 fragments were used for each treatment conditions. After 48 hours of incubation at 37°C, the fragments were pooled and enzymatically digested and filtered into single cell suspensions, as described above. Flow cytometry was conducted and the supernatant was collected from each well to assess IFN γ and CCL5 levels using a Human IFN γ ELISA Set (BD OptEIA, 555142) and ELISA MAX™ Deluxe Set Human CCL5 (Biolegend, 440804), respectively, according to the manufacturers' instructions.

2.2.5.20 MTT assay

To assess tumor cell viability in co-culture experiments, an MTT assay was used as follows. The medium from the co-culture wells was removed and the wells were gently washed once with PBS to remove suspension cells. MTT (Sigma-Aldrich) was then added at 500 µg/ml and the tumor cells were incubated at 37°C for 2–3 hours. Formazan crystals were resuspended in 90 µl of dimethyl sulfoxide (DMSO; Sigma-Aldrich) and absorbance was measured at a wavelength of 570 nm.

2.2.5.21 Bioinformatic analysis of published gene expression data of human melanoma samples

We received the normalized Nanostring RNA expression data from the NCT01502293 trial (Oncosec), in which patients received IL-12-encoding mRNA by intra-tumoral electroporation (Algazi et al., 2019). The gene signatures for different immune sub-populations were retrieved from the PanCancerImmunology Nanostring panel. The transcripts within the “Cytotoxic cells” signature can't be attributed to a single cell type and are found in other signature lists of both NK and CD8 T cells. Therefore, its transcripts were merged with the cytotoxic NK and CD8 T cells resulting in the “Cytotoxic CD8+ T cells” and “Cytotoxic NK cells” signatures. Importantly, neither “Cytotoxic CD8+ T cells” and “Cytotoxic NK cells” contained the CCL5 transcript. Downstream analysis of all Nanostring data was performed using R version 4.0.2 and visualized in GraphPad Prism 9.

Immune cell infiltration was estimated by calculating a signature score as described by Cursons et al. 2019. Briefly, all transcripts for each sample were ordered by decreasing expression and the signature score was defined as:

$$1 - \frac{\text{mean rank of signature transcripts}}{\text{number of all transcripts}}$$

Thus, a high signature score indicates enrichment of signature transcripts among genes with high expression. To find genes that correlate with the Cytotoxic NK cells signature score, we performed a linear regression for signature scores with log-transformed transcript counts. p-values were adjusted by the Benjamini-Hochberg correction method.

We also reanalyzed RNAseq data of samples from tumor patients treated with anti-PD-1 antibodies (nivolumab; Riaz *et al.*, 2017) . Data was downloaded from the GEO under accession number GSE91061. Only patients with both pre- and post-treatment samples and evaluated responses were analyzed. Counts were normalized by library size using edgeR and displayed as log counts per million using GraphPad Prism 9. Paired two-way ANOVA with multiple comparisons and the post-hoc test were used to calculate significances for increased CCL5 expression upon treatment in CB. The availability of RNAseq data allowed the use of more complex gene signatures than with Nanostring data above. Therefore, we used the signatures described by Tirosh *et al* and Cursons *et al.* for this analysis (Souza-Fonseca-Guimaraes *et al.*, 2019; Tirosh *et al.*, 2016). As we wanted to correlate signatures with CCL5 expression, CCL5 was excluded from the T cell signature provided by Tirosh *et al.* 2016. Signature scores were calculated as described above.

2.2.5.22 Statistical analysis

For normally-distributed datasets, we used 2-tailed Student's t test and one-way ANOVA followed by Holm-Sidak multiple comparison test. When variables were not normally distributed, we performed non-parametric Mann-Whitney or Kruskal-Wallis tests. For survival analysis, p values were computed using the Log Rank test. Two-way ANOVA was used to compare tumor growth curves and grouped data sets. p values > 0.05 were considered not significant, p values < 0.05 were considered significant. * p value < 0.05, ** p value < 0.01, *** p value < 0.001, **** p value < 0.0001.

2.2.6 Acknowledgments

We thank members of the Cancer Immunology and Cancer Immunotherapy Laboratory at the Department of Biomedicine for helpful discussions and suggestions. We are grateful to A. Ignatenko and B. Simic for cloning viral constructs and to F. Weiss, and P. Freitag for producing and providing the biological reagents. We thank Priska Auf der Maur (University Hospital of Basel) for designing the graphical abstract. This work benefited from clinical data provided by OncoSec Medical Incorporated. This work was funded by the Schweizerische Nationalfonds Grant CRSII5_170929 to A.Z. and A.P., by the Schweizerische Nationalfonds Grant 320030_188576/1 to A.Z. and by the National Cancer Institute of the National Institutes of Health under award number F32CA189372 (to S.N.S.), and by the University of Zurich Forschungskredit 2017 ID 3761 (to D.B.).

2.2.7 Authors contributions

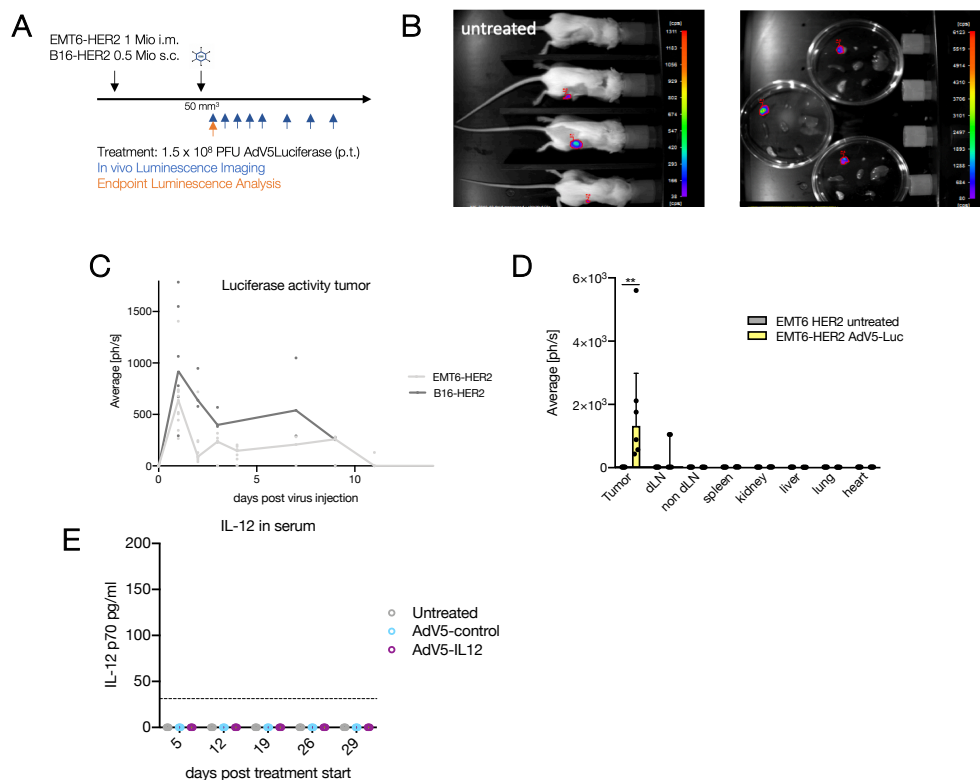
N.K. designed the study, performed experiments, analyzed data, and wrote the manuscript. M.P.T., M.N., F.W., V.K., M.B. and D.S.T. planned and performed experiments and generated and analyzed data. D.B., S.N.S., D.B., K.P.H and P.Z. designed, cloned or produced biological reagents. D.S. and E.B. processed and analyzed data. M.P.T., M.N., D.B., S.N.S., H.L., M.A.S., A.S.K. and A.P. provided input for research design and interpretation and edited the manuscript. A.Z. directed the study and wrote the manuscript. All authors reviewed and approved the manuscript.

2.2.8 Declaration of interests

The authors declare no competing interests.

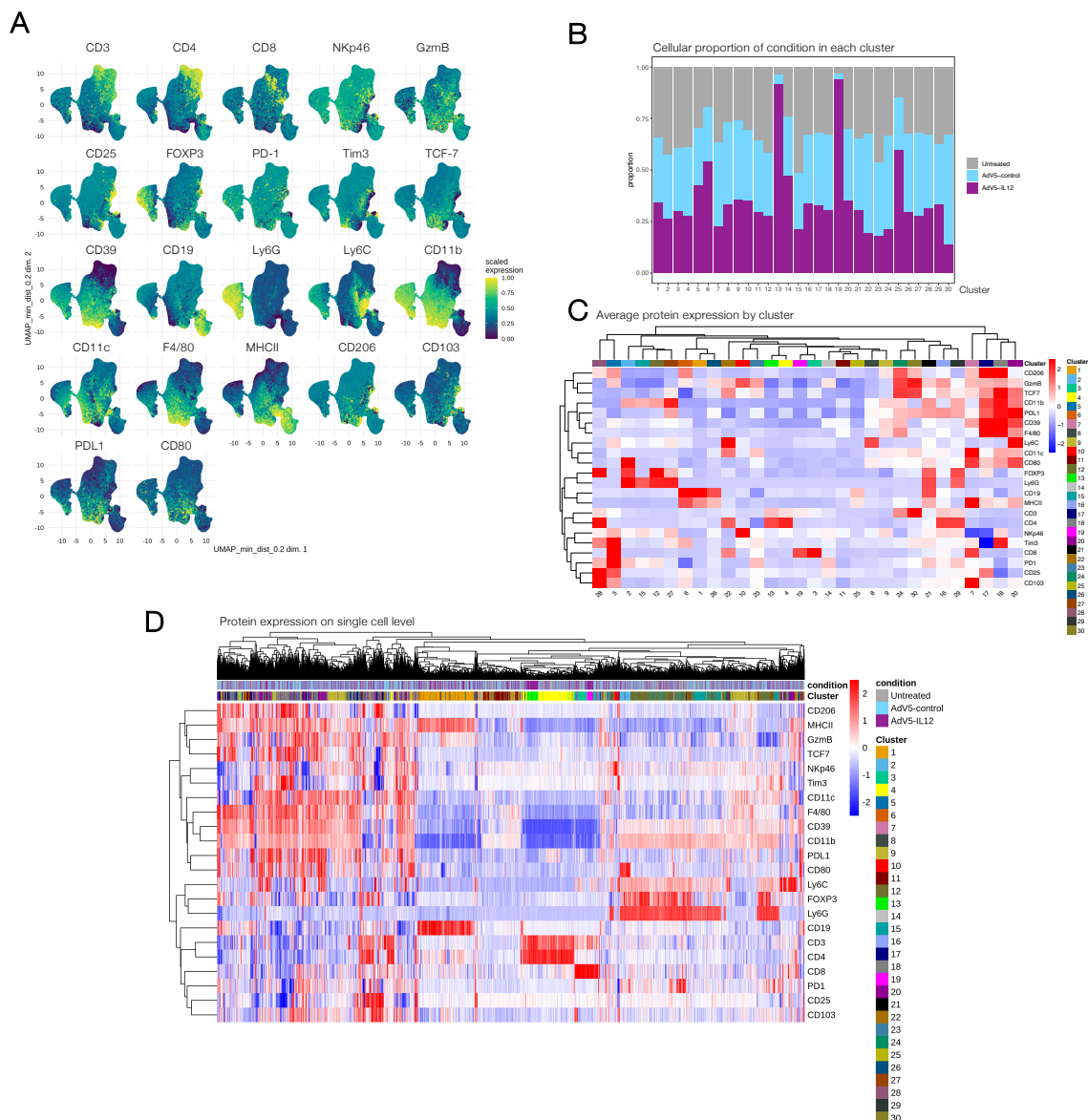
2.2.9 Supplementary figures

Figure S1: Related to Figure 1: Pharmacokinetics of HER2-targeted and shielded vectors



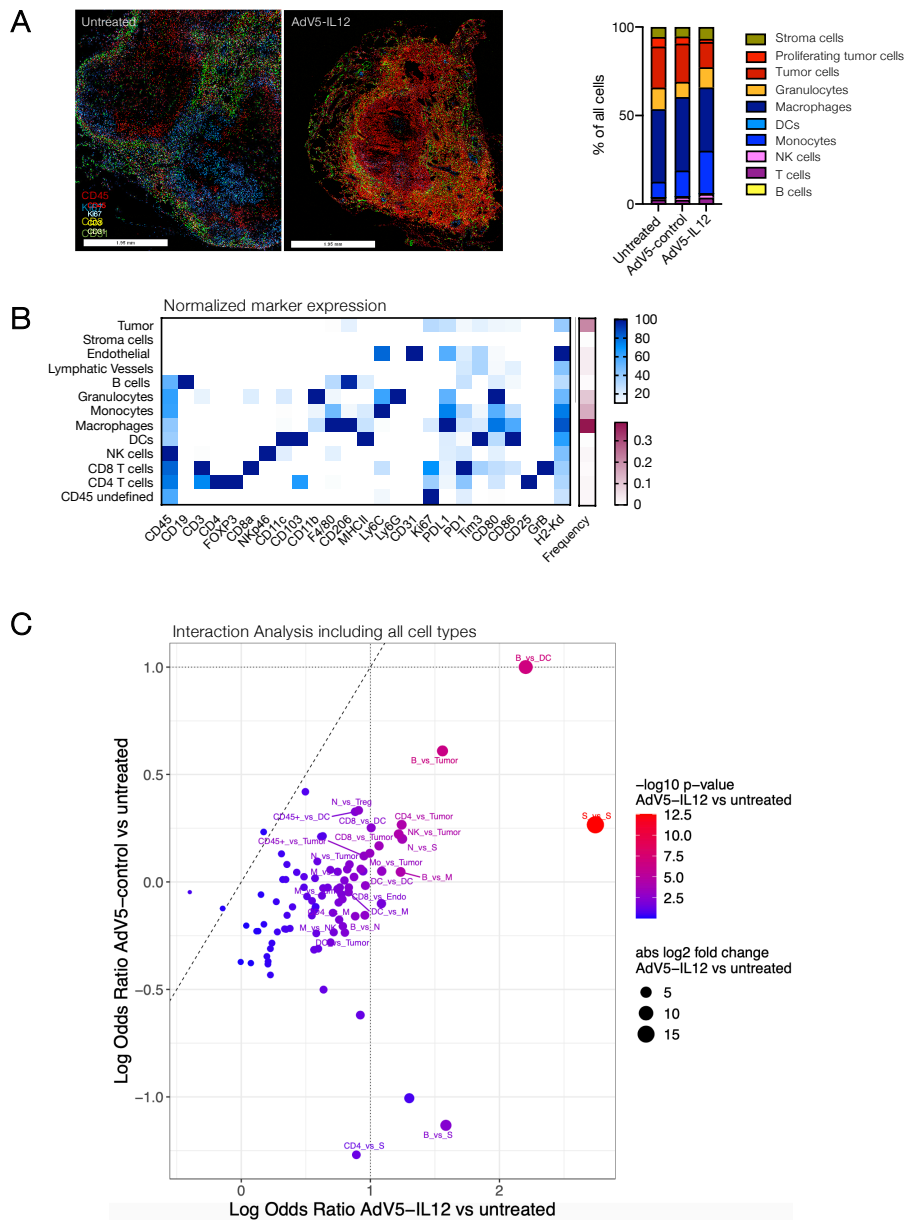
A-C: Wildtype (WT) mice were engrafted with 1 mio EMT6-HER2 (i.m.) or 0.5 mio B16-HER2 (s.c.). Mice were p.t. treated with AdV5-Luciferase on day 7 or day 11 (tumor size 30–70 mm³), respectively. The luciferase signal was live imaged at the indicated time points (blue arrows; day 1, 2, 3, 4, 5, 7, 9, 11 and 13 post virus injection). Representative luciferase signal in three treated and one untreated animal one day post AdV5-Luciferase injection are shown. After isolation of tumor, draining lymph node, non-draining lymph node, spleen, kidney, liver, heart and lung, luciferase signal was measured again. **C:** Quantification of *in vivo* luciferase signal in EMT6-HER2 (light grey) and B16-HER2 (dark grey) tumors. **D:** Quantification of luciferase signal one day post AdV5-Luciferase treatment in isolated indicated organs of EMT6-HER2 bearing mice. **A-D:** n= 6 mice per condition. *p < 0.05, **p < 0.01, ***p < 0.001, ****p < 0.0001. Error bar values represent SD. For comparisons between grouped data sets, two-way ANOVA with multiple comparisons was used. **E:** Wildtype (WT) mice were engrafted with 1 mio EMT6-HER2 intramammarily (i.m.). From day 7 (tumor size 30–70 mm³), mice were treated with 1.5x10⁸ PFU of HER2-targeted and shielded adenoviral vectors (peritumorally) encoding for IL-12 or empty control cassette (AdV5-control) on day 7, 9, 11 and 14. On the indicated days, serum was collected and IL-12 concentration was determined by ELISA. Dotted line denotes detection limit of the ELISA. Contribution: NK planned, organized, conducted and analyzed the experiments and prepared figure.

Figure S2: Related to Figure 2: Cellular consequences of AdV5-IL12 in EMT6-HER2:



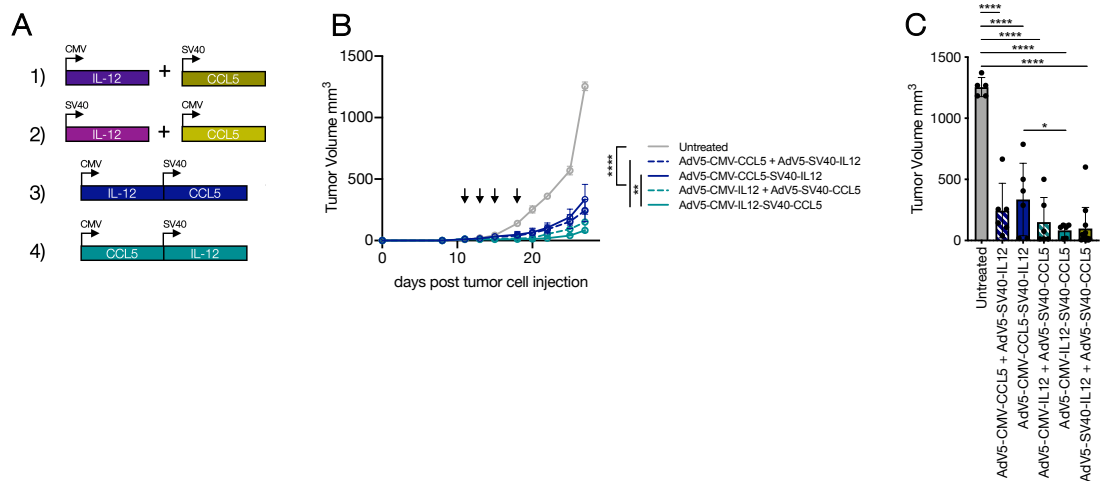
A-C: Wildtype (WT) mice were engrafted with 1 mio EMT6-HER2 intramammarily (i.m.). Starting from day 7 (tumor size 30–70 mm³), mice were treated with 1.5x10⁸ PFU of HER2-targeted and shielded adenoviral vectors (peritumorally) encoding IL-12 or empty control cassette (AdV5-control) on day 7, 9 and 11. On day 12 post inoculation, tumors were isolated and single cell suspensions were analyzed by flow cytometry. n= 5-6 mice per condition. **A:** UMAP-projection of pooled conditions showing expression analyzed proteins supporting cell-type assignments. **B:** Percentage of cells in each cluster by treatment. **C:** Heatmap showing average protein expression by cluster. **D:** Heatmap showing protein expression of 2 x 10⁴ random cells assigned to conditions (Untreated, AdV5-control or AdV5-IL12) and cluster. DS conducted clustering of multidimensional flow cytometry data. NK prepared figure.

Figure S3: Related to Figure 2: Interaction analysis after AdV5-IL12 treatment in EMT6-HER2:



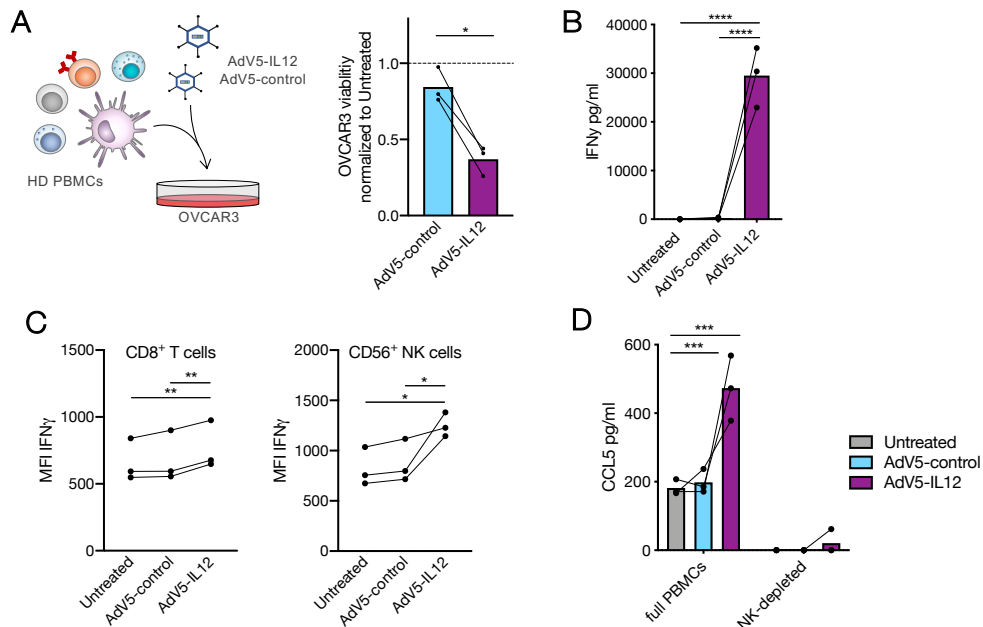
A-B: Wildtype (WT) mice were engrafted with 1 mio EMT6-HER2 intramammarily (i.m.). Starting from day 7 (tumor size 30–70 mm³), mice were treated with 1.5x10⁸ PFU of HER2-targeted and shielded adenoviral vectors (peritumorally) encoding for IL-12 or empty control cassette (AdV5-control) on day 7, 9 and 11. On day 12 post inoculation, tumors were isolated, embedded in OCT and analyzed by multiparameter immuno-fluorescence microscopy. n= 3 mice per condition. **A:** Representative IF pictures are showing untreated and AdV5-IL12 treated tumors (CD45: red, Ki67: blue, CD3: yellow, CD31: green) including quantification of main clusters between conditions. **B:** Heatmap showing normalized marker expression and frequency of identified main populations. **C:** Visualization of log odds ratios and p values for changes in all cell-cell type interactions between experimental conditions. Contribution: NK planned, organized, conducted and analyzed the experiments and prepared figure. MPT and EB assisted to analyze multi-dimensional microscopy analysis. FW established CODEX methodology under the supervision of NK.

Figure S4: Related to Figure 4: Design of combinatorial adenoviral vectors:



A: Design of combinatorial vectors compared to mixture of single viruses. **B-C:** Mice were treated with each 1.5×10^8 PFU AdV5-IL12 and AdV5-CCL5 or 1.5×10^8 PFU combinatorial vectors on day 11, 13, 15 and 18 (tumor size 30–70 mm³) after B16-HER2 inoculation as indicated (black arrows). **B:** Tumor growth curves are shown. **C:** Quantification of tumor volume on day 27 post tumor inoculation. **B-C:** n = 5-6 mice per condition. *p < 0.05, **p < 0.01, ***p < 0.001, ****p < 0.0001. Error bar values represent SD or SEM (tumor growth curves). For comparisons between three or more groups, one-way ANOVA with multiple comparisons was used. Two-way ANOVA was used to compare tumor growth curves. Contribution: DB and SNS cloned viral constructs. NK planned, organized, conducted and analyzed the experiments and prepared figure.

Figure S5: Related to Figure 6: AdV5-hu-IL12 induces CCL5 expression in human co-cultures:



A-D: Healthy donor PBMCs were co-cultured with OVCAR-3 cells which were transduced with HER2-targeted AdV5 encoding human IL-12 or control virus. **B:** Quantification of OVCAR-3 viability normalized to untreated co-cultures after 96h. **C:** IFN γ expression was determined in supernatants after 5 d. **C:** IFN γ expression (MFI) in CD8 T cells and NK cells after 96 h. **D:** CCL5 expression in supernatants of co-cultures with full PBMCs or NK-depleted PBMCs after 5 d. **A-D:** n = each 3 donors. *p < 0.05, **p < 0.01, ***p < 0.001, ****p < 0.0001. 2-tailed paired Student's t test was used. For comparisons between three or more groups, paired one-way ANOVA with multiple comparisons was used. Contribution: NK and MN planned, organized and conducted experiments. NK analyzed data and prepared figure.

3 Summary

In spite of clinical success, cancer immunotherapy still fails to evoke durable tumor rejection in the vast majority of patients. While the current treatment modalities are predominantly T cell-centric, leaving aside the impact of innate immunity, recent evidence has highlighted the fundamental role of innate immune cells in orchestrating cancer immunity.

In this work, I present how enhanced anti-cancer immunity can be achieved by rationally engaging key cellular interplays of both adaptive and innate immunity utilizing adenoviral vectors: First, I introduce a modular assembly system for the efficient generation and production of high-capacity adenoviral vectors as a platform for tumor-targeted cancer immunotherapy. As proof of concept, we show that a single HCA₂ encoding the cytokines IL-2, IL-12, as well as an anti-PD-1 antibody, yielded comparable amounts of payloads produced by a mixture of single-payload HCA₂s, and resulted in equal tumor regression and prolonged survival in tumor mouse models.

Second, I present work which aims to assess the potential of these vectors to improve cancer immunotherapy by augmenting anti-tumorigenic T cell- NK cell- DC crosstalk. In detail, I here describe the following major findings: (1) IL-12, induced by an engineered viral vector for tumor-targeting, enforces a tumor-eliminating positive feedback loop, enhances CD8 T cell-DC interactions and achieves protective immunity, (2) intra-tumoral NK cells producing cDC1 attractants such as CCL5 are required for IL-12-mediated tumor rejection, and (3) attraction of cDC1s by local delivery of CCL5 can compensate for the lack of NK cell function and boost responses to IFN γ -inducing therapies, such as IL-12 and immune checkpoint inhibition (ICI).

This work provides evidence that lack of intra-tumoral cDC1 recruitment by NK cells represents a major barrier for T cell-based therapies. It will be exciting to determine if and which tumor-derived factors might mediate resistance by limiting functionality of DCs and NK cells within the tumor microenvironment. In addition, identifying such factors will help to define predictive markers for T cell-focused therapies, such as ICI and provide new avenues beyond CCL5 to improve their efficacy by rationally designing combinatorial therapies.

4 Acknowledgements

First of all, I would like to thank Alfred Zippelius for accommodating, accompanying, supporting and encouraging me over the last years. Thank you for giving me the right tasks at the right moments to push my boundaries.

I owe special thanks to Abhishek Kashyap, who supervised me in the first years of my PhD. Thank you for sharing all your knowledge and expertise about science with me, as well as pointing out the importance of personal development outside of the lab.

I would like to thank all the members of the cancer immunology and cancer immunotherapy labs. Thank you for all your help, input, discussions, lunch breaks and time we spent outside of the lab. Working with you has always been very productive and enjoyable at the same time.

Special thanks go to Marcel Trefny, Laura Fernandez Rodriguez and Dominic Schmid for all our fruitful collaborations, intense discussions, the input you gave me and for cheering me up when I needed it.

I would also especially like to thank our technicians, Béatrice Dolder, Petra Herzig, Mélanie Buchi and Reto Ritschard for your immense help and for keeping the lab running.

Thank you, Franziska Werner and Victoria Koch for being such amazing master students. I really enjoyed the time we worked and spend together (including all our other master/MD students: Nicolai, Mirza, Emanuele, Adrian and Eva). You will do well in the future, I'm sure!

Another particular thank you goes to all my collaboration partners, especially the Plückthun Lab in Zurich, in particular Dominik Brücher and Sheena Smith, the Pinschewer Lab, the Hess Lab, especially to Jonas Lötscher and Adrià Martí i Líndez, and to Ewelina Bartoszek and David Schreiner. Thank you for all your help, scientific exchange and insights into new projects.

I am very grateful to the members of my PhD advisory committee and my external experts: Christoph Hess, Mikaël Pittet, Anja Wege and Jan Böttcher for taking the time to discuss my projects constructively.

Besides all this scientific help, I want to acknowledge my friends, especially Sabine Winkler, Sophia Wiedemann, Theresa Rohm, Alexandra Kosareva and Natalia Rodrigues Mantuano. Thank you for the phenomenal hours we spent chatting, dancing, laughing, crying, gaming, traveling, cooking and enjoying life. #Basel2024

Finally, I would like to thank my parents, Hans and Brigitte Kirchhammer, as well as my sister Isabel Dintner (including Tim, Valentin and Felix). Thank you for always supporting me and accepting my decisions. I could not imagine a better family.

And thank you Michal, for all your scientific input and for creating our own perfect little world.

5 References

- Ahmadzadeh, M., and Rosenberg, S.A. (2006). IL-2 administration increases CD4⁺CD25^{hi} Foxp3⁺ regulatory T cells in cancer patients. *Blood* 107, 2409–2414.
- Akbari, P., Huijbers, E.J.M., Themeli, M., Griffioen, A.W., and van Beijnum, J.R. (2019). The tumor vasculature an attractive CAR T cell target in solid tumors. *Angiogenesis* 22, 473–475.
- Algazi, A., Bhatia, S., Agarwala, S., Molina, M., Lewis, K., Faries, M., Fong, L., Levine, L.P., Franco, M., Oglesby, A., et al. (2019). Intratumoral delivery of tavokinogene telseplasmid yields systemic immune responses in metastatic melanoma patients. *Ann. Oncol.*
- Algazi, A.P., Twitty, C.G., Tsai, K.K., Le, M., Pierce, R., Browning, E., Hermiz, R., Canton, D.A., Bannavong, D., Oglesby, A., et al. (2020). Phase II Trial of IL-12 Plasmid Transfection and PD-1 Blockade in Immunologically Quiescent Melanoma. *Clin. Cancer Res.* 26, 2827–2837.
- Allen, R.J., and Byrnes, A.P. (2019). Interaction of adenovirus with antibodies, complement, and coagulation factors. *FEBS Lett.* 593, 3449–3460.
- Ansell, S.M., Lesokhin, A.M., Borrello, I., Halwani, A., Scott, E.C., Gutierrez, M., Schuster, S.J., Millenson, M.M., Cattray, D., Freeman, G.J., et al. (2015). PD-1 blockade with nivolumab in relapsed or refractory Hodgkin's lymphoma. *N. Engl. J. Med.* 372, 311–319.
- Arduin, E., Arora, S., Bamert, P.R., Kuiper, T., Popp, S., Geisse, S., Grau, R., Calzascia, T., Zenke, G., and Kovarik, J. (2015). Highly reduced binding to high and low affinity mouse Fc gamma receptors by L234A/L235A and N297A Fc mutations engineered into mouse IgG2a. *Mol. Immunol.* 63, 456–463.
- Ayers, M., Luceford, J., Nebozhyn, M., Murphy, E., Loboda, A., Kaufman, D.R., Albright, A., Cheng, J.D., Kang, S.P., Shankaran, V., et al. (2017). IFN- γ -related mRNA profile predicts clinical response to PD-1 blockade. *J. Clin. Invest.* 127, 2930–2940.
- Baitsch, L., Baumgaertner, P., Devèvre, E., Raghav, S.K., Legat, A., Barba, L., Wieckowski, S., Bouzourene, H., Deplancke, B., Romero, P., et al. (2011). Exhaustion of tumor-specific CD8⁺ T cells in metastases from melanoma patients. *J. Clin. Invest.* 121, 2350–2360.
- Baker, A.T., Aguirre-Hernández, C., Haldén, G., and Parker, A.L. (2018). Designer oncolytic adenovirus: Coming of age. *Cancers (Basel)*. 10, 201.
- Barry, K.C., Hsu, J., Broz, M.L., Cueto, F.J., Binnewies, M., Combes, A.J., Nelson, A.E., Loo, K., Kumar, R., Rosenblum, M.D., et al. (2018). A natural killer–dendritic cell axis defines checkpoint therapy–responsive tumor microenvironments. *Nat. Med.* 24, 1178–1191.
- Barry, M.A., Rubin, J.D., and Lu, S.C. (2020). Retargeting adenoviruses for therapeutic applications and vaccines. *FEBS Lett.* 594, 1918–1946.
- Bjorklund, T. (2018). Repairing the brain: Gene therapy. *J. Parkinsons. Dis.* 8, S123–S130.
- Blank, C.U., Haining, W.N., Held, W., Hogan, P.G., Kallies, A., Lugli, E., Lynn, R.C., Philip, M., Rao, A., Restifo, N.P., et al. (2019). Defining 'T cell exhaustion.' *Nat. Rev. Immunol.* 19, 665–674.
- Bots, S.T.F., and Hoeben, R.C. (2020). Non-human primate-derived adenoviruses for future use as oncolytic agents? *Int. J. Mol. Sci.* 21, 1–20.
- Böttcher, J.P., and Reis e Sousa, C. (2018). The Role of Type 1 Conventional Dendritic Cells in Cancer Immunity. *Trends in Cancer* 4, 784–792.
- Böttcher, J.P., Bonavita, E., Chakravarty, P., Blees, H., Cabeza-Cabrerizo, M., Sammicheli, S., Rogers, N.C., Sahai, E., Zelenay, S., and Reis e Sousa, C. (2018). NK Cells Stimulate Recruitment of cDC1 into the Tumor Microenvironment Promoting Cancer Immune Control. *Cell* 172, 1022–1037.e14.
- Bronger, H., Singer, J., Windmüller, C., Reuning, U., Zech, D., Delbridge, C., Dorn, J., Kiechle, M., Schmalfeldt, B., Schmitt, M., et al. (2016). CXCL9 and CXCL10 predict survival and are regulated by cyclooxygenase inhibition in advanced serous ovarian cancer. *Br. J. Cancer* 115, 553–563.
- Brücher, D., Franc, V., Smith, S.N., Heck, A.J.R., and Plückthun, A. (2020). Malignant tissues produce divergent antibody glycosylation of relevance for cancer gene therapy effectiveness. *MAbs*.

- Brücher, D., Kirchhammer, N., Smith, S.N., Schumacher, J., Schumacher, N., Kolibius, J., Freitag, P.C., Schmid, M., Weiss, F., Keller, C., et al. (2021). iMATCH - an integrated modular assembly-system for therapeutic 2 combination high-capacity adenovirus gene therapy. *Mol. Ther. - Methods Clin. Dev.*
- Brummelman, J. (2018). High-dimensional single cell analysis identifies stem-like cytotoxic CD8+ T cells infiltrating human tumors. *J. Exp. Med.* *215*, 2520–2535.
- Brunetti-Pierri, N., Palmer, D.J., Beaudet, A.L., Carey, K.D., Finegold, M., and Ng, P. (2004). Acute Toxicity after High-Dose Systemic Injection of Helper-Dependent Adenoviral Vectors into Nonhuman Primates. *Hum. Gene Ther.* *15*, 35–46.
- Brunetti-Pierri, N., Ng, T., Iannitti, D., Cioffi, W., Stapleton, G., Law, M., Breinholt, J., Palmer, D., Grove, N., Rice, K., et al. (2013). Transgene expression up to 7 years in nonhuman primates following hepatic transduction with helper-dependent adenoviral vectors. *Hum. Gene Ther.* *24*, 761–765.
- Cabeza-Cabrerizo, M., van Blijswijk, J., Wienert, S., Heim, D., Jenkins, R.P., Chakravarty, P., Rogers, N., Frederico, B., Acton, S., Beerling, E., et al. (2019). Tissue clonality of dendritic cell subsets and emergency DCpoiesis revealed by multicolor fate mapping of DC progenitors. *Sci. Immunol.* *4*.
- Casagrande, N., Borghese, C., Visser, L., Mongiat, M., Colombatti, A., and Aldinucci, D. (2019). CCR5 antagonism by maraviroc inhibits hodgkin lymphoma microenvironment interactions and xenograft growth. *Haematologica* *104*, 564–575.
- Cavazzana-Calvo, M., Hacein-Bey, S., De Saint Basile, G., Gross, F., Yvon, E., Nusbaum, P., Selz, F., Hue, C., Certain, S., Casanova, J.L., et al. (2000). Gene therapy of human severe combined immunodeficiency (SCID)-X1 disease. *Science (80-.)*. *288*, 669–672.
- Chahal, P.S., Schulze, E., Tran, R., Montes, J., and Kamen, A.A. (2014). Production of adeno-associated virus (AAV) serotypes by transient transfection of HEK293 cell suspension cultures for gene delivery. *J. Virol. Methods* *196*, 163–173.
- Chan, K.K., and Bass, A.R. (2020). Autoimmune complications of immunotherapy: pathophysiology and management. *BMJ* *369*.
- Chen, D.S., and Mellman, I. (2013). Oncology meets immunology: The cancer-immunity cycle. *Immunity* *39*, 1–10.
- Chng, J., Wang, T., Nian, R., Lau, A., Hoi, K.M., Ho, S.C.L., Gagnon, P., Bi, X., and Yang, Y. (2015). Cleavage efficient 2A peptides for high level monoclonal antibody expression in CHO cells. *MAbs* *7*, 403–412.
- Cornish, G.H., Sinclair, L. V., and Cantrell, D.A. (2006). Differential regulation of T-cell growth by IL-2 and IL-15. *Blood* *108*, 600–608.
- Coughlan, L. (2020). Factors Which Contribute to the Immunogenicity of Non-replicating Adenoviral Vected Vaccines. *Front. Immunol.* *11*, 909.
- Cursons, J. (2019). A gene signature predicting natural killer cell infiltration and improved survival in melanoma patients. *Cancer Immunol. Res.* *7*, 1162–1174.
- Cursons, J., Souza-Fonseca-Guimaraes, F., Foroutan, M., Anderson, A., Hollande, F., Hediye-Zadeh, S., Behren, A., Huntington, N.D., and Davis, M.J. (2019). A gene signature predicting natural killer cell infiltration and improved survival in melanoma patients. *Cancer Immunol. Res.* *7*, 1162–1174.
- D'Amico, L., Menzel, U., Prummer, M., Müller, P., Buchi, M., Kashyap, A., Haessler, U., Yermanos, A., Gébleux, R., Briendl, M., et al. (2019). A novel anti-HER2 anthracycline-based antibody-drug conjugate induces adaptive anti-tumor immunity and potentiates PD-1 blockade in breast cancer. *J. Immunother. Cancer* *7*, 16.
- Danthinne, X., and Imperiale, M.J. (2000). Production of first generation adenovirus vectors: A review. *Gene Ther.* *7*, 1707–1714.
- Day, D., and Siu, L.L. (2016). Approaches to modernize the combination drug development paradigm. *Genome Med.* *8*, 1–14.
- Debré, P., Combadiere, B., Boissonnas, A., Bonduelle, O., Maho, M., Lavergne, E., Combadière, C., and

- Iga, M. (2021). Increases Tumor Cell Infiltration Overexpression Delays Tumor Growth and Intratumoral CC Chemokine Ligand 5. *J Immunol Ref.* 173, 3755–3762.
- Diab, A., Tannir, N.M., Bentebibel, S.E., Hwu, P., Papadimitrakopoulou, V., Haymaker, C., Kluger, H.M., Gettinger, S.N., Sznol, M., Tykodi, S.S., et al. (2020). Bempegaldesleukin (NKTR-214) plus nivolumab in patients with advanced solid tumors: Phase I dose-escalation study of safety, efficacy, and immune activation (PIVOT-02). *Cancer Discov.* 10, 1158–1173.
- DiMasi, J.A., and Grabowski, H.G. (2007). Economics of new oncology drug development. *J. Clin. Oncol.* 25, 209–216.
- Dormond, E., and Kamen, A.A. (2011). Manufacturing of adenovirus vectors: production and purification of helper dependent adenovirus. *Methods Mol. Biol.* 737, 139–156.
- Dreier, B., and Plückthun, A. (2012). Rapid selection of high-affinity binders using ribosome display. *Methods Mol. Biol.* 805, 261–286.
- Dreier, B., Honegger, A., Hess, C., Nagy-Davidescu, G., Mittl, P.R.E., Grütter, M.G., Belousova, N., Mikheeva, G., Krasnykh, V., and Plückthun, A. (2013). Development of a generic adenovirus delivery system based on structure-guided design of bispecific trimeric DARPin adapters. *Proc. Natl. Acad. Sci. U. S. A.* 110.
- Dunn, G.P., Old, L.J., and Schreiber, R.D. (2004). The immunobiology of cancer immunosurveillance and immunoediting. *Immunity* 21, 137–148.
- Dutcher, J.P., Schwartzentruber, D.J., Kaufman, H.L., Agarwala, S.S., Tarhini, A.A., Lowder, J.N., and Atkins, M.B. (2014). High dose interleukin-2 (Aldesleukin) - expert consensus on best management practices-2014. *J. Immunother. Cancer* 2, 26.
- Egen, J.G., and Allison, J.P. (2002). Cytotoxic T lymphocyte antigen-4 accumulation in the immunological synapse is regulated by TCR signal strength. *Immunity* 16, 23–35.
- Ehrke-Schulz, E., Zhang, W., Schiwon, M., Bergmann, T., and Solanki, M. (2016). Cloning and large-scale production of high-capacity adenoviral vectors based on the human adenovirus type 5. *J. Vis. Exp.* 1–15.
- Ehrke-Schulz, E., Schiwon, M., Leitner, T., Dávid, S., Bergmann, T., Liu, J., and Ehrhardt, A. (2017). CRISPR/Cas9 delivery with one single adenoviral vector devoid of all viral genes. *Sci. Rep.* 7, 17113.
- El-Kenawi, A.E., and El-Remessy, A.B. (2013). Angiogenesis inhibitors in cancer therapy: Mechanistic perspective on classification and treatment rationales. *Br. J. Pharmacol.* 170, 712–729.
- Emerman, M., and Temin, H.M. (1984). Genes with promoters in retrovirus vectors can be independently suppressed by an epigenetic mechanism. *Cell* 39, 459–467.
- Fang, J., Qian, J.J., Yi, S., Harding, T.C., Tu, G.H., VanRoey, M., and Jooss, K. (2005). Stable antibody expression at therapeutic levels using the 2A peptide. *Nat. Biotechnol.* 23, 584–590.
- Fang, J., Yi, S., Simmons, A., Tu, G.H., Nguyen, M., Harding, T.C., VanRoey, M., and Jooss, K. (2007). An antibody delivery system for regulated expression of therapeutic levels of monoclonal antibodies *In Vivo*. *Mol. Ther.* 15, 1153–1159.
- Fausther-Bovendo, H., and Kobinger, G.P. (2014). Pre-existing immunity against Ad vectors: Humoral, cellular, and innate response, what's important? *Hum. Vaccines Immunother.* 10, 2875–2884.
- Fehniger, T.A., Cooper, M.A., Nuovo, G.J., Cella, M., Facchetti, F., Colonna, M., and Caligiuri, M.A. (2003). CD56bright natural killer cells are present in human lymph nodes and are activated by T cell-derived IL-2: A potential new link between adaptive and innate immunity. *Blood* 101, 3052–3057.
- Flavahan, W.A., Gaskell, E., and Bernstein, B.E. (2017). Epigenetic plasticity and the hallmarks of cancer. *Science* (80-.). 357.
- Flynn, R., Buckler, J.M., Tang, C., Kim, F., and Dichek, D.A. (2010). Helper-dependent adenoviral vectors are superior in vitro to first-generation vectors for endothelial cell-targeted gene therapy. *Mol. Ther.* 18, 2121–2129.
- Galluzzi, L., Chan, T.A., Kroemer, G., Wolchok, J.D., and López-Soto, A. (2018). The hallmarks of successful anticancer immunotherapy. *Sci. Transl. Med.* 10.

- Galon, J., and Bruni, D. (2019). Approaches to treat immune hot, altered and cold tumours with combination immunotherapies. *Nat. Rev. Drug Discov.* 18, 197–218.
- Gao, J., Mese, K., Bunz, O., and Ehrhardt, A. (2019). State-of-the-art human adenovirus vectorology for therapeutic approaches. *FEBS Lett.* 593, 3609–3622.
- Gardner, A., de Mingo Pulido, Á., and Ruffell, B. (2020). Dendritic Cells and Their Role in Immunotherapy. *Front. Immunol.* 11, 1–14.
- Garon, E.B., Rizvi, N.A., Hui, R., Leighl, N., Balmanoukian, A.S., Eder, J.P., Patnaik, A., Aggarwal, C., Gubens, M., Horn, L., et al. (2015). Pembrolizumab for the treatment of non-small-cell lung cancer. *N. Engl. J. Med.* 372, 2018–2028.
- Garrido, F., Ruiz-Cabello, F., Cabrera, T., Pérez-Villar, J.J., López-Botet, M., Duggan-Keen, M., and Stern, P.L. (1997). Implications for immunosurveillance of altered HLA class I phenotypes in human tumours. *Immunol. Today* 18, 89–95.
- Garris, C.S., Arlauckas, S.P., Kohler, R.H., Trefny, M.P., Garren, S., Piot, C., Engblom, C., Pfirschke, C., Siwicki, M., Gungabeesoon, J., et al. (2018). Successful Anti-PD-1 Cancer Immunotherapy Requires T Cell-Dendritic Cell Crosstalk Involving the Cytokines IFN- γ and IL-12. *Immunity*.
- Gaspar, H.B., Parsley, K.L., Howe, S., King, D., Gilmour, K.C., Sinclair, J., Brouns, G., Schmidt, M., Kalle, C. Von, Barington, T., et al. (2004). Gene therapy of X-linked severe combined immunodeficiency by use of a pseudotyped gammaretroviral vector. *Lancet* 364, 2181–2187.
- Gerhard, G.M., Bill, R., Messemaker, M., Klein, A.M., and Pittet, M.J. (2021). Tumor-infiltrating dendritic cell states are conserved across solid human cancers. *J. Exp. Med.* 218.
- Gibson, D., Young, L., and Chuang, R. (2009). Enzymatic assembly of DNA molecules up to several hundred kilobases. *Nat. Methods* 6, 12–16.
- Giudicelli, V. (2006). IMGT/LIGM-DB, the IMGT(R) comprehensive database of immunoglobulin and T cell receptor nucleotide sequences. *Nucleic Acids Res.* 34, D781–D784.
- Goltsev, Y., Samusik, N., Kennedy-Darling, J., Bhate, S., Hale, M., Vazquez, G., Black, S., and Nolan, G.P. (2018). Deep Profiling of Mouse Splenic Architecture with CODEX Multiplexed Imaging. *Cell* 174, 968-981.e15.
- Gordon, K., Del Medico, A., Sander, I., Kumar, A., and Hamad, B. (2019). Gene therapies in ophthalmic disease. *Nat. Rev. Drug Discov.* 18, 415–416.
- Gorziglia, M.I., Lapceovich, C., Roy, S., Kang, Q., Kadan, M., Wu, V., Pechan, P., and Kaleko, M. (1999). Generation of an Adenovirus Vector Lacking E1, E2a, E3, and All of E4 except Open Reading Frame 3. *J. Virol.* 73, 6048–6055.
- Goswami, R., Subramanian, G., Silayeva, L., Newkirk, I., Doctor, D., Chawla, K., Chattopadhyay, S., Chandra, D., Chilukuri, N., and Betapudi, V. (2019). Gene therapy leaves a vicious cycle. *Front. Oncol.* 9, 297.
- Greber, U.F. (2020). Adenoviruses – Infection, pathogenesis and therapy. *FEBS Lett.* 594, 1818–1827.
- Greber, U.F., and Flatt, J.W. (2019). Adenovirus entry: From infection to immunity. *Annu. Rev. Virol.* 6, 177–197.
- Hanahan, D., and Weinberg, R.A. (2011). Hallmarks of cancer: The next generation. *Cell* 144, 646–674.
- Haryadi, R., Ho, S., Kok, Y.J., Pu, H.X., Zheng, L., Pereira, N.A., Li, B., Bi, X., Goh, L.T., Yang, Y., et al. (2015). Optimization of heavy chain and light chain signal peptides for high level expression of therapeutic antibodies in CHO cells. *PLoS One* 10, 1–16.
- Haslam, A., and Prasad, V. (2019). Estimation of the percentage of US patients with cancer who are eligible for and respond to checkpoint inhibitor immunotherapy drugs. *JAMA Netw. Open* 2, e192535.
- He, T.C., Zhou, S., Da Costa, L.T., Yu, J., Kinzler, K.W., and Vogelstein, B. (1998). A simplified system for generating recombinant adenoviruses. In *Proceedings of the National Academy of Sciences of the United States of America*, (National Academy of Sciences), pp. 2509–2514.

- Hegde, P.S., and Chen, D.S. (2020). Top 10 Challenges in Cancer Immunotherapy. *Immunity* 52, 17–35.
- Hellmann, M.D., Paz-Ares, L., Bernabe Caro, R., Zurawski, B., Kim, S.-W., Carcereny Costa, E., Park, K., Alexandru, A., Lupinacci, L., de la Mora Jimenez, E., et al. (2019). Nivolumab plus Ipilimumab in Advanced Non–Small-Cell Lung Cancer. *N. Engl. J. Med.* 381, 2020–2031.
- Herberman, R.B., Nunn, M.E., Holden, H.T., and Lavrin, D.H. (1975). Natural cytotoxic reactivity of mouse lymphoid cells against syngeneic and allogeneic tumors. II. Characterization of effector cells. *Int. J. Cancer* 16, 230–239.
- Hildner, K., Edelson, B.T., Purtha, W.E., Diamond, M., Matsushita, H., Kohyama, M., Calderon, B., Schraml, B.U., Unanue, E.R., Diamond, M.S., et al. (2008). Batf3 deficiency reveals a critical role for CD8 α + dendritic cells in cytotoxic T cell immunity. *Science* (80-.). 322, 1097–1100.
- Hinrichs, C.S., Spolski, R., Paulos, C.M., Gattinoni, L., Kerstann, K.W., Palmer, D.C., Klebanoff, C.A., Rosenberg, S.A., Leonard, W.J., and Restifo, N.P. (2008). IL-2 and IL-21 confer opposing differentiation programs to CD8+ T cells for adoptive immunotherapy. *Blood* 111, 5326–5333.
- Huang, K.-W., Hsu, F.-F., Qiu, J.T., Chern, G.-J., Lee, Y.-A., Chang, C.-C., Huang, Y.-T., Sung, Y.-C., Chiang, C.-C., Huang, R.-L., et al. (2020). Highly efficient and tumor-selective nanoparticles for dual-targeted immunogene therapy against cancer. *Sci. Adv.* 6, eaax5032.
- Hubberstey, A. V., Pavliv, M., and Parks, R.J. (2002). Cancer therapy utilizing an adenoviral vector expressing only E1A. *Cancer Gene Ther.* 9, 321–329.
- Huntington, N.D., Cursons, J., and Rautela, J. (2020). The cancer–natural killer cell immunity cycle. *Nat. Rev. Cancer* 20, 437–454.
- Hurteau, J.A., Blessing, J.A., DeCesare, S.L., and Creasman, W.T. (2001). Evaluation of recombinant human interleukin-12 in patients with recurrent or refractory ovarian cancer: A gynecologic oncology group study. *Gynecol. Oncol.* 82, 7–10.
- Jager, L., Hausl, M., Rauschhuber, C., Wolf, N., and Kay, M. (2009). A rapid protocol for construction and production of high-capacity adenoviral vectors. *Nat. Protoc.* 4, 547–564.
- Jeannet, G. (2010). Essential role of the Wnt pathway effector Tcf-1 for the establishment of functional CD8 T cell memory. *Proc. Natl Acad. Sci. USA* 107, 9777–9782.
- Jiao, X., Velasco-Velazquez, M.A., Wang, M., Li, Z., Rui, H., Peck, A.R., Korkola, J.E., Chen, X., Xu, S., DuHadaway, J.B., et al. (2018). CCR5 Governs DNA damage repair and breast cancer stem cell expansion. *Cancer Res.* 78, 1657–1671.
- Jung, S.Y., Kang, K.W., Lee, E.Y., Seo, D.W., Kim, H.L., Kim, H., Kwon, T.W., Park, H.L., Kim, H., Lee, S.M., et al. (2018). Heterologous prime–boost vaccination with adenoviral vector and protein nanoparticles induces both Th1 and Th2 responses against Middle East respiratory syndrome coronavirus. *Vaccine* 36, 3468–3476.
- Kakarla, S., Song, X.T., and Gottschalk, S. (2012). Cancer-associated fibroblasts as targets for immunotherapy. *Immunotherapy* 4, 1129–1138.
- Kalbasi, A., and Ribas, A. (2020). Tumour-intrinsic resistance to immune checkpoint blockade. *Nat. Rev. Immunol.* 20, 25–39.
- Karnoub, A.E., Dash, A.B., Vo, A.P., Sullivan, A., Brooks, M.W., Bell, G.W., Richardson, A.L., Polyak, K., Tubo, R., and Weinberg, R.A. (2007). Mesenchymal stem cells within tumour stroma promote breast cancer metastasis. *Nature* 449, 557–563.
- Kärre, K. (2002). NK Cells, MHC Class I Molecules and the Missing Self. *Scand. J. Immunol.* 55, 221–228.
- Kennedy, M.K., Picha, K.S., Shanebeck, K.D., Anderson, D.M., and Grabstein, K.H. (1994). Interleukin-12 regulates the proliferation of Th1, but not Th2 or Th0, clones. *Eur. J. Immunol.* 24, 2271–2278.
- Kilinc, M.O., Rowswell-Turner, R.B., Gu, T., Virtuoso, L.P., and Egilmez, N.K. (2009). Activated CD8 + T-Effector/Memory Cells Eliminate CD4 + CD25 + Foxp3 + T-Suppressor Cells from Tumors via FasL Mediated Apoptosis . *J. Immunol.* 183, 7656–7660.
- Kim, J.H., Lee, S.-R., Li, L.-H., Park, H.-J., Park, J.-H., Lee, K.Y., Kim, M.-K., Shin, B.A., and Choi, S.-Y.

- (2011). High Cleavage Efficiency of a 2A Peptide Derived from Porcine Teschovirus-1 in Human Cell Lines, Zebrafish and Mice. *PLoS One* 6, e18556.
- Kurtulus, S. (2019). Checkpoint blockade immunotherapy induces dynamic changes in PD-1-CD8+ tumor-infiltrating T cells. *Immunity* 50, 181–194.
- Larkin, J., Chiarion-Sileni, V., Gonzalez, R., Grob, J.-J., Rutkowski, P., Lao, C.D., Cowey, C.L., Schadendorf, D., Wagstaff, J., Dummer, R., et al. (2019). Five-Year Survival with Combined Nivolumab and Ipilimumab in Advanced Melanoma. *N. Engl. J. Med.* 381, 1535–1546.
- Lasek, W., Zagodzinski, R., and Jakobisiak, M. (2014). Interleukin 12: still a promising candidate for tumor immunotherapy? *Cancer Immunol Immunother* 3, 419–435.
- Leach, D.R., Krummel, M.F., and Allison, J.P. (1996). Enhancement of antitumor immunity by CTLA-4 blockade. *Science* (80-.). 271, 1734–1736.
- Lee, H. (2019). Integrated molecular and immunophenotypic analysis of NK cells in anti-PD-1 treated metastatic melanoma patients. *Oncoimmunology* 8.
- Lee, C.S., Bishop, E.S., Zhang, R., Yu, X., Farina, E.M., Yan, S., Zhao, C., Zeng, Z., Shu, Y., Wu, X., et al. (2017). Adenovirus-mediated gene delivery: Potential applications for gene and cell-based therapies in the new era of personalized medicine. *Genes Dis.* 4, 43–63.
- Lee, D., Liu, J., Junn, H.J., Lee, E.J., Jeong, K.S., and Seol, D.W. (2019). No more helper adenovirus: production of gutless adenovirus (GLAd) free of adenovirus and replication-competent adenovirus (RCA) contaminants. *Exp. Mol. Med.* 51, 1–18.
- Levine, J.H., Simonds, E.F., Bendall, S.C., Davis, K.L., Amir, E.A.D., Tadmor, M.D., Litvin, O., Fienberg, H.G., Jager, A., Zunder, E.R., et al. (2015). Data-Driven Phenotypic Dissection of AML Reveals Progenitor-like Cells that Correlate with Prognosis. *Cell* 162, 184–197.
- Li, C., Jiang, P., Wei, S., Xu, X., and Wang, J. (2020). Regulatory T cells in tumor microenvironment: New mechanisms, potential therapeutic strategies and future prospects. *Mol. Cancer* 19, 116.
- Licursi, M., Christian, S.L., Pongnopparat, T., and Hirasawa, K. (2011). In vitro and in vivo comparison of viral and cellular internal ribosome entry sites for bicistronic vector expression. *Gene Ther.* 18, 631–636.
- Lo, M., Kim, H.S., Tong, R.K., Bainbridge, T.W., Vernes, J.M., Zhang, Y., Lin, Y.L., Chung, S., Dennis, M.S., Zuchero, Y.J.Y., et al. (2017). Effector-attenuating substitutions that maintain antibody stability and reduce toxicity in mice. *J. Biol. Chem.* 292, 3900–3908.
- Long, G. V., Dummer, R., Hamid, O., Gajewski, T.F., Caglevic, C., Dalle, S., Arance, A., Carlino, M.S., Grob, J.J., Kim, T.M., et al. (2019). Epcadostat plus pembrolizumab versus placebo plus pembrolizumab in patients with unresectable or metastatic melanoma (ECHO-301/KEYNOTE-252): a phase 3, randomised, double-blind study. *Lancet Oncol.* 20, 1083–1097.
- van der Loo, J.C.M., and Wright, J.F. (2016). Progress and challenges in viral vector manufacturing. *Hum. Mol. Genet.* 25, R42–R52.
- De Luca, M., Aiuti, A., Cossu, G., Parmar, M., Pellegrini, G., and Robey, P.G. (2019). Advances in stem cell research and therapeutic development. *Nat. Cell Biol.* 21, 801–811.
- Lundstrom, K. (2018). Viral Vectors in Gene Therapy. *Diseases* 6, 42.
- Luo, J., Deng, Z.L., Luo, X., Tang, N., Song, W.X., Chen, J., Sharff, K.A., Luu, H.H., Haydon, R.C., Kinzler, K.W., et al. (2007). A protocol for rapid generation of recombinant adenoviruses using the AdEasy system. *Nat. Protoc.* 2, 1236–1247.
- Masteller, E.L., Chuang, E., Mullen, A.C., Reiner, S.L., and Thompson, C.B. (2000). Structural Analysis of CTLA-4 Function In Vivo. *J. Immunol.* 164, 5319–5327.
- Maude, S.L., Frey, N., Shaw, P.A., Aplenc, R., Barrett, D.M., Bunin, N.J., Chew, A., Gonzalez, V.E., Zheng, Z., Lacey, S.F., et al. (2014). Chimeric Antigen Receptor T Cells for Sustained Remissions in Leukemia. *N. Engl. J. Med.* 371, 1507–1517.
- Meric-Bernstam, F., Larkin, J., Tabernero, J., and Bonini, C. (2020). Enhancing anti-tumour efficacy with immunotherapy combinations. *Lancet*.

- Mingozzi, F., and High, K.A. (2013). Immune responses to AAV vectors: Overcoming barriers to successful gene therapy. *Blood* 122, 23–36.
- Mizuguchi, H., Xu, Z., Ishii-Watabe, A., Uchida, E., and Hayakawa, T. (2000). IRES-Dependent Second Gene Expression Is Significantly Lower Than Cap-Dependent First Gene Expression in a Bicistronic Vector. *Mol. Ther.* 1, 376–382.
- Mizuguchi, H., Koizumi, N., Hosono, T., Ishii-Watabe, A., Uchida, E., Utoguchi, N., Watanabe, Y., and Hayakawa, T. (2002). CAR-or αv integrin-binding ablated adenovirus vectors, but not fiber-modified vectors containing RGD peptide, do not change the systemic gene transfer properties in mice. *Gene Ther.* 9, 769–776.
- Mokhtari, R.B., Homayouni, T.S., Baluch, N., Morgatskaya, E., Kumar, S., Das, B., and Yeger, H. (2017). Combination therapy in combating cancer. *Oncotarget* 8, 38022–38043.
- Morris, M.A., Gibb, D.R., Picard, F., Brinkmann, V., Straume, M., and Ley, K. (2005). Transient T cell accumulation in lymph nodes and sustained lymphopenia in mice treated with FTY720. *Eur. J. Immunol.* 35, 3570–3580.
- Motzer, R.J., Rakhit, A., Thompson, J.A., Nemunaitis, J., Murphy, B.A., Ellerhorst, J., Schwartz, L.H., Berg, W.J., and Bukowski, R.M. (2001). Randomized multicenter phase II trial of subcutaneous recombinant human interleukin-12 versus interferon- $\alpha 2a$ for patients with advanced renal cell carcinoma. *J. Interf. Cytokine Res.* 21, 257–263.
- Motzer, R.J., Tannir, N.M., McDermott, D.F., Arén Frontera, O., Melichar, B., Choueiri, T.K., Plimack, E.R., Barthélémy, P., Porta, C., George, S., et al. (2018). Nivolumab plus Ipilimumab versus Sunitinib in Advanced Renal-Cell Carcinoma. *N. Engl. J. Med.* 378, 1277–1290.
- Motzer, R.J., Rini, B.I., McDermott, D.F., Arén Frontera, O., Hammers, H.J., Carducci, M.A., Salaman, P., Escudier, B., Beuselinck, B., Amin, A., et al. (2019). Nivolumab plus ipilimumab versus sunitinib in first-line treatment for advanced renal cell carcinoma: extended follow-up of efficacy and safety results from a randomised, controlled, phase 3 trial. *Lancet Oncol.* 20, 1370–1385.
- Müller, P., Kreuzaler, M., Khan, T., Thommen, D.S., Martin, K., Glatz, K., Savic, S., Harbeck, N., Nitz, U., Gluz, O., et al. (2015). Trastuzumab emtansine (T-DM1) renders HER2+ breast cancer highly susceptible to CTLA-4/PD-1 blockade. *Sci. Transl. Med.* 7.
- Murooka, T.T., Rahbar, R., and Fish, E.N. (2009). CCL5 promotes proliferation of MCF-7 cells through mTOR-dependent mRNA translation. *Biochem. Biophys. Res. Commun.* 387, 381–386.
- Muruve, D.A., Cotter, M.J., Zaiss, A.K., White, L.R., Liu, Q., Chan, T., Clark, S.A., Ross, P.J., Meulenbroek, R.A., Maelandsmo, G.M., et al. (2004). Helper-dependent adenovirus vectors elicit intact innate but attenuated adaptive host immune responses in vivo. *J. Virol.* 78, 5966–5972.
- Myers, J.A., and Miller, J.S. (2021). Exploring the NK cell platform for cancer immunotherapy. *Nat. Rev. Clin. Oncol.* 18, 85–100.
- Nakao, S., Arai, Y., Tasaki, M., Yamashita, M., Murakami, R., Kawase, T., Amino, N., Nakatake, M., Kurosaki, H., Mori, M., et al. (2020). Intratumoral expression of IL-7 and IL-12 using an oncolytic virus increases systemic sensitivity to immune checkpoint blockade. *Sci. Transl. Med.* 12, eaax7992.
- Natoli, M., Bonito, N., Robinson, J.D., Ghaem-Maghami, S., and Mao, Y. (2020). Human ovarian cancer intrinsic mechanisms regulate lymphocyte activation in response to immune checkpoint blockade. *Cancer Immunol. Immunother.* 69, 1391–1401.
- Neshat, S.Y., Tzeng, S.Y., and Green, J.J. (2020). Gene delivery for immunoengineering. *Curr. Opin. Biotechnol.* 66, 1–10.
- Nguyen, K.G., Vrabel, M.R., Mantooth, S.M., Hopkins, J.J., Wagner, E.S., Gabaldon, T.A., and Zaharoff, D.A. (2020). Localized Interleukin-12 for Cancer Immunotherapy. *Front. Immunol.* 11, 1–36.
- O'Donnell, J.S., Teng, M.W.L., and Smyth, M.J. (2019). Cancer immunoediting and resistance to T cell-based immunotherapy. *Nat. Rev. Clin. Oncol.* 16, 151–167.
- Palmer, D., and Ng, P. (2003). Improved system for helper-dependent adenoviral vector production. *Mol. Ther.* 8, 846–852.

- Palmer, D.J., Turner, D.L., and Ng, P. (2020). A single “all-in-one” helper-dependent adenovirus to deliver donor DNA and CRISPR/Cas9 for efficient homology-directed repair. *Mol. Ther. - Methods Clin. Dev.* 17, 441–447.
- Parks, R.J., Chen, L., Anton, M., Sankar, U., and Rudnicki, M.A. (1996). A helper-dependent adenovirus vector system: Removal of helper virus by Cre-mediated excision of the viral packaging signal. *Proc. Natl. Acad. Sci. U. S. A.* 93, 13565–13570.
- Parks, R.J., Eveleigh, C.M., and Graham, F.L. (1999). Use of helper-dependent adenoviral vectors of alternative serotypes permits repeat vector administration. *Gene Ther.* 6, 1565–1573.
- Pentcheva-Hoang, T., Egen, J.G., Wojnoonski, K., and Allison, J.P. (2004). B7-1 and B7-2 selectively recruit CTLA-4 and CD28 to the immunological synapse. *Immunity* 21, 401–413.
- Plückthun, A. (2015). Designed ankyrin repeat proteins (DARPs): Binding proteins for research, diagnostics, and therapy. *Annu. Rev. Pharmacol. Toxicol.* 55, 489–511.
- Porter, C.E., Rosewell Shaw, A., Jung, Y., Yip, T., Castro, P.D., Sandulache, V.C., Sikora, A., Gottschalk, S., Iltman, M.M., Brenner, M.K., et al. (2020). Oncolytic adenovirus armed with BiTE, cytokine, and checkpoint inhibitor enables CAR T cells to control the growth of heterogeneous tumors. *Mol. Ther.* 6, 1251–1262.
- Poulin, K.L., McFall, E.R., Chan, G., Provost, N.B., Christou, C., Smith, A.C., and Parks, R.J. (2020). Fusion of Large Polypeptides to Human Adenovirus Type 5 Capsid Protein IX Can Compromise Virion Stability and DNA Packaging Capacity. *J. Virol.* 94.
- Prat, A., Navarro, A., Paré, L., Reguart, N., Galván, P., Pascual, T., Martínez, A., Nuciforo, P., Comerma, L., Alos, L., et al. (2017). Immune-related gene expression profiling after PD-1 blockade in non-small cell lung carcinoma, head and neck squamous cell carcinoma, and melanoma. *Cancer Res.* 77, 3540–3550.
- Qin, J., Zhang, L., Cliff, K., Hular, I., and Xiang, A. (2010). Systematic Comparison of Constitutive Promoters and the Doxycycline-Inducible Promoter. *PLoS One* 5, e10611.
- Rafei-Shamsabadi, D., Lehr, S., von Bubnoff, D., and Meiss, F. (2019). Successful combination therapy of systemic checkpoint inhibitors and intralesional interleukin-2 in patients with metastatic melanoma with primary therapeutic resistance to checkpoint inhibitors alone. *Cancer Immunol. Immunother.* 68, 1417–1428.
- Renaud-Gabardos, E., Hantelys, F., Morfoisse, F., Chaufour, X., Garmy-Susini, B., and Prats, A.-C. (2015). Internal ribosome entry site-based vectors for combined gene therapy. *World J. Exp. Med.* 5, 11–20.
- Riaz, N., Havel, J.J., Makarov, V., Desrichard, A., Urba, W.J., Sims, J.S., Hodi, F.S., Martín-Algarra, S., Mandal, R., Sharfman, W.H., et al. (2017). Tumor and Microenvironment Evolution during Immunotherapy with Nivolumab. *Cell* 171, 934-949.e15.
- Ribas, A., and Wolchok, J.D. (2018). Cancer immunotherapy using checkpoint blockade. *Science* (80-.). 359, 1350–1355.
- Ricobaraza, A., Gonzalez-Aparicio, M., Mora-Jimenez, L., Lumberras, S., and Hernandez-Alcoceba, R. (2020). High-capacity adenoviral vectors: Expanding the scope of gene therapy. *Int. J. Mol. Sci.* 21.
- Riley, R.S., June, C.H., Langer, R., and Mitchell, M.J. (2019). Delivery technologies for cancer immunotherapy. *Nat. Rev. Drug Discov.* 18, 175–196.
- Roberts, E.W., Broz, M.L., Binnewies, M., Headley, M.B., Nelson, A.E., Wolf, D.M., Kaisho, T., Bogunovic, D., Bhardwaj, N., and Krummel, M.F. (2016). Critical Role for CD103+/CD141+ Dendritic Cells Bearing CCR7 for Tumor Antigen Trafficking and Priming of T Cell Immunity in Melanoma. *Cancer Cell* 30, 324–336.
- Rosewell, A., Vetrini, F., and Ng, P. (2011). Helper-Dependent Adenoviral Vectors.
- Rotte, A. (2019). Combination of CTLA-4 and PD-1 blockers for treatment of cancer. *J. Exp. Clin. Cancer Res.* 38, 1–12.
- Ruan, M.Z.C., Cerullo, V., Cela, R., Clarke, C., Lundgren-Akerlund, E., Barry, M.A., and Lee, B.H.L. (2016). Treatment of osteoarthritis using a helper-dependent adenoviral vector retargeted to chondrocytes. *Mol.*

Ther. - Methods Clin. Dev. 3, 16008.

Ruffell, B., Chang-Strachan, D., Chan, V., Rosenbusch, A., Ho, C.M.T., Pryer, N., Daniel, D., Hwang, E.S., Rugo, H.S., and Coussens, L.M. (2014). Macrophage IL-10 Blocks CD8+ T Cell-Dependent Responses to Chemotherapy by Suppressing IL-12 Expression in Intratumoral Dendritic Cells. *Cancer Cell* 26, 623–637.

Sade-Feldman, M. (2018). Defining T cell states associated with response to checkpoint immunotherapy in melanoma. *Cell* 175, 998–1013.

Saleh, R., and Elkord, E. (2020). FoxP3+ T regulatory cells in cancer: Prognostic biomarkers and therapeutic targets. *Cancer Lett.* 490, 174–185.

Samstein, R.M., Lee, C.H., Shoushtari, A.N., Hellmann, M.D., Shen, R., Janjigian, Y.Y., Barron, D.A., Zehir, A., Jordan, E.J., Omuro, A., et al. (2019). Tumor mutational load predicts survival after immunotherapy across multiple cancer types. *Nat. Genet.* 51, 202–206.

Samusik, N., Good, Z., Spitzer, M.H., Davis, K.L., and Nolan, G.P. (2016). Automated mapping of phenotype space with single-cell data. *Nat. Methods* 13, 493–496.

Sánchez-Paulete, A.R., Cueto, F.J., Martínez-López, M., Labiano, S., Morales-Kastresana, A., Rodríguez-Ruiz, M.E., Jure-Kunkel, M., Azpilikueta, A., Quetglas, J.I., Sancho, D., et al. (2016). Abstract 4908: Cancer immunotherapy with immunomodulatory anti-CD137 and anti-PD-1 monoclonal antibodies requires Btl3-dependent dendritic cells. (American Association for Cancer Research (AACR)), pp. 4908–4908.

Sandig, V., Youil, R., Bett, J., Franlin, L.L., and Oshima, M. (2000). Optimization of the helper-dependent adenovirus system for production and potency in vivo. *Proc. Natl. Acad. Sci. U. S. A.* 97, 1002–1007.

Schmid, M., Ernst, P., Honegger, A., Suomalainen, M., Zimmermann, M., Braun, L., Stauffer, S., Thom, C., Dreier, B., Eibauer, M., et al. (2018). Adenoviral vector with shield and adapter increases tumor specificity and escapes liver and immune control. *Nat. Commun.* 9, 1–16.

Schreiber, R.D., Old, L.J., and Smyth, M.J. (2011). Cancer immunoediting: Integrating immunity's roles in cancer suppression and promotion. *Science* (80-.). 331, 1565–1570.

Sedighi, M., Zahedi Bialvaei, A., Hamblin, M.R., Ohadi, E., Asadi, A., Halajzadeh, M., Lohrasbi, V., Mohammadzadeh, N., Amirani, T., Krutova, M., et al. (2019). Therapeutic bacteria to combat cancer; current advances, challenges, and opportunities. *Cancer Med.* 8, 3167–3181.

Seliger, B. (2019). Combinatorial Approaches with Checkpoint Inhibitors to Enhance Anti-tumor Immunity. *Front. Immunol.* 10, 999.

Sharma, P., and Allison, J.P. (2020). Dissecting the mechanisms of immune checkpoint therapy. *Nat. Rev. Immunol.* 20, 75–76.

Sharma, P., Hu-Lieskovan, S., Wargo, J.A., and Ribas, A. (2017). Primary, Adaptive, and Acquired Resistance to Cancer Immunotherapy. *Cell* 168, 707–723.

Shayakhmetov, D.M., Eberly, A.M., Li, Z.-Y., and Lieber, A. (2005). Deletion of Penton RGD Motifs Affects the Efficiency of both the Internalization and the Endosome Escape of Viral Particles Containing Adenovirus Serotype 5 or 35 Fiber Knobs. *J. Virol.* 79, 1053–1061.

Siddiqui, I. (2019). Intratumoral Tcf1+PD-1+CD8+ T cells with stem-like properties promote tumor control in response to vaccination and checkpoint blockade immunotherapy. *Immunity* 50, 195-211.e10.

Simmons, A.D., Moskalenko, M., Creson, J., Fang, J., Yi, S., VanRoey, M.J., Allison, J.P., and Jooss, K. (2008). Local secretion of anti-CTLA-4 enhances the therapeutic efficacy of a cancer immunotherapy with reduced evidence of systemic autoimmunity. *Cancer Immunol. Immunother.* 57, 1263–1270.

Slade, N. (2001). Viral vectors in gene therapy. In *Periodicum Biologorum, (Diseases)*, pp. 139–143.

Smith, A.C., Poulin, K.L., and Parks, R.J. (2009). DNA Genome Size Affects the Stability of the Adenovirus Virion. *J. Virol.* 83, 2025–2028.

Smith, S.N., Schubert, R., Simic, B., Brücher, D., Schmid, M., Kirk, N., Freitag, P.C., Gradinaru, V., and Plückthun, A. (2021). The SHREAD gene therapy platform for paracrine delivery improves tumor localization and 3 intratumoral effects of a clinical antibody. *Proc. Natl Acad. Sci. USA.*

- Souza-Fonseca-Guimaraes, F., Cursons, J., and Huntington, N.D. (2019). The Emergence of Natural Killer Cells as a Major Target in Cancer Immunotherapy. *Trends Immunol.*
- Spranger, S., Dai, D., Horton, B., and Gajewski, T.F. (2017). Tumor-Residing Batf3 Dendritic Cells Are Required for Effector T Cell Trafficking and Adoptive T Cell Therapy. *Cancer Cell* 31, 711-723.e4.
- Sudan, R. (2020). Cytokines in cancer immunotherapy. In *Systems and Synthetic Immunology*, (Springer Singapore), pp. 255–269.
- Sun, J., Wei, Q., Zhou, Y., Wang, J., Liu, Q., and Xu, H. (2017). A systematic analysis of FDA-approved anticancer drugs. *BMC Syst. Biol.* 11.
- Takeishi, H., and Ushijima, T. (2019). Accumulation of genetic and epigenetic alterations in normal cells and cancer risk. *Npj Precis. Oncol.* 3, 1–8.
- Thommen, D.S., Koelzer, V.H., Herzig, P., Roller, A., Trefny, M., Dimeloe, S., Kialainen, A., Hanhart, J., Schill, C., Hess, C., et al. (2018). A transcriptionally and functionally distinct pd-1 + cd8 + t cell pool with predictive potential in non-small-cell lung cancer treated with pd-1 blockade. *Nat. Med.* 24.
- Tirosh, I., Izar, B., Prakadan, S.M., Wadsworth, M.H., Treacy, D., Trombetta, J.J., Rotem, A., Rodman, C., Lian, C., Murphy, G., et al. (2016). Dissecting the multicellular ecosystem of metastatic melanoma by single-cell RNA-seq. *Science* (80-). 352, 189–196.
- Topalian, S.L., Hodi, F.S., Brahmer, J.R., Gettinger, S.N., Smith, D.C., McDermott, D.F., Powderly, J.D., Carvajal, R.D., Sosman, J.A., Atkins, M.B., et al. (2012). Safety, activity, and immune correlates of anti-PD-1 antibody in cancer. *N. Engl. J. Med.* 366, 2443–2454.
- Trüb, M., Uhlenbrock, F., Claus, C., Herzig, P., Thelen, M., Karanikas, V., Bacac, M., Amann, M., Albrecht, R., Ferrara-Koller, C., et al. (2020). Fibroblast activation protein-targeted-4-1BB ligand agonist amplifies effector functions of intratumoral T cells in human cancer. *J Immunother Cancer* 8, 238.
- Tugues, S., Burkhard, S.H., Ohs, I., Vrohings, M., Nussbaum, K., Vom Berg, J., Kulig, P., and Becher, B. (2015). New insights into IL-12-mediated tumor suppression. *Cell Death Differ.* 22, 237–246.
- Ura, T., Okuda, K., and Shimada, M. (2014). Developments in viral vector-based vaccines. *Vaccines* 2, 624–641.
- Voabil, P., de Bruign, M., Roelofsen, L.M., Hendriks, S.H., Brokamp, S., van den Braber, M., Broeks, A., Sanders, J., Herzig, P., Zippelius, A., et al. Immunological response of human cancers to PD-1 blockade. *Nat. Med.*
- Waldman, A.D., Fritz, J.M., and Lenardo, M.J. (2020). A guide to cancer immunotherapy: from T cell basic science to clinical practice. *Nat. Rev. Immunol.* 20, 651–668.
- Wang, S., Astsaturov, I.A., Bingham, C.A., McCarthy, K.M., Von Mehren, M., Xu, W., Alpaugh, R.K., Tang, Y., Littlefield, B.A., Hawkins, L.D., et al. (2012). Effective antibody therapy induces host-protective antitumor immunity that is augmented by TLR4 agonist treatment. *Cancer Immunol. Immunother.* 61, 49–61.
- Wei, S.C., Anang, N.A.A.S., Sharma, R., Andrews, M.C., Reuben, A., Levine, J.H., Cogdill, A.P., Mancuso, J.J., Wargo, J.A., Pe'er, D., et al. (2019). Combination anti-CTLA-4 plus anti-PD-1 checkpoint blockade utilizes cellular mechanisms partially distinct from monotherapies. *Proc. Natl. Acad. Sci. U. S. A.* 116, 22699–22709.
- Weiss, G.R., O'Donnell, M.A., Loughlin, K., Zonno, K., Laliberte, R.J., and Sherman, M.L. (2003). Phase 1 Study of the Intravesical Administration of Recombinant Human Interleukin-12 in Patients With Recurrent Superficial Transitional Cell Carcinoma of the Bladder. *J. Immunother.* 26, 343–348.
- West, W. (1989). Continuous infusion recombinant interleukin-2 (rIL-2) in adoptive cellular therapy of renal carcinoma and other malignancies. *Cancer Treat. Rev.*
- Wirth, T., and Ylä-Herttuala, S. (2014). Gene therapy used in cancer treatment. *Biomedicines* 2, 149–162.
- Wolchok, J.D., Chiarion-Sileni, V., Gonzalez, R., Rutkowski, P., Grob, J.-J., Cowey, C.L., Lao, C.D., Wagstaff, J., Schadendorf, D., Ferrucci, P.F., et al. (2017). Overall Survival with Combined Nivolumab and Ipilimumab in Advanced Melanoma. *N. Engl. J. Med.* 377, 1345–1356.

Wold, W., and Toth, K. (2014). Adenovirus Vectors for Gene Therapy, Vaccination and Cancer Gene Therapy. *Curr. Gene Ther.* *13*, 421–433.

Xu, Z., Qiu, Q., Tian, J., Smith, J., and Conenello, G. (2013). Coagulation factor X shields adenovirus type 5 from attack by natural antibodies and complement. *Nat. Med.* *19*, 452–457.

Yan, M., Parker, B.A., Schwab, R., and Kurzrock, R. (2014). HER2 aberrations in cancer: Implications for therapy. *Cancer Treat. Rev.* *40*, 770–780.

Yang, L., Huang, J., Ren, X., Gorska, A.E., Chytil, A., Aakre, M., Carbone, D.P., Matrisian, L.M.M., Richmond, A., Lin, P.C., et al. (2008). Abrogation of TGF β Signaling in Mammary Carcinomas Recruits Gr-1+CD11b+ Myeloid Cells that Promote Metastasis. *Cancer Cell* *13*, 23–35.

Zhao, Y., Lee, C.K., Lin, C.H., Gassen, R.B., Xu, X., Huang, Z., Xiao, C., Bonorino, C., Lu, L.F., Bui, J.D., et al. (2019). PD-L1:CD80 Cis-Heterodimer Triggers the Co-stimulatory Receptor CD28 While Repressing the Inhibitory PD-1 and CTLA-4 Pathways. *Immunity* *51*, 1059-1073.e9.

Zhou, H.S., Zhao, T., Rao, X.M., and Beaudet, A.L. (2002). Production of helper-dependent adenovirus vector relies on helper virus structure and complementing. *J. Gene Med.* *4*, 498–509.

Zilionis, R., Engblom, C., Pfirschke, C., Savova, V., Zemmour, D., Saatcioglu, H.D., Krishnan, I., Maroni, G., Meyerovitz, C. V., Kerwin, C.M., et al. (2019). Single-Cell Transcriptomics of Human and Mouse Lung Cancers Reveals Conserved Myeloid Populations across Individuals and Species. *Immunity* *50*, 1317-1334.e10.

Zippelius, A., Batard, P., Rubio-Godoy, V., Bioley, G., Liénard, D., Lejeune, F., Rimoldi, D., Guillaume, P., Meidenbauer, N., Mackensen, A., et al. (2004). Effector Function of Human Tumor-Specific CD8 T Cells in Melanoma Lesions: A State of Local Functional Tolerance. *Cancer Res.* *64*, 2865–2873.

Zorn, E., Nelson, E.A., Mohseni, M., Porcheray, F., Kim, H., Litsa, D., Bellucci, R., Raderschall, E., Canning, C., Soiffer, R.J., et al. (2006). IL-2 regulates FOXP3 expression in human CD4+CD25+ regulatory T cells through a STAT-dependent mechanism and induces the expansion of these cells in vivo. *Blood* *108*, 1571–1579.

flowCore: flowCore: Basic structures for flow cytometry data version 2.2.0 from Bioconductor.

CATALYST: Cytometry dATa anALYSIS Tools version 1.14.0 from Bioconductor.

GitHub - JinmiaoChenLab/Rphenograph: Rphenograph: R implementation of the PhenoGraph algorithm.

CRAN - Package pheatmap.

6 Curriculum Vitae

Nicole Kirchhammer

✉ nicole.kirchhammer@unibas.ch

☎ +41 612652355

📍 Hebelstrasse 20 4031 Basel

Research

07/2021– currently	Postdoctoral Fellow Cancer Immunology University of Basel Dpt. of Biomedicine – Prof. Dr. Alfred Zippelius	Basel
05/2017 – 06/2021	PhD student “Tumor-targeted immunotherapy using an engineered adenoviral vector platform” University of Basel Dpt. of Biomedicine – Prof. Dr. Alfred Zippelius	Basel
06/2017 – 09/2017	Research stay within PhD education at Collaborator’s side Production of adenoviral vectors University of Zurich Dpt. of Biochemistry – Prof. Dr. Andreas Plückthun	Zurich

Education

2014 – 2016	Master of Science in Molecular Medicine – <i>summa cum laude</i> University of Regensburg Specialization in Cancer Immunology, Immunology and Epidemiology	Regensburg
Master thesis	“In vitro evaluation of potential tumor-therapeutic effects of novel monoclonal, chimeric rabbit anti-Her2 antibodies in comparison to Trastuzumab and Pertuzumab” Dpt. of Gynecology and Obstetrics – Prof. Dr. Gero Brockhoff	
2011 – 2014	Bachelor of Science in Molecular Medicine – <i>magna cum laude</i> University of Regensburg	Regensburg
Bachelor thesis	“Molecular studies of selected, by histone modification regulated candidate genes in glioblastoma” Dpt. of Neuropathology – Prof. Dr. Markus Riemenschneider	

Additional Education

02/2021	Clinical Study project management course	Basel
10/2020	Training for Persons Responsible for Directing Animal Experimentation (LTKII)	Zurich
2019	antelope@novartis mentorship	Basel
04/2019	Finance basics for innovators and entrepreneurs	Basel
10/2018	Business Skills- Crash Course	Basel
2018/2017/2015	Introduction to R, Analysis of genomics data with R/Bioconductor, Methods course “Gene Expression Analysis”	Basel Regensburg
10/2013	Laboratory Animal Course (FELASA Category B)	Regensburg

Supervising and Mentoring Activities

05/2020 – 05/2021	Supervision of Master's thesis, Victoria Koch
04/2019 – 12/2019	Supervision of Master's thesis, Franziska Werner

Posters and Presentations

In addition to regularly presenting my work at institute seminars, lab meetings and graduate scholars:

02/2020	Invited Speaker at 2 nd Swiss Cytometry Meeting 2020 "A novel genetically engineered adenoviral vector platform for tumor-targeted cancer immunotherapy"	Lausanne
10/2019	Invited Speaker at Oncolytic Viruses Congress "Adenoviral vectors for cancer immunotherapeutics"	Regensburg
03/2019	Poster presentation at University of Basel Immunology Community Retreat Engelberg "Paracrine delivery of cancer immunotherapeutics"	
11/2018	Poster presentation at Basel Breast Consortium Annual Meeting "Paracrine delivery of cancer immunotherapeutics"	Basel

Publications and Patents

Bruecher D*, Kirchhammer N*, Smith SN, Schumacher J, Kolibius J, Freitag PC, Schmid M, Weiss F, Keller C, Grove M, Grove M, Greber U, Zippelius A, Plückthun A. iMATCH – an intuitive modular assembly-system for therapeutic combination high-capacity adenovirus gene therapy. *Molecular Therapy – Methods & Clinical Development*, 2021

Bonilla WV, Kirchhammer N*, Marx AF*, Kaller SM, Kryzaniak MA, Lu M, Darbre S, Schmidt S, Raguz J, Berka U, Vincenti I, Pauzuolis M, Günther S, Magnus C, Merkler D, Orlander K, Zippelius A, Pinschewer D. Heterologous arenavirus vector prime – boost overrules self-tolerance for massive tumor-specific CD8 T cell attack. *Cell reports medicine* 2021

Lötscher J, Marti Lindez AA, Kirchhammer N, Griodano Attianese G, Criolioli E, Trefny M, Lenz M, Strati P, Litzler L, Koch V, Lee D, Dehio PG, Künzli M, Loliger JG, Burgener AV, Schreiner D, Balmer ML, King C, Irving M, Zippelius A, Reith W, Hess C. Shaping memory with magnesium – how moderate activation of LFA-1 with magnesium optimizes CD8+ T cell effector function. Submitted

Stanczak MA, Mantuano N*, Kirchhammer N*, Sanin DE, Wang J, Trefny MP, Monaco G, Gray AG, Petrone A, Wang J, Kashyap AS, Glatz K, Kasenda B, Normington K, Broderick J, Peng L, Pearce OMT, Pearce EL, Bertozzi CR, Zippelius A and Läubli H. Targeting cancer glycosylation repolarizes tumor-associated macrophages allowing effective immune checkpoint blockade. Submitted

Wege AK, Kirchhammer N, Kazandjian LV, Prassl S, Brandt M, Piendl G, Ortmann O, Fischer S, Brockhoff G. A novel rabbit derived anti-HER2 antibody with pronounced therapeutic effectiveness on HER2-positive breast cancer cells in vitro and in humanized tumor mice (HTM), *Journal of translational medicine* 2020

Mantuano N, Stanczak MA, Oliveria IA, Kirchhammer N, Filardy A, Monaco G, Santos RC, Fonsceca AC, Fontes M, Bastos CS, Dias WB, Zippelius A, Todeschini AR and Läubli H. Hyperglycemia enhances cancer immune evasion by inducing alternative macrophage polarization through increased O-GlcNAcylation. *Cancer Research* 2020

Kashyap AS, Zhao Y, Fernandez-Rodriguez L, Monaco G, Trefny MP, Yoshida N, Martin K, Sharma A, Olieric N, Shah P, Stanczak MA, Kirchhammer N, Park SM, Wieckowski S, Läubli H, Zagani R, Kasenda B, Steinmetz MO, Reinecker HC, Zippelius A. GEFH1 signaling upon microtubule destabilization is required for dendritic cell activation and specific anti-tumor responses. *Cell Reports* 2019

Rom-Jurek E-M, Kirchhammer N, Ugocsai P, Ortmann O, Wege AK, Brockhoff G. Regulation of programmed death ligand 1 (PD-L1) expression in breast cancer cell lines *in vitro* and in immunodeficient and humanized tumor mice. *International Journal of Molecular Sciences*. 2018

MAB Discovery GmbH, Fischer S & Brandt M, Her-2 binding antibodies, 2016-05-06, EP2016016 8619

*authorship equally shared